ABSTRACT

Clark, William Isaac. Fixed-Abrasive Diamond Wire Saw Machining. (Under the direction of Dr. Albert Shih)

The goal of this research was to investigate the use of fixed abrasive diamond wire saw machining with wood and foam ceramic materials. Fixed abrasive diamond wire saw machining was developed in recent years to allow for thin kerf slicing of advanced semiconductor materials. The main advantages of this machining technology for the use in wood machining are its thin kerf loss and unidirectional cutting capability.

The design of cutting experiments using a spooled wire saw is presented. The first experiment tested the response of machining wood repeatedly with the same process parameters. The next experiments tested the effect of changing wire axial speed and saw rocking motion conditions for pine and oak wood materials. Finally, an experiment was designed to machine three types of foam ceramic materials.

A data acquisition system was constructed and signal-processing techniques for removing noise were developed. The data collection system was used to record forces and certain machine parameters during wire cutting. The machined surfaces for the wood materials were measured to determine their roughness. A Scanning Electron Microscope was used to examine new and used wire as well as cutting debris to study the effects of wire wear. Finally, the results and the direction of future work in this area are discussed.

FIXED-ABRASIVE DIAMOND WIRE SAW MACHINING

by
WILLIAM ISAAC CLARK

A thesis submitted to the Graduate Faculty of
North Carolina State University
in partial fulfillment of the
requirements for the Degree of Master of Science

DEPARTMENT OF MECHANICAL AND AEROSPACE ENGINEERING

Raleigh

2001

APPROVED BY:

______________________________ ______________________________

____

Chair of Advisory Committee

BIOGRAPHY

William Clark was born outside of Nashville, Tennessee in November of 1977. He is the son of Douglas H. Clark and Mindy J. Clark. After attending The University of North Carolina at Asheville for two years, William transferred to North Carolina State University to complete an undergraduate degree in Mechanical Engineering. William spent the last 18 months pursuing a Master of Science Degree in Mechanical Engineering under the guidance of Dr. Albert J. Shih. More recently, William accepted an offer to work with the Naval Surface Warfare Research Center in Dahlgren, Virginia after completion of his degree.

ACKNOWLEDGEMENTS

I would like to thank some of the people who helped me conduct this research project. First of all, Dr. Albert J. Shih worked as my advisor to first set up the project and to help in every step of its completion. Sam McSpadden helped tremendously during my work in the HTML program at ORNL. Richard Lemaster provided funding, support, and advice from the Wood Tooling and Machining Research Group.

TABLE OF CONTENTS

LIST OF FIGURES

Chapter 1

Chapter 2

Chapter 3

Chapter 4

Chapter 5

Chapter 6

LIST OF TABLES

Chapter 2

Chapter 4

Chapter 5

NOMENCLATURE

Symbol	Description
DF	Yoke downfeed
V	Wire velocity
θ	Wire bow angle
H	Height error from wire bow
L	Guide pulley center distance
D	Capacitance sensor face diameter
R^2	Correlation factor
δ	Height error from workpiece width
W	Workpiece width
α	Rocking motion angle
ψ	Wire inclination angle actually achieved
T_1	Tension in wire to right of workpiece
T_2	Tension in wire to left of workpiece
F_C	Horizontal cutting force
F_T	Vertical thrust force
F_x	Horizontal force measured by dynamometer
F_y	Vertical force measured by dynamometer

1 INTRODUCTION

The development and use of large, 200 mm and 300 mm (8 inch and 12 inch) diameter single crystal silicon wafers has revitalized interest in wire saw machining technologies. Slicing single crystal silicon into thin wafers with minimum warp, uniform thickness, and low kerf loss is a critical step in semiconductor manufacturing. Figure 1.1 shows the traditional inner diamond saw blade used to slice a single crystal silicon ingot into wafers. The thickness of the saw blade creates kerf loss, the waste of material from machining. To minimize this kerf loss, wire saw machining technology, as shown in Figure 1.2, was developed in the 90s and was applied to silicon wafer production in the late 90s.

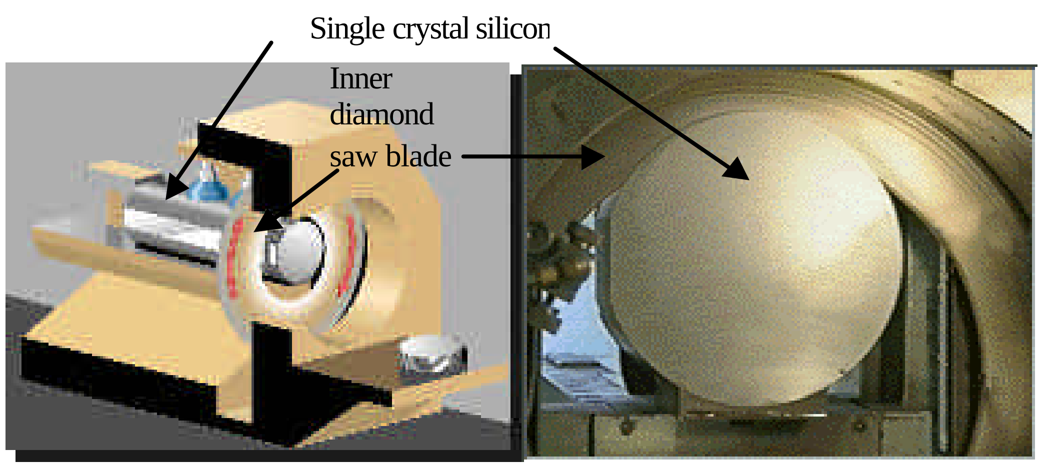

Figure 1.1: Traditional inner diamond saw blade for silicon wafer slicing. [Mitsubushi, 1998]

As shown in Figure 1.2, a thin, high-tensile strength steel wire is wound around three or four polyethylene rollers as it passes between two spools of wire (1 and 6 in Figure 1.2(a)). The spacing between the wires is controlled by precisely ground grooves on the Polyethylene rollers, as shown in the close-up view in Figure 1.2(b). For slicing silicon wafers, loss abrasive slurry is used. The abrasive slurry is fed from a plate (5 in Figure 1.2(a)) to the wire and is carried by the wire to the workpiece. A small portion of the abrasive is impregnated as a third-body between the wire and the silicon workpiece to generate the cutting action. A set of 200 to 300 silicon wafers, each one 12 inch in diameter, can be cut in about 6 to 8 hours [Merritt, 1999], which is much more efficient than the traditional inner diamond saw blade slicing method shown in Fig. 1.1. To further reduce the processing time and to machine other harder and more difficult-to-machine semiconductor materials, such as silicon carbide, new diamond impregnated wires and wire saw machines have been developed. These have led to the use of fixed abrasive diamond wire saw machining for other materials and industries, including the wood machining in furniture manufacturing.

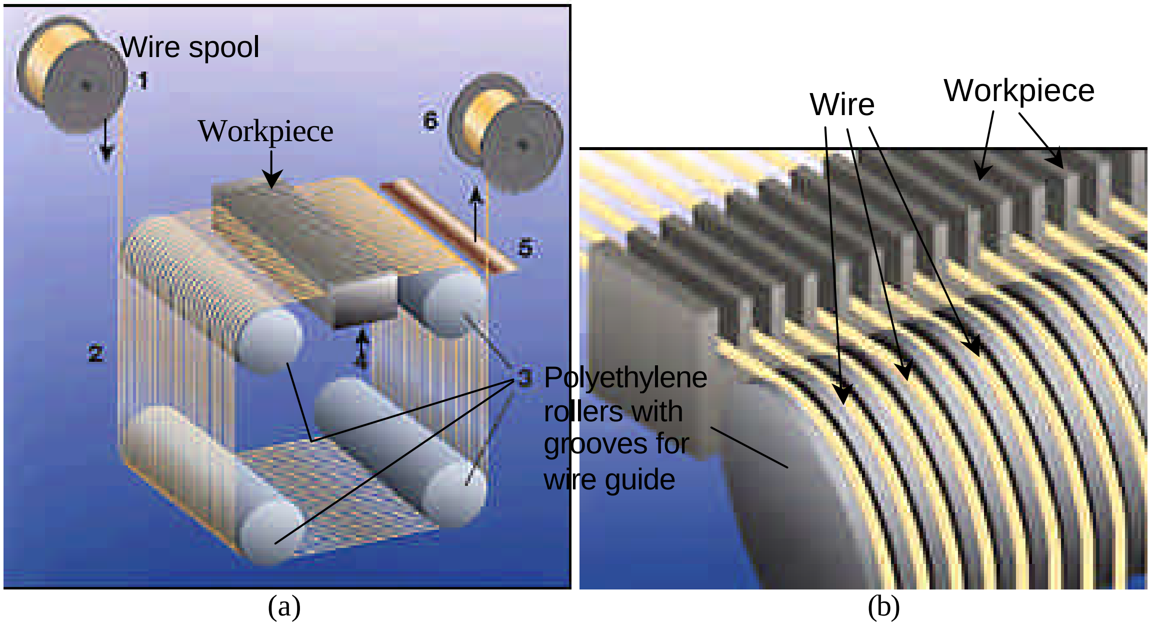

Figure 1.2: (a) Configuration of the wire saw slicing of wafer and (b) close-up view of the grooves in the plastic wire guide and the slicing of workpiece. [Bekaert, 1999]

1.1 Fixed Abrasive Diamond Wire

There are competing methods of producing fixed-abrasive diamond wire. Each supplier uses a different method to affix diamond particles to a metal wire core. The first type of wire from Supplier 1, Laser Technology West (LTW), is shown in Figure 1.3(a) and under higher magnification in 1.4(a). This brand of wire uses an additional layer of binding material, coated by the electroplating method, to cover the diamonds in an attempt to affix the diamonds to the wire. This hides the diamonds from view, making them difficult to find in both figures. Other brands of fixed abrasive diamond wire use different methods to bind the diamonds in place. SEM pictures of unused wire segments from the other two suppliers, Suppliers 2 and 3, are shown in Figures 1.3(b) and 1.3(c), respectively. Higher magnification images of both are shown in Figures 1.4(b) and 1.4(c). The diamond wires from Suppliers 2 and 3 have diamond grains that are very obvious. The diamonds seen in Figure 1.3(c) are smaller than those used by other two suppliers. Figure 1.3 and Figure 1.4 reveal that significantly different methods developed to manufacture the fixed-abrasive diamond wire.

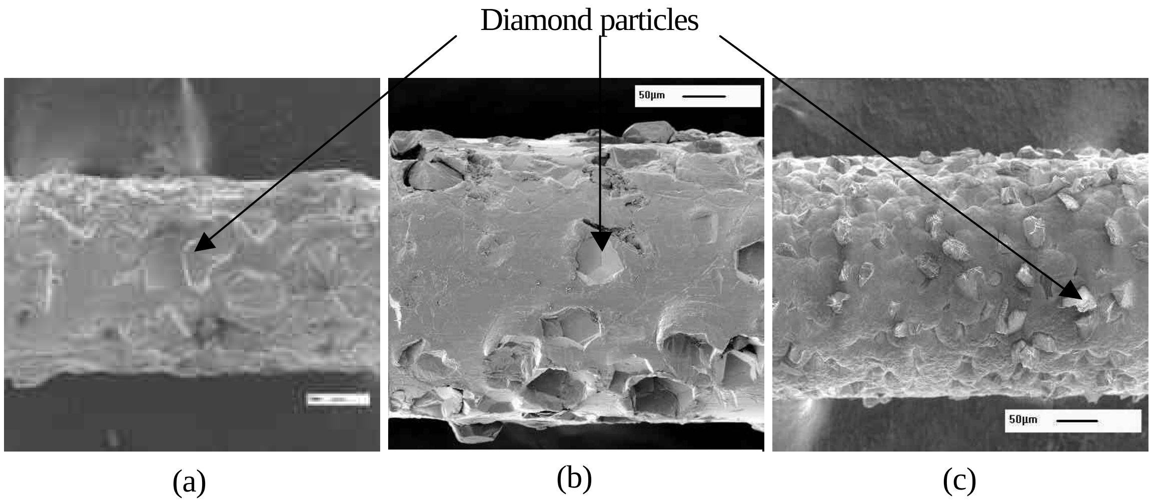

Figure 1.3: Segment of a new diamond wire from (a) Supplier 1, (b) Supplier 2, and (c) Supplier 3.

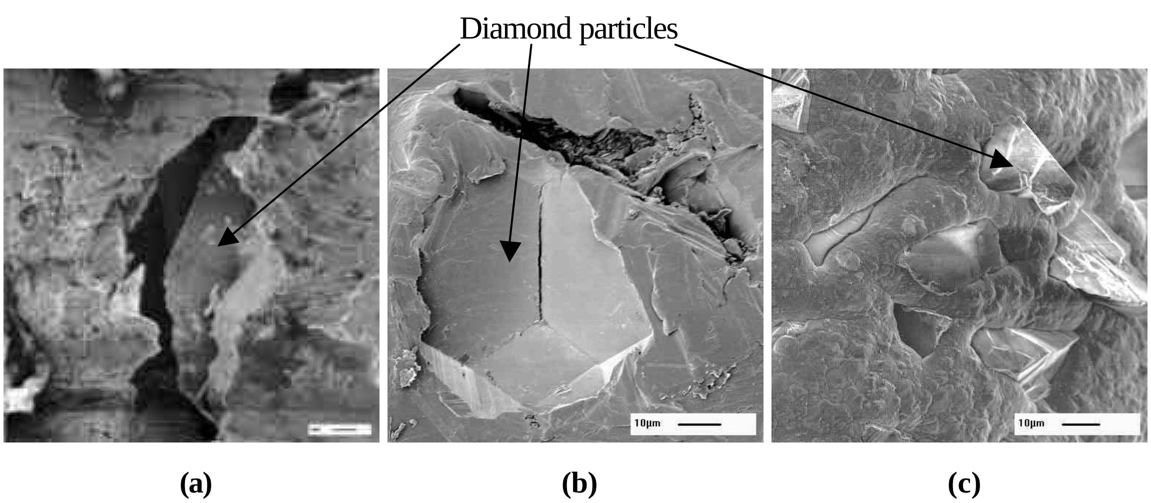

Figure 1.4: Individual diamonds on wires from (a) Supplier 1, (b) Supplier 2, and (c) Supplier 3.

The first type of fixed abrasive diamond wire has a metal matrix outer layer affixing diamond particles to the inner metal wire. If the diamond particles extend beyond the metal, they can be used to cut a workpiece as the wire is pulled across it. The diamond wire in Figure 1.4(b) works the same way, except that their diamonds are never buried beneath a binding material. Each diamond particle acts as an individual cutting tool. In this, diamond wire cutting is very similar to grinding operations.

1.2 Methods of Fixed Abrasive Diamond Wire Machining

The three types of wire saw machining of wood to be studied are shown in Figure 1.5. The first method, as shown in Figure 1.5(a), is to use a long wire, stored in two spools, to cut the wood workpiece. Fresh, uncut diamond wire can be continuously introduced during machining, which makes this type of wire saw cutting more precise, but also more expensive. This type of wire saw cutting is commonly used for wafer slicing in the semiconductor industry. For wood machining, the workpiece can move moved in two translational directions, as shown in Figure 1.6(a), or in two translational and one rotational directions, as shown in Figure 1.6(b). The other two types of wire saw machining, as shown in Figures 1.5(b) and 1.5(c), use looped continuous and reciprocal/oscillating diamond wire, respectively. The looped diamond wire saw cutting (Figure 1.5(b)) is like the band saw but is a lot more flexible. The reciprocal/oscillating wire saw cutting (Figure 1.5(c)) could be conducted with existing scroll saw machines.

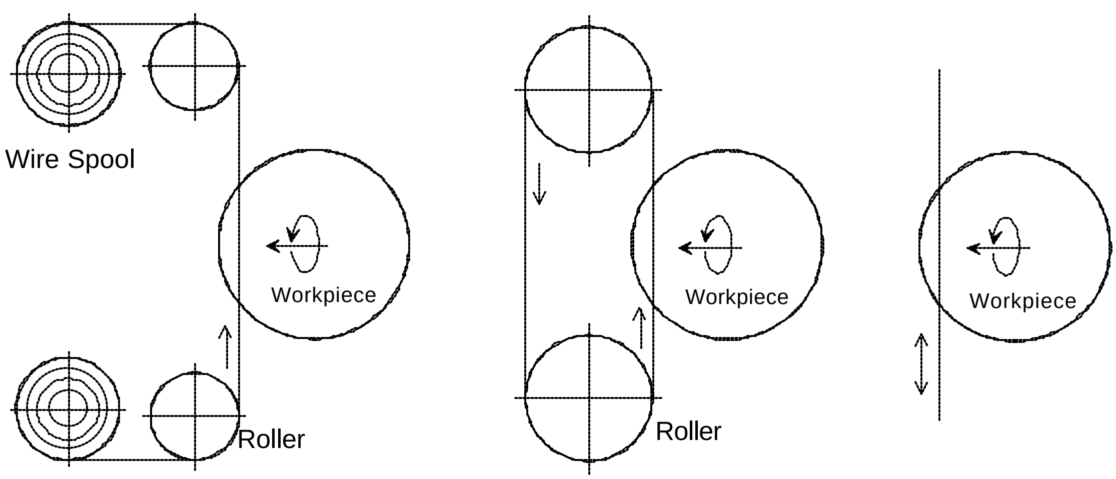

(a) **(b)** **(c)**

Figure 1.5: Three types of wire saw cutting of wood, (a) cutting with a long wire stored in two spools, (b) looped wire saw, and (c) reciprocal/oscillating wire saw cutting.

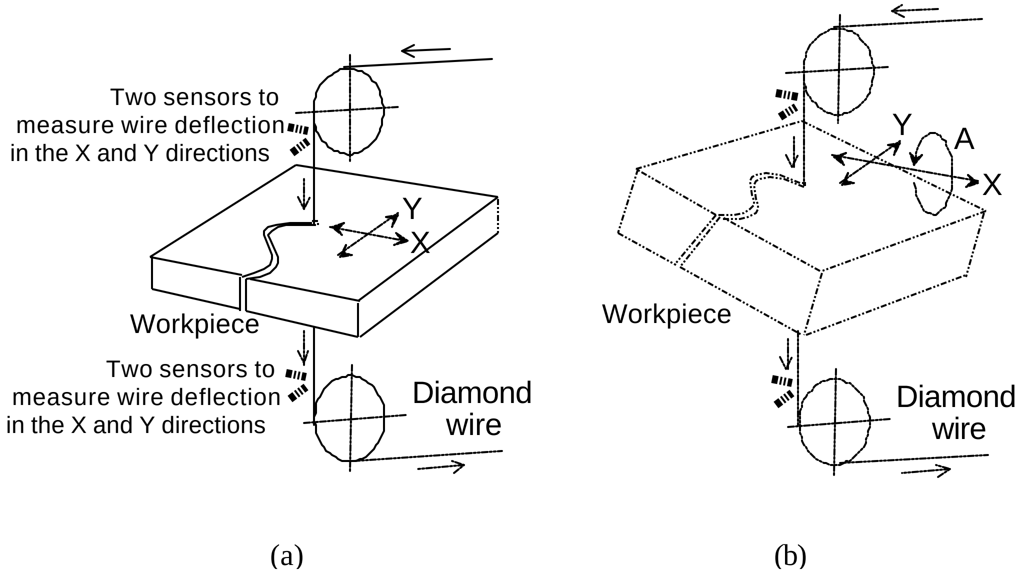

Figure 1.6: Wire saw cutting of wood workpiece and location of wire deflection capacitance sensors, (a) X-Y contouring, and (b) X-Y contouring plus rotation (A-axis) of the workpiece.

During all three types of wire saw cutting, the wood workpiece can be moved in both X and Y translational directions, as shown in Figure 1.6(a) or in the combination of X and Y plus a twist of the workpiece, A-axis in Figure 1.6(b

1.3 Advantages of Fixed Abrasive Diamond Wire Machining

Fixed abrasive diamond wire saw machining wields several advantages over competing machining methods. The four major advantages, thin kerf, unidirectional cutting capability, low noise, and low dust are described in the following sections.

1.3.1 Thin Kerf

The diamond wire saw could replace some current circular saw and band saw applications for thin-kerf wood machining. Thin-kerf can reduce the waste of wood material.

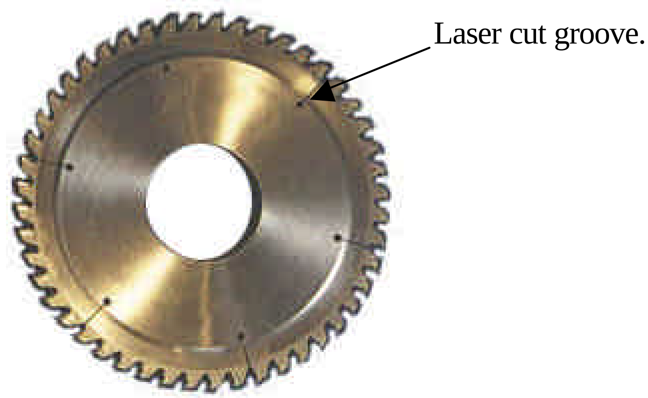

Figure 1.7: Typical circular saw blade for cutting wood [Super Thin Saws, 2001].

A thin kerf circular saw blade, made by Super Thin Saws, is shown in Figure 1.7. The technology of circular saw wood machining has made significant advances in the past five decades. Thin kerf circular saw blades are now applied in many high-end wood-machining operations such as rip saw operations. To use super thin kerf circular saw blades, a well-balanced blade and a machine with an accurate, low-runout spindle are necessary. Most of the thin-kerf circular saw blades have laser-cut grooves with different shapes to help increase the frequency of resonant modes of vibration. Figure 1.7 shows examples of the laser cut grooves. Another common practice to increase the resonant frequencies of the circular saw blade is to use a steel roller to roll a ring on the blade or to use a laser to heat-treat rings or areas on the surface. Both methods create compressive residual stress on the blade surface to increase resonant frequencies. Developments of thin-kerf circular saw blade are summarized by Kirbach [1989], Parker and Mote [1989], Schajer and Mote [1983], Mote and Szymani [1977], Szymani and Mote [1977], Mote and Nieh [1973], and Mote [1964]. With all these developments, there is still a limit on the thickness required for a circular saw blade. The diamond wire saw could provide a quantum leap over the current super thin circular saw on thin-kerf wood machining technology.

A study was conducted to survey the kerf of circular saw blades used in industry today. The results are summarized in Figure 1.8. One millimeter is the limit for state-of-the-art super thin circular saw blades. The diameter of the diamond wire starts at 0.4 mm and could be as thin as 0.12 mm. Compared to conventional circular sawing, which ranges from 1 to 3.5 mm, the diamond wire saw could offer an order of magnitude less kerf loss. Figure 1.8 illustrates the great potential for low kerf loss in the diamond wire saw machining of wood. This survey covers the regular and thin-kerf circular saw blades made by DeWalt of Black & Decker and the special-made super thin saw blades made by Super Thin Saws, Inc. at Waterbury VT.

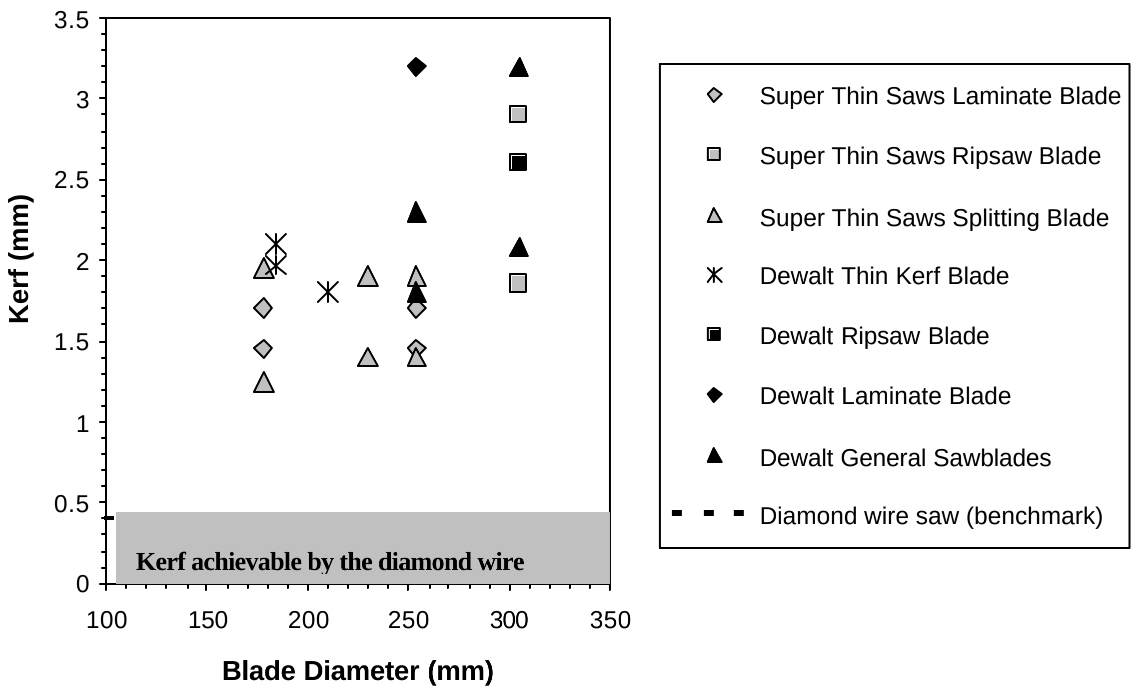

Figure 1.8: Comparison of the kerf in circular and diamond wire saw machining.

An example that was used to show the benefit of super thin circular saw blades is applied to illustrate the advantage of the diamond wire saw. As shown in Figure 1.9, the numbers of 4.5 mm wide slabs able to be cut out from a 34 mm wide wood block are:

- 5 by the regular circular saw blade with 2.87 mm kerf,
- 6 by the super thin circular saw blade with 1.40 mm kerf, and
- 7 by the diamond wire saw with 0.42 mm kerf.

Using the diamond wire saw, two extra pieces can be cut over the regular circular saw and one extra piece can be cut over the super thin circular saw. This demonstrates the advantage of the thin-kerf in diamond wire saw.

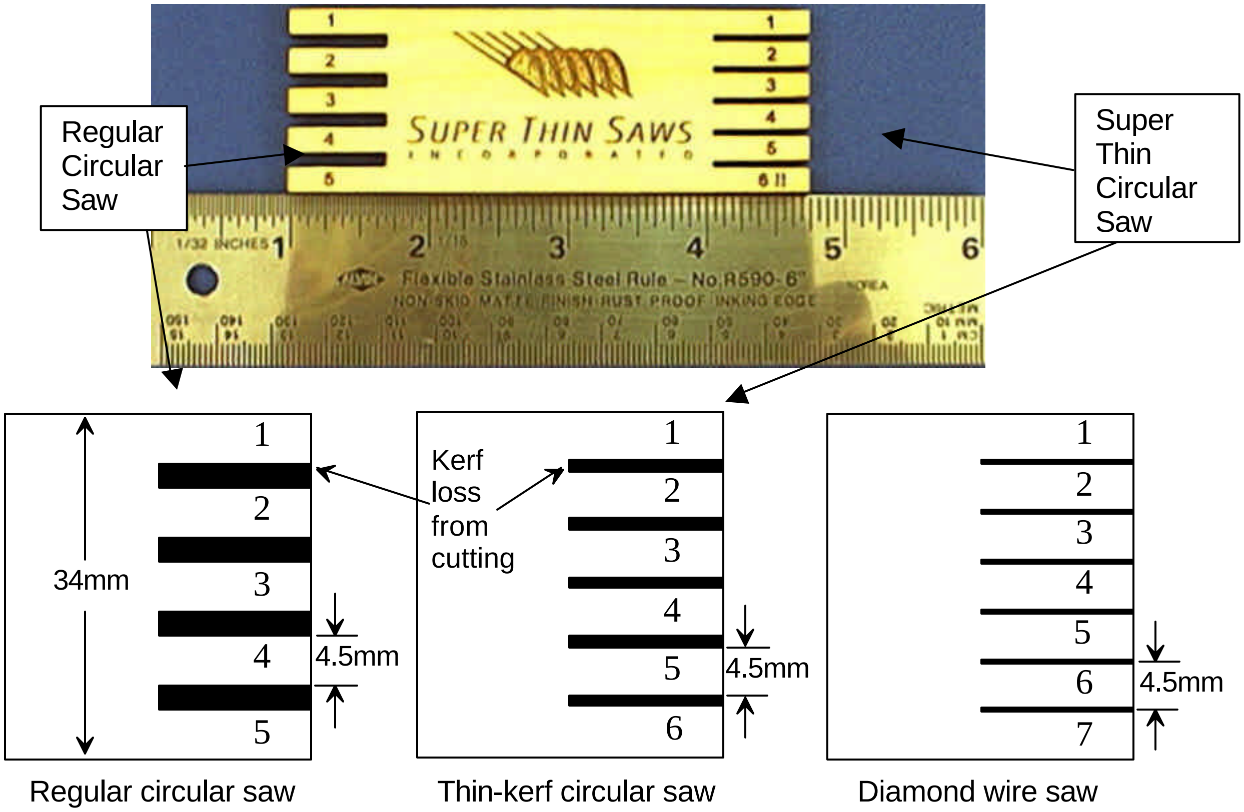

Figure 1.9: An example to compare the kerf loss in regular and thin-kerf circular saw and diamond wire saw and to illustrate the benefit of thin-kerf diamond wire saw to reduce waste.

1.3.2 Unidirectional Cutting Capability

Wood machining lacks a flexible contour cutting method. Furniture companies typically use band saws to cut a desired 2D contour out of wood products. During contour cutting, the band saw blade is twisted in order to change direction, which limits the curvature on cut parts. Diamond wire, due to its symmetry, can cut in any direction equally well. This advantage of diamond wire saw cutting was demonstrated on the test cut in Figure 1.10. Besides contouring in the X-Y directions, an additional twist of the workpiece, A-axis in Figure 1.6, can be added for another dimension of flexibility.

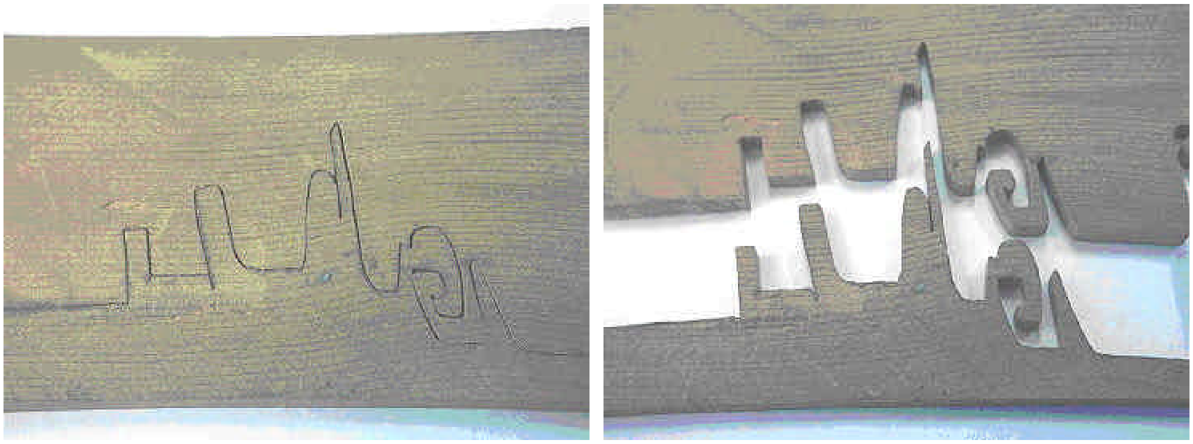

Figure 1.10: A sample machined by a 0.4 mm diameter scroll/ reciprocal diamond wire saw, (a) trace of wire saw path on a pine pencil slat, and (b) separation of two pieces after cutting.

1.3.3 Low Noise

Noise is a major problem in the furniture manufacturing plants, where machines and operators work close together in a confined space. The Occupational Safety and Health Administration (OSHA) of the US Department of Labor has strict regulations on the level of noise in the workplace. Circular saws and band saws are typically noisy machines, creating pure tone noise levels far exceeding the nominal 85 dB-A threshold. Fixed abrasive diamond wire cutting is much quieter and could help reduce the overall noise level in the plant, eliminate the cost of expensive noise reduction programs, and enhance the environment for workers.

1.3.4 Low Dust

Like noise exposure, OSHA also regulates exposure to dust. The dust generated in machining wood is known to be a fire and health hazard. Wood dust becomes a potential health problem when wood particles from processes such as sanding and cutting become airborne. Breathing the airborne μm and sub-μm size wood dust may cause allergic respiratory effects, mucosal, and nonallergic respiratory effects. The diamond has a small cutting kerf and will, therefore, generate less dust

1.4 Development of Fixed Abrasive Diamond Wire Machining

Most of the technological developments in the field of fixed abrasive diamond wire machining are relatively new. The following literature review provides an overview of both the patented wire machining technologies and the limited literary material on the subject. Following that is a description of some of the newest technical developments in wire machining.

1.4.1 Literature Review

Diamond wire saw machining is a relatively new technology. Most of these technical breakthroughs occurred in the past few years and are published as patents. The process to use diamond wire to cut brittle semiconductor materials was first developed by H. Mech [1974a, 1974b] at Motorola in the 70s. There are only 3 patents in the '70s [McLaughlin, 1977] and 2 patents in the '80s [Wells, 1985 Wells and Hatfield, 1987 on wire saw related machining technology. The number of patents exploded in the '90s [Kurokawa, 1990; Takeuchi, 1991; Toyama et al. 1993; Bonzo et al., 1996]. There are more than five patents each year since 1998 on the development of new diamond wire and wire saw machine [Hauser, 1998a; Hauser, 1998b; Toyama, 1998; Hodsden, 1998; Hauser, 1998c; Hauser, 1999; Miyoshi et al., 1999; Toyama, 1999; Hodsden, 1999; Asakawa and Oishi, 2000; Buljan and Andrews, 2000, Egglhuber, 2000; Hodsden and Hodsden, 2000; Ikehara, 2000; Katamachi, 2000; Ueoka et al., 2000, Witte and Ragan, 2000; Yu, 2000; Nagatsuka et al., 2001; Ohashi and Matsuzawa, 2001; Egglhuber, 2001; Oishi et al., 2001; Onizaki and Ogawa, 2001; Hodsden, 2001; Hodsden and Luedders, 2001; Hodsden and Hodsden, 2001].

Besides these patents, Li, Kao, and Prasad [1998] have presented a model and analysis of the contact between the abrasive and workpiece due to rolling indentation in the free-abrasive wire saw machining of a silicon wafer. Sahoo, et al. [1998] uses the finite element method to analyze the vibration modes in wire saw cutting of thin wafers. Bhagavat and Kao [1999] and Bhagavat, et al. [2000] present a model and finite element analysis of the elesto-hydrodynamic interaction in free-abrasive diamond wire machining. Ishikawa et al. [1994], Tokura, et al. [1992], and Ito and Murata [1987] include some preliminary experimental wire saw machining results. This review illustrates the lack of research on fixed-abrasive diamond wire saw machining.

1.4.2 Recent Developments

There have been several advances in recent years in the field of fixed abrasive diamond wire that make it an attractive technology for use by the wood machining industry. It is important to point out that wire saw machining of wood is not a totally new idea. There have been many unsuccessful attempts in the past to develop similar wire or band saw technologies for flexible, thin-kerf wood machining. In the past decade, several major technical developments in wire saw machining have prevailed in the semiconductor industry. These new technologies, which may be transferable to wood machining, are summarized as follows:

1.4.2.1 New Bond and Laser Treated Diamond Wire

A new method using a laser to condition the metal bond, which is electroplated on the thin wire to hold the diamond, has been invented and started production [Hodsen, 2001]. Several laser processes are applied to temper and harden the metal bond, which is used to hold the diamond grit to the wire. New metal bond materials have also been invented to strengthen the diamond grit on a thin wire. These inventions were driven by the semiconductor industry for precise, cost-effective slicing of wafers. For the woodworking industry, the new diamond wire opens a new research area. The bond on the wire has to withstand not only the force applied on the diamond grit but also the repetitive bending stress as it rolls around a roller, as shown in Figure 1.11. The bond on the diamond wire needs to have both ductility and strength. In summary, there are some recent breakthroughs in technology to make new diamond wire, which is the cornerstone for the research on diamond wire saw machining of wood.

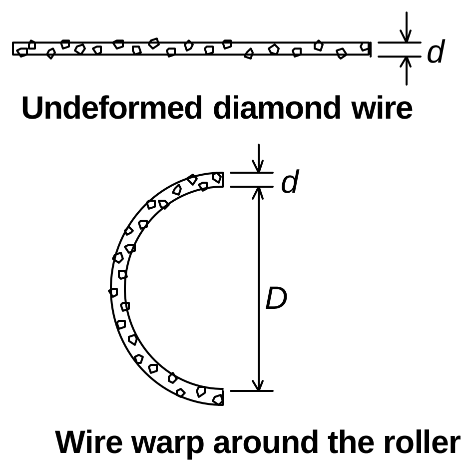

Figure 1.11: Strain created by wrapping the wire on a roller.

1.4.2.2 High Speed Wire Saw Machining

Experiments in semiconductor wire sawing demonstrate that high wire speeds can reduce the cutting force on each diamond grit, lower the wire wear and diamond pullout, and achieve higher material removal rates. The maximum wire speed on newly developed diamond wire saw machines has gradually increased from 10 m/s in 1998 to 20 m/s or higher in 2000.

1.4.2.3 Rocking Motion Wire Sawing

Figures 1.12(a) and 1.12(b) illustrate the difference between traditional and rocking motion wire saw machining. The length of contact between the wire and workpiece changes in the traditional wire saw machining, as shown by w_1 and w_2 in Figure 1.12(a). The additional rocking motion of the wire relative to the workpiece, as shown in Figure 1.12(b), can maintain a small and consistent length of contact between the wire and workpiece. In cutting silicon and silicon carbide wafers, the rocking motion wire saw has demonstrated the advantages of enhanced material removal rate, reduced wire wear, and improved quality of cut

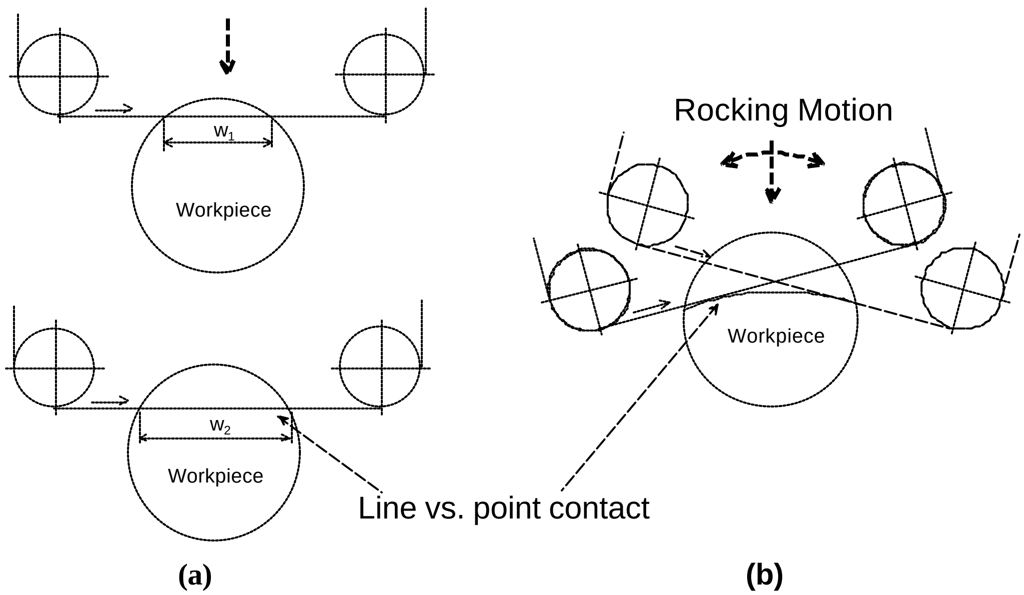

Figure 1.12. A comparison of (a) traditional and (b) rocking-motion diamond wire saw machining.

1.4.2.4 Non-Contact, In-Process Wire Deflection Sensor

A technology was developed by Laser Technology West of Colorado Springs, CO to use a capacitance sensor for real-time, in-process measurement of the deflection of the diamond wire. The electrical capacitance between the sensor and the diamond wire changes as a function of the distance between them. This principle was used for accurate measurement of the wire deflection without actual contact. The capacitance sensor is routinely used to measure to 0.1 degree-scale accuracy. If two capacitance sensors are used, the orientation of the wire in two directions can be detected. This allows for precision 2D contour cutting

1.4.2.5 Looped Wire

A new development by the Well Diamond Wire Saw, Inc. of Norcross, GA is to braze the ends of a diamond wire together, as shown in Figure 1.13, to make a looped diamond wire. Laser Technology West has patented a technology to make the looped diamond wire without using any brazing media [Hodsden and Hodsden, 2000]. These looped diamond wires can be used in a machine similar to a band saw for precise, flexible form cutting of wood.

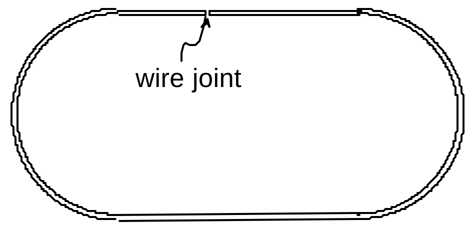

Figure 1.13: Blazing the ends of a diamond wire to make a looped wire saw.

Diamond wire saw machining, even for the semiconductor industry, is a relatively new technology. Most of these technical breakthroughs occurred in the past few years, and have not appeared in many traditional literary sources.

2 EXPERIMENT SETUP

This chapter describes how the experiment was arranged. It includes sections describing the equipment used to conduct the experiments and the materials the experiments were conducted on. There is also a section describing how the process parameters were chosen to form the testing matrixes.

2.1 Equipment Utilized

Many tools were used in this study to conduct the experiments and to analyze the results. The following sections describe the major equipment used such as the wire saw, the fixed abrasive diamond wire, components in the dynamometer system, the scanning electron microscope used, and the devices used to measure surface roughness.

2.1.1 Diamond Wire Saw

A Millennium Series rocking motion slicing fixed abrasive diamond wire saw was used in this study. This saw utilizes the spool-to-spool model of cutting, where the wire reverses direction periodically. The machine possesses the ability to conduct rocking motion cutting at three speeds (slow, medium, and fast) at up to 5 degrees of wire rock. The wire is run between two spools. The leading wire spool is connected to a motor that pulls the wire to produce the wire movement, and the trailing wire spool is connected to a motor that opposes this movement to provide wire tension. When the wire travels fully from one spool to the other, the direction of wire movement reverses, switching the function of each motor between leading and trailing functions. The wire speed is user selectable for any speed between 2.5 and 15 m/s. The wire tension supplied by the trailing motor is programmable between 13 and 50 N.

This wire saw slices be feeding the cutting wire down into the workpiece. To achieve this, the whole wire yoke structure, including both wire spools and all four wire guide pulleys, is mounted is mounted on two vertical slides. A stepping motor controls a ball screw, which drives the yoke mechanism up or down. The stepping motor possesses 240 steps per rotation, and its gearing results in 10 motor rotations for every 2.54 mm linear downfeed. The two methods of downfeed rate control are wire bow angle rate and specified linear downfeed rate. For the bow angle controlled downfeed rate, the machine can be programmed to find a downfeed rate that causes a set wire bow angle of anywhere between 0.1 and 5 degrees. The specified linear downfeed rates are user selectable between 0.0254 and 0.635 mm/s.

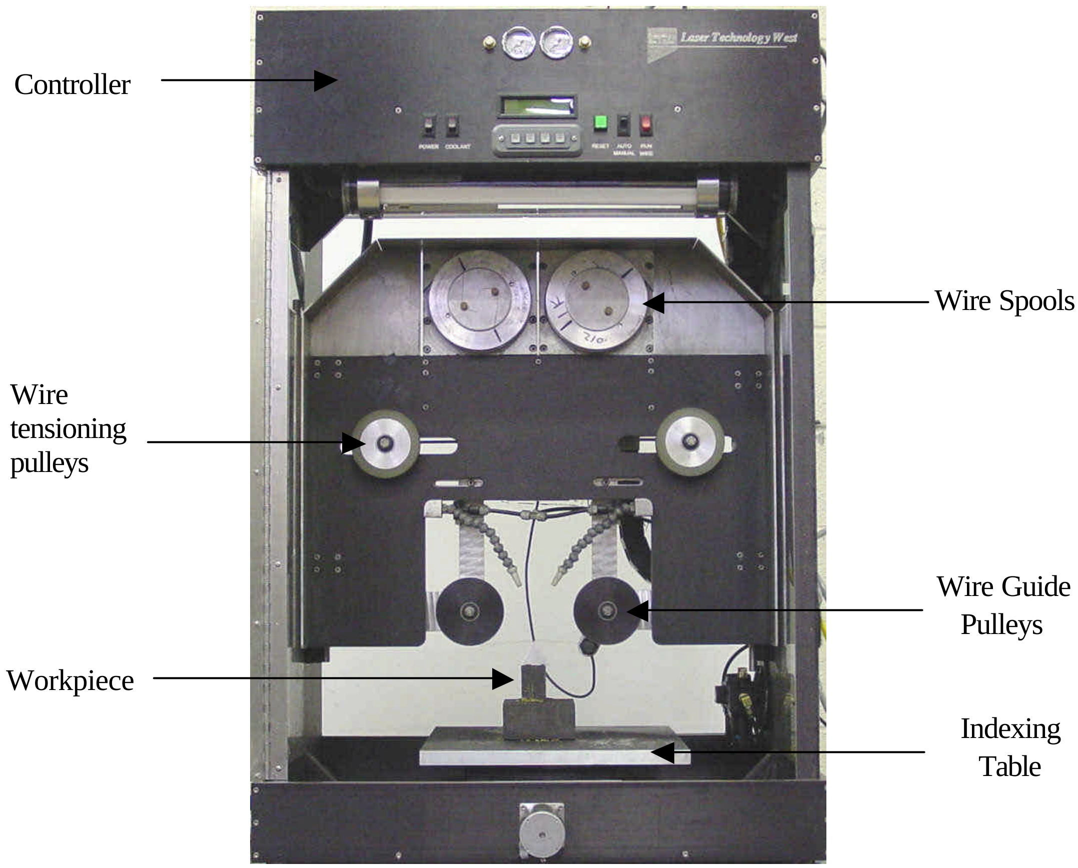

Figure 2.1: Wire saw used in this experiment.

2.1.2 Diamond Wire

Wire used in this study was all standard 0.3 mm nominal diameter wire from Laser Tech West. The specified size of the diamond particles used with this wire is 80 µm. One length of wire was used to cut each material type, and the typical wire length was 180 meters.

2.1.3 Dynamometer

A Kistler brand model 9255B 3-axis force dynamiter was used to measure the cutting forces exhibited on the work pieces during cutting. The dynamometer signals were routed through a

Kistler 3 channel charge amplifier with calibration factors of 3.93 and 7.86 pC per mechanical unit for the vertical and the two horizontal force channels, respectively. The dynamometer used is rated to record forces in the range of –20 to 20 kN and above the threshold of 0.01 N. A Kistler 1687B5 3-conductor armored cable was used to connect the dynamometer to the charge amplifier.

2.1.4 Data Acquisition

A National Instruments PC-based data acquisition system was used to record force signals from the dynamometer and three process signals from the wire saw machine's controller. These signals were collected inside a National Instruments SCB-68 terminator block. A model 184749A-02 shielded cable connected the terminator block to an AT-MIO-16E-1 model PC-based ISA data acquisition card. This card has a theoretical sampling rate of 1.25 million samples per second spread across 16 single ended channels. The card supports 8 channels if they are measured as differential signals.

2.1.5 Scanning Electron Microscope

A Hitachi S-800 scanning electron microscope was used to take SEM micrographs of selected specimens of diamond wire, cutting debris, and machined workpiece surfaces. The voltage was set to 5 kV for every image. But since the cutting debris and machined surfaces consisted primarily of nonconductive materials, the specimens required a coating layer of conductive material. A gold/platinum sputtering machine was used in these cases to coat the specimens.

2.1.6 Surface Roughness Measurement

A Talysurf 120 contact stylus surface roughness measurement machine was used to obtain values for R_a, R_P, and R_q for the machined wood surfaces. This machine uses a diamond stylus to measure the height of the workpiece surface along a profile line. Each measurement used 6 consecutive 0.8 mm cutoff lengths for a listed overall profile length of 5.7 mm.

An optical Rodenstock RM600 surface roughness measurement machine was also used to measure selected surfaces. This machine shines a beam of concentrated light at a point focused on the surface of the workpiece. The indexing table supporting the workpiece is then moved through a programmed horizontal distance. The reflection of the concentrated light beam is used to generate a dataset of workpiece surface height along the beam's path. This dataset is then used to compute various surface roughness parameters for the line segment examined.

2.2 Materials Used

Pine and Oak wood materials were chosen as the main wood materials due to their high rate of use in industry. Pine is a common soft wood used in furniture products, while oak is one of the most common hardwoods used. The industry standard "one-by" workpiece width of 19 mm was used. Examples of red oak, white pine, and Douglas fir materials from this experiment are shown in Figures 2.2(a), 2.2(b), and 2.2(c), respectively.

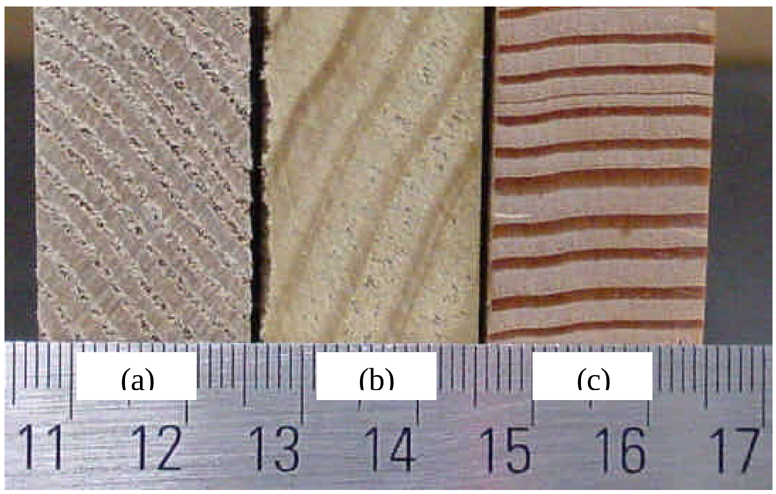

Figure 2.2: Wood workpiece materials (a) oak, (b) pine, and (c) fir.

Douglas fir was used due to its ability to form boards with nearly orthogonal grains. Virtually every readily available oak or pine workpiece will have curved and misaligned grain structures. This means that a wire saw machining the workpiece would always use a cut path through different grain types. The Douglas fir, however, contains relatively straight grains, which are orientated along the workpiece edges. The difference in workpiece grain orientation between the fir and the oak and pine materials can be seen in Figure 2.2. The light bands form the early wood grains, and the smaller dark bands form the late wood. The fir material was used to determine the effect of grain type on machining.

The three advanced ceramic foam materials also examined in the study are silica fused silicon carbide (SiC), transformation toughened zirconia (TTZ), and zirconia-toughened alumina (ZTA). These three materials are shown in Figure 2.3(a), 2.3(b), and 2.3(c). These materials are all open cell foams. For a constant wire downfeed rate, wire saw machining of foam materials results in a lower material removal rate than for continuous solid materials.

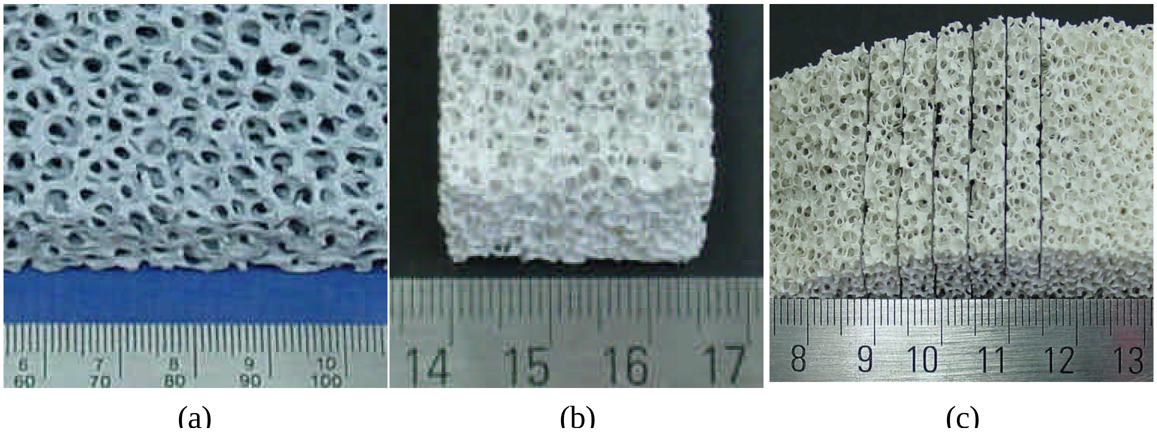

Figure 2.3: Foam ceramic workpiece materials of (a) SiC, (b) TTZ, and (c) ZTA.

2.3 Experiment Design

Initially, a feasibility test was designed to observe machining results across a long series of cuts with the same parameters. In this initial test, a set downfeed rate of 0.0508 mm/s was selected, wire speed was selected to be 4.5 m/s, and wire tension was programmed to be 18 N. Yellow pine was selected as the workpiece material. Rocking motion was used at the full amplitude (5 degrees) with the medium speed setting. Table 2.1 lists the process parameters used in the wire endurance test. The downfeed rate, wire tension, workpiece width, and cut depth are consistent with what the main wood experiments also used. The wire speed and rocking motion conditions were chosen to provide typical values.

Table 2.1. Pine endurance test parameters.

Workpiece Width	19 mm
Cut Depth	25.4 mm
Wire Diameter	0.3 mm
Diamond Size	80 μm
Downfeed Rate	0.0508 mm/s
Wire Tension	18 N
Wire Speed	4.5 m/s
Rocking Motion Conditions	5 degrees, Medium Speed (0.3 Hz)

After the initial endurance test was completed, a testing matrix was designed to examine wood machining more thoroughly. The key parameters of wire speed and rocking motion were varied through three values each for both pine and oak materials. Table 2.2 lists the machining parameters that remained constant during these tests, and Table 2.3 shows the experiment matrix.

Table 2.2. Common pine and oak experiment parameters.

Workpiece Width	19 mm
Cut Depth	25.4 mm
Wire Diameter	0.3 mm
Diamond Size	80 µm
Downfeed Rate	0.0508 mm/s
Wire Tension	18 N

Table 2.3. Pine and oak experiment matrix.

Pine and Oak Workpiece				
Wire Speed (m/s)	Rocking Motion (5 degree amplitude)			
	None	Slow (0.15 Hz)	Medium (0.3 Hz)	Fast (0.5 Hz)
4.5	x	x	x	x
6	x	x	x	x
9	x	x	x	x

Initial tests with machining the foam ceramic materials showed a potential for faster slicing. Therefore, experiments were also conducted at the yoke's highest programmable downfeed rate. Instead of conducting a full range of rocking motion experiments, the two extremes (no rocking and full fast rocking) were compared at the faster downfeed rate.

Table 2.4: Foam ceramic experiment matrix.

Foam Ceramics: SiC, ZTA, TTZ				
Rock motion		No rock		Fast rock
Down feed rate (mm/s)		0.0508	0.635	0.635
Wire speed (m/s)	4.5	x	x	x
	6	x	x	x

x: Experiment conducted

3 DATA ACQUISITION

The important parameters to be measured in this study all exist as voltages, allowing for PC-based data acquisition. This chapter describes which signals were measured by the data collection system, what hardware was used in system, the noise problems encountered in measuring the signals, and the signal processing techniques used on the recorded signals.

3.1 Measured Signals

In all, there were 5 signals measured by the data acquisition system used in this study. Of the three available force channels from the dynamometer, only the two channels measuring forces in the horizontal cut and vertical thrust directions were used. Also, three signals representing the yoke height, wire bow, and wire speed from the wire saw's controller were measured. The following sections provide a brief description of each signal.

3.1.1 Yoke Motor

The machine's yoke contains the wire drive motors, wire tension pulleys, wire guide pulleys, and the capacitance bow sensor. The entire yoke is mounted on two vertical slides, and a stepping motor and ball screw assembly control its height. The stepping motor outputs a square wave of 0-12 volts every time it rotates a step, and the saw's controller uses this signal to compute yoke height and speed.

The saw controls the cut depth by turning the step motor the number of steps required to move the yoke a set distance. The saw controls the downfeed rate by simply controlling the motor's rotational speed. Data acquisition of this signal works backwards from this by recording the number and frequency of steps and using that to calculate position and velocity.

There are 250 steps in the motor for every complete rotation, and the ball screw converts this to linear movement at a rate of 2.54 mm per revolution. This means that every motor step moves the yoke by 0.01016 mm.

3.1.2 Capacitance Sensor

Whenever a wire is used to cut, it is subjected to thrust forces that bow the wire. Knowledge of how much the wire bows is necessary to determine the actual depth of cut and is useful for approximating the magnitude of the forces generated during cutting. Figure 3.1 illustrates some of the important parameters in wire bow. The wire guide pulleys, whose nominal downfeed rate DF is controlled by the movement of the machine's yoke, push the wire as it cuts a stationary workpiece. The wire will reverse its direction periodically, so its velocity V will either be to the left or the right.

Figure 3.1 shows how a wire bow angle θ will cause the actual cut depth to differ from the nominal wire depth by an amount H. Knowledge of the discrepancy H is necessary for computing the actual cut depth and the actual cutting rate. The actual depth will just be the difference between the height H and the depth of the wire guide pulleys. The actual cutting velocity will be the sum of the nominal downfeed rate DF and the derivative of H with respect to time.

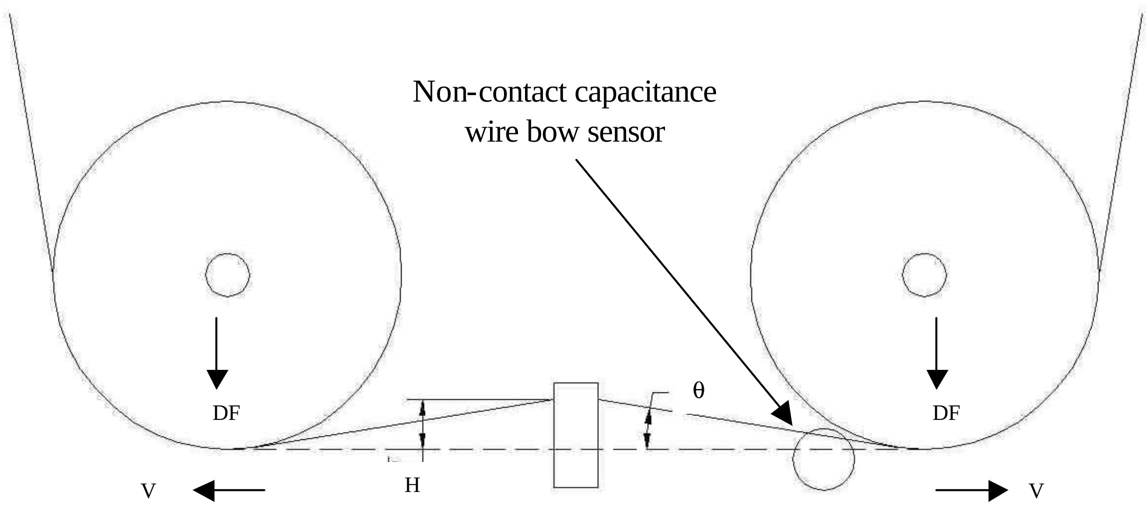

Figure 3.1: Wire bow process parameters.

The wire saw used in this study has a non-contact capacitance sensor that is used to detect the degree to which the wire becomes bowed. The sensor is positioned so that the wire passes across the top half of its circular face. When the wire is not bowed, it spans horizontal across the sensor. At this position, the sensor outputs a baseline voltage corresponding to the capacitance between the wire and the sensor face. As the wire bows upward, less of the wire passes across the sensor's face, resulting in a lower capacitance between the sensor and the wire. Since the sensor actually outputs a signal inversely proportional to capacitance, the signal magnitude actually increases with wire bow angle.

The wire saw's controller already has a function built in to calibrate the sensor's output voltage to the wire's bow angle. Factors affecting the correlation between sensor voltage and wire bow angle include: the initial horizontal wire height relative to the sensor, the distance between the wire's guide pulleys L, the wire diameter and composition, the distance between the wire and the sensor face, etc. The user can adjust the sensor's position to affect how where the wire will pass across it. The wire diameter and composition can change whenever the wire is replaced with another wire size, brand, or type. Also, as the wire wears, its diameter, composition, and electrical properties may change. Because these factors can change for every cut, the sensor output to bow angle correlation can be recalibrated as needed. The calibration procedure occurs as follows:

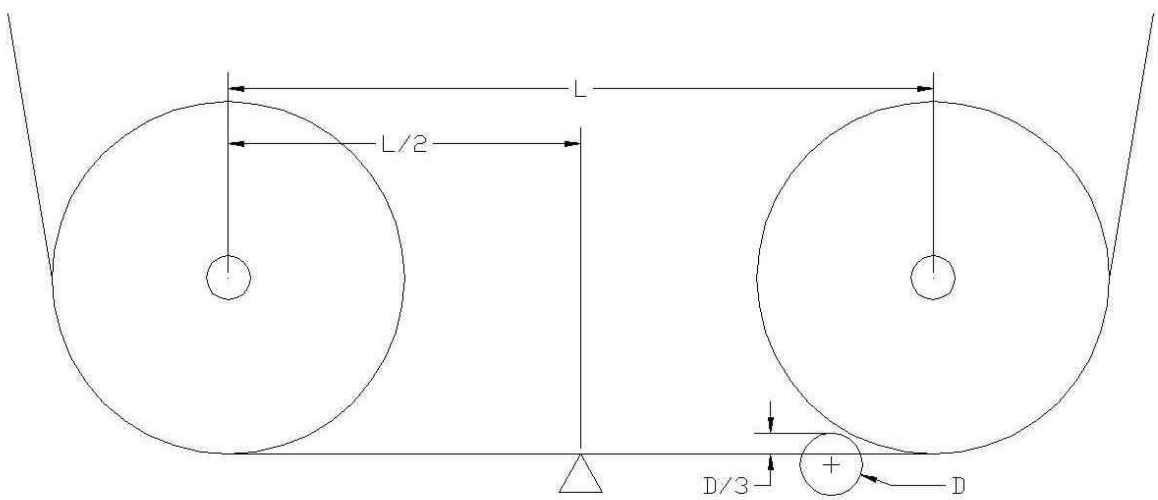

Figure 3.2: Dimensions during wire bow calibration.

1. The wire to be used is first loaded onto the saw, the capacitance sensor is positioned as desired, and the wire guide pulleys are spaced to the desired width. The saw's manufacturer suggests positioning the sensor so that the wire passes across the sensor's face at a height of approximately 2/3 of the sensor's diameter D, as shown in Figure 3.2. The wire guide pulleys need to be spaced wide enough to allow the workpiece enough room to pass between them.
2. A triangular rod is placed in the machine's cutting area as if it were a workpiece, and the machine's yoke is manually jogged down until the wire is just touching, but not bowed by, the top corner of the triangle. It is important to center the triangle tool between the two wire guide pulleys to ensure symmetric bending.

3. The user sets the machine controller to "calibrate bow sensor" mode and inputs the distance L between the guide pulleys' center points.
4. The machine feeds the yoke down until the input geometry suggests the wire should be bowed one degree. The controller pauses the yoke positioning motor for an instant and measures the sensor's output voltage.
5. The yoke is again lowered until the wire bow should be two degrees and another sensor output voltage measurement occurs. This repeated for bow angles θ of 3, 4, 5, and 6 degrees.
6. The yoke is then lifted to its starting position where there is no bow, and the calibration ends.

At the end of this calibration, the saw's controller can use the calibration data to determine the wire bow angle based on the sensor's output voltage. The manufacturer claims accuracy on the angle of 0.1 degrees.

During bow angle calibrations for this study, signals for the vertical force, capacitance sensor output voltage, and yoke positioning motor output were recorded. The recorded signals were first conditioned as described later in Section 3.4. Then the times at which the yoke positioning motor paused at known bow angles during the calibration were found. The sensor's output voltage and the dynamometer's vertical force readings were found at each of these times. These force and bow sensor voltage data points were plotted against the wire bow angle at the 7 known θ values. Appropriate curve fits were then found to determine functional relationships for bow angle and vertical force values from capacitance sensor output voltages.

It is important to note that these relationships are only useful for wire bow in the range experienced during the calibration procedure. For example, these calibration equations could not necessarily deal with wire bow angle θ of more than 6 degrees or wire bow of negative angles (bowed down).

Each bow sensor calibration depends on many variables listed earlier in this section. The cutting wire, one such factor, was changed whenever the workpiece material changed. For this reason, a new bow sensor calibration was performed every time the workpiece material was changed. All calibration equations were chosen so that the correlation factor R^2 was at least 0.99.

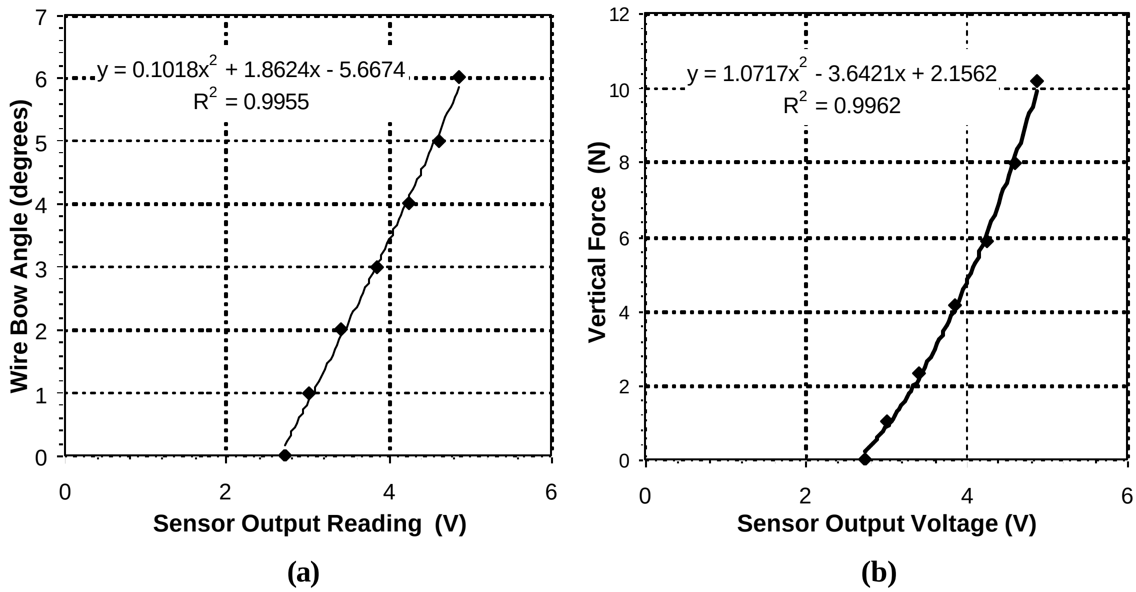

Figure 3.3: Sample calibration curves for (a) bow angle and (b) vertical thrust force from pine experiments.

Unfortunately, there are circumstances that can change how the capacitance bow sensor outputs its voltage. These circumstances must be taken into consideration if meaningful results are to be obtained. The three issues, changes in workpiece width, workpiece centering, and rocking motion are described below.

The calibration is normally performed with an aluminum triangular rod to allow the wire to bow against a point contact. During cutting, however, the wire will be bending against a workpiece of finite width. While the measured wire bow angle could be the same, the height of the cut, H, will depend on the workpiece width W. Figure 3.4 shows how there will be another height difference of δ between the actual height of cut and the height achieved during calibration for the same bow angle θ.

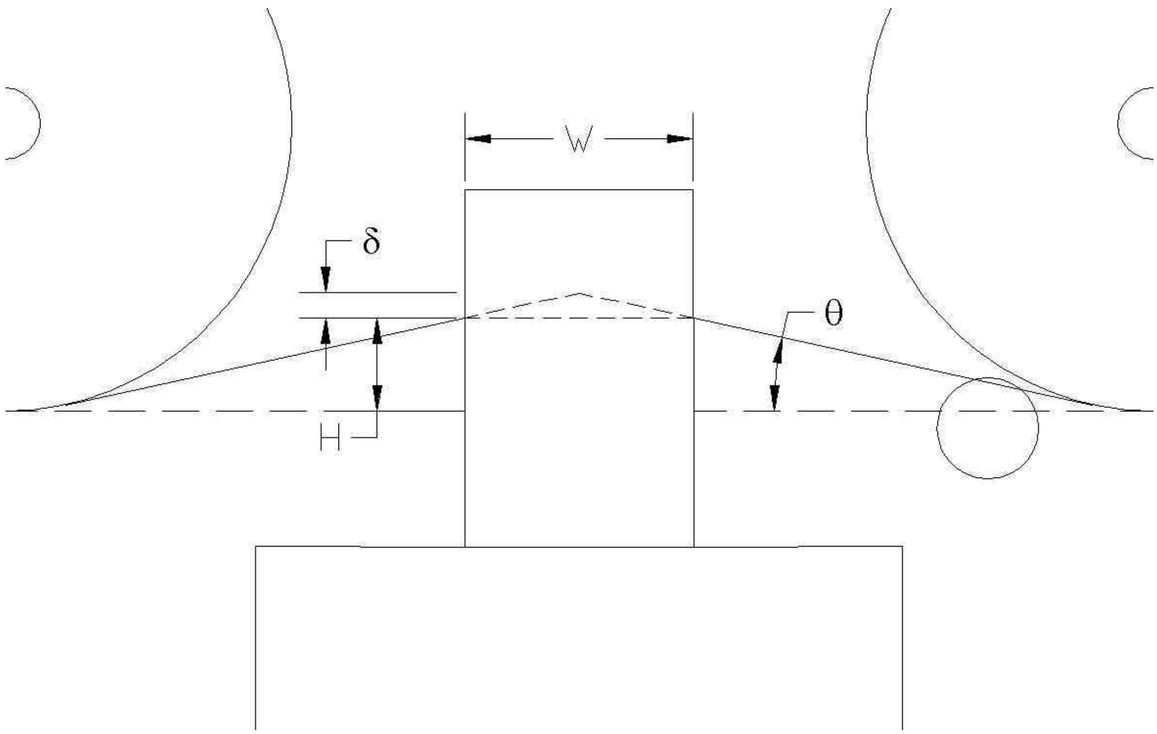

Figure 3.4: Actual depth of cut.

By the geometry listed above in Figures 3.1, 3.2, and 3.4, δ is found by:

$$\tan(q) = \frac{d}{\left(\frac{W}{2}\right)}$$

$$d = \frac{2\tan(q)}{W}$$

Similarly, the actual cut height can be found by:

$$\tan(q) = \frac{d+H}{\left(\frac{L}{2}\right)}$$

$$H = \frac{2\tan(q)}{L} - d = \frac{2\tan(q)}{L} - \frac{2\tan(q)}{W} = 2\tan q\left(\frac{1}{L} - \frac{1}{W}\right)$$

The saw only possesses one capacitance sensor to measure wire bow. If the workpiece is perfectly centered between the wire guide pulleys and the cutting is assumed to be even across the workpiece width, then symmetry implies the bow angle will be the same on either side. If the workpiece is not perfectly centered, there will be a difference between the bow angles on the left and right sides of the workpiece. However, the workpiece would have to be significantly out of center for it to adversely affect the angle measurement. If one of the wood workpieces used in this study were out of center by the entire value of its width W (19mm), then the measured angle would only differ from the workpiece-centered case measurement by 0.25 degrees. This is above the manufacturer's claim of 0.1^{o} sensor accuracy.

Rocking motion raises and lowers the wire guide pulleys to rock the wire clockwise and counterclockwise through a specified angle. Figure 3.5 shows the three main wire positions during rocking motion, rocked fully clockwise (a), rocked fully counterclockwise (b), and horizontal (c). The wire must exist as in Figure 3.5(c) each time it moves between the extreme positions of 3.5(a) and (b).

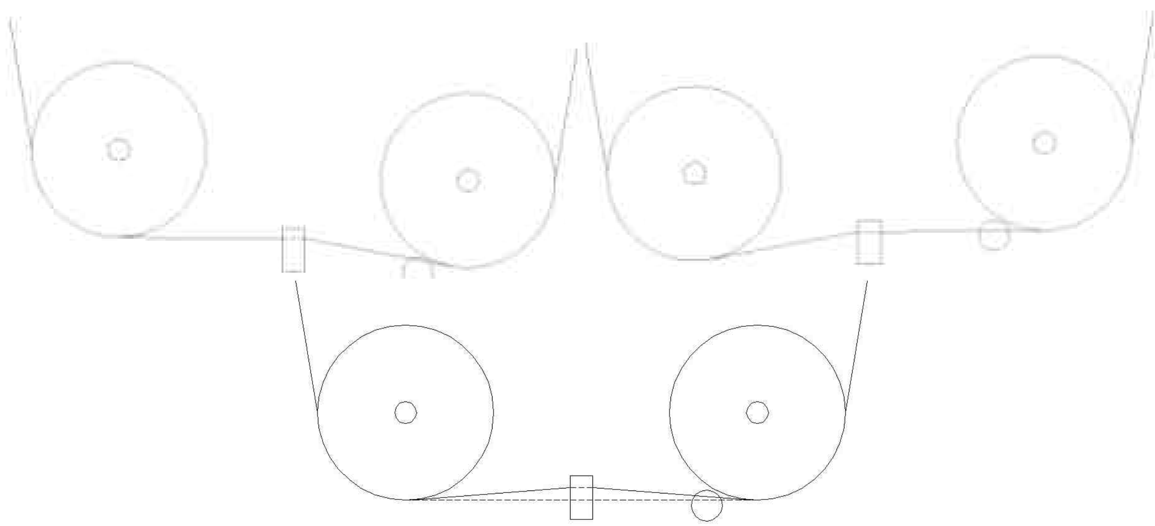

(a) (c) (b)

Figure 3.5: Rocking motion in (a) clockwise, (b) counterclockwise, and (c) horizontal positions.

The capacitance sensor is affixed to the base of the right guide pulley; and is therefore raised and lowered by the same amount. When the wire is rocked clockwise by an angle α, the length of wire passing in front of the sensor face shortens. Let the angle recorded by the bow sensor be the angle ψ. At the clockwise rocking position, this angle ψ will be the same as α if there is no bow, and it will be $\alpha + \theta$ if there is already wire bow present. If this total angle ψ is more than 6 degrees, then the signal moves outside the range the sensor was calibrated to measure.

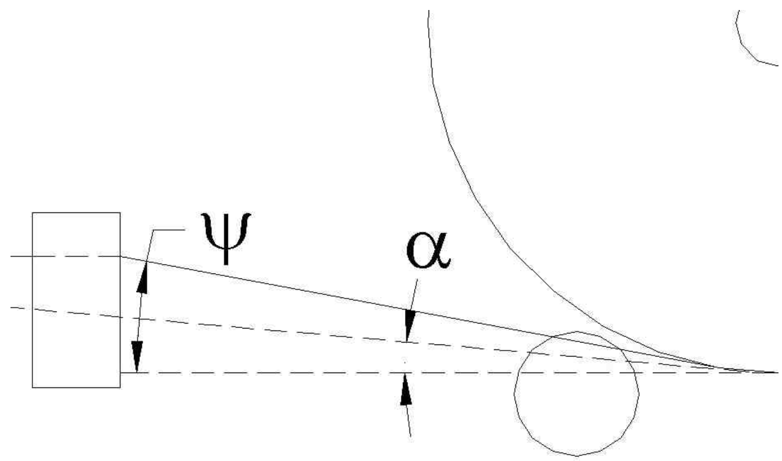

Figure 3.6: Wire angles at clockwise rocking position.

Similarly, when the wire is then rocked counterclockwise by an angle α, the wire lowers relative to the sensor face. For the small angles this rocking motion operates under, this has the effect of lengthening the amount of wire passing in front of the sensor. This will increase the wire-sensor capacitance and lower the sensor output voltage and the subsequent value of ψ. If the nominal wire bow angle θ is larger than the rock angle α, ψ will still be within the calibrated range. But if α is larger than θ (if the wire rocks past horizontal), ψ passes out of the calibrated voltage range. This is shown in Figure 3.7 where the wire rocks just past the horizontal to produce a negative angle.

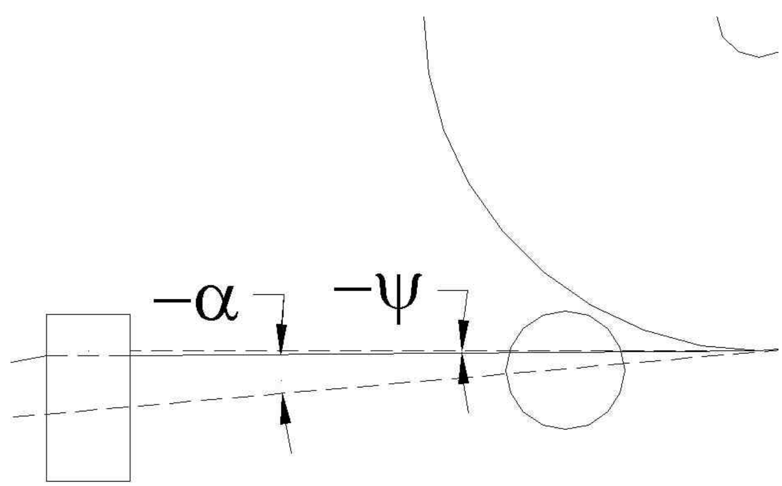

Figure 3.7: Negative angles at counterclockwise rocking position.

Rocking motion affects the capacitance sensor's output signal by inducing a sinusoidal curve whose peaks and troughs fall above and below the nominal output voltage. The crest of the wave represents the angle of α plus θ from clockwise rotation, and the trough occurs when the wire is rotated fully counterclockwise. Rocking motion positions that produce a crest and a trough are shown in Figure 3.5(a) and (b), respectively. The mean value between peak and trough represents the nominal wire bow angle θ that occurs each time the wire guide pulleys become horizontal to each other. This nominal wire bow position is shown in Figure 3.5(c). The sinusoidal signal and the technique to account for it is described later in section 3.5.

3.1.3 Wire Speed

The two wire spools that collect and dispense the wire as it moves are mounted on the shafts of motors. These two motors provide both the wire velocity and the wire tension. The leading motor collecting wire will rotate at a set speed to achieve the programmed wire speed, and the trailing motor will resist the lead motor to provide the programmed amount of wire tension. One of the motors outputs an analog voltage proportional to its rotational speed, and the saw's controller uses this to approximate the wire's axial speed.

The base diameter of the wire spools is 100 mm. First assume that the wire is wrapped at the base wire diameter. For the range of programmable wire speeds of 2.5 to 15 m/s, the corresponding motor rotational speeds of 8 to 47.75 revolutions per second.

Next, assume that a long wire is threaded in the machine so that most of the wire is on one source spool moving to the other destination spool at a motor speed of the full 47.75 revolutions per second. The diameter of the wire on the destination spool is still just 100 mm because it is empty, but the diameter of the wire on the source spool is 108 mm because the wire wraps on top of itself. The wire will move at the speed of the driving (destination) motor. At the beginning of the wire transfer, the linear wire speed is the programmed 15 m/s. But near the end of the wire transfer as the destination spool is filled with wire, the linear wire speed increases to over 16 m/s. The motor rotational speed remains the same, but since the wire diameter increases by 8%, the wire speed will also.

This shows that, since the controller only fixes the motor rotational speed, the wire speed selected for a cut program is only approximate. This was not a problem for this investigation since precise control of wire speed was not required, but it may be important in future experiments.

3.1.4 Horizontal Cutting Force

The horizontal force channel measured in this study uses a piezoelectric transducer to measure along the direction of wire movement. As each individual diamond particle plows through the workpiece material, it will produce a net force that can be broken up into two components: the cutting force and the thrust force. The cutting force lies in the direction of diamond particle movement. So, if the wire cuts flat across, one horizontal dynamometer channel can record this parameter. The algebraic sign of the force will change when the wire changes direction, but the mechanics of cutting should be the same for each direction.

While cutting with rocking motion, the cutting force may no longer be aligned with this dynamometer channel at all times. This will be discussed later in section 4.3.

3.1.5 Vertical Thrust Force

The vertical force channel measured in this study uses another piezoelectric transducer in the dynamometer. The thrust force generated by each diamond particle acts normal to its cutting force and into the workpiece. For this grinding wheel, all the thrust forces are in the same direction and simply add up to form the overall thrust force. The diamond wire is round, however, so particles will interact with the workpiece over a range of angles. The net sum of the individual thrust forces will still point in the direction of wire downfeed because the angled components of the thrust forces cancel themselves out. This should hold true as long as wire feed proceeds in only the vertical direction.

During a cut, the vertical thrust force measured by the dynamometer should always point in the direction of wire downfeed rate. In a cut program with a constant feed rate, constant wire speed, and isotropic workpiece material properties, the vertical thrust force should not change much with respect to time.

3.2 Hardware Setup

An overall sketch of the data collection system is shown in Figure 3.8. Each signal was routed to a National Instruments AT-MIO-16E-1 data acquisition card to allow for computer recordings of each signal during cutting experiments.

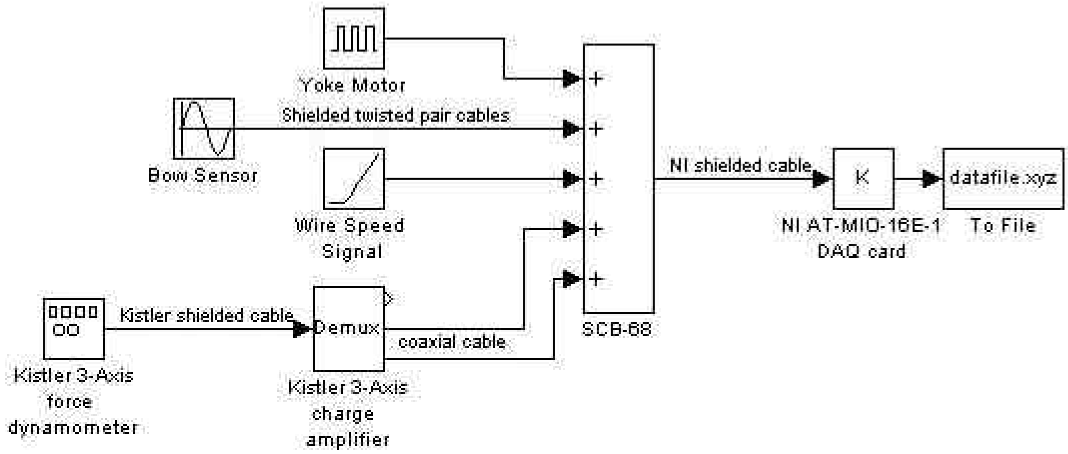

Figure 3.8: Sketch of data collection system used.

A 4 pair shielded twisted-pair cable was used to carry the three signals recorded from the saw's controller. Each of these three signals were connected in differential mode, so each used a pair of wires to carry the signal and the signal's ground to the terminator block. The bow sensor and wire speed signals used the saw controller's ground pin out as their ground. The yoke motor signal used a pair of 100-kΩ resistors between its signal and ground as a voltage divider. The wire pair for each signal was connected to the NI SCB-68 terminator block so that their difference was recorded as the desired signal. The fourth wire pair in the cable was used to connect the terminator block ground circuit to the wire saw aluminum chassis.

The three force channels of the dynamometer were connected to the charge amplifier through a 3-channel shielded cable. Coaxial cables were connected between the charge amplifier and the terminator block for the two force channels of interest. The main wire carried the signal voltage, and the cable shielding was subtracted in the terminator block as the ground to obtain the measured signal. Another shielded cable connected the computer chassis ground to the force channel ground in the terminator block.

From the terminator block, the five signals were routed through a NI shielded cable to the National Instruments data acquisition card. Each signal was recorded as a buffered dataset by the LabVIEW application Controlink developed by Controlink Systems, LLC. The force channels were recorded at a sampling rate of 4096 samples per second, and the signals from the saw were recorded at a rate of 256 samples per second.

3.3 Dynamometer

Any force measurement system will undergo a deformation due to the measured force. In many cases, the deformation is the measurement of the force. Piezoelectric force transducers undergo a deformation, but it is usually small enough to be ignored

The piezoelectric effect is when a crystal outputs a charge due to a change in load. A 3-axis force dynamometer has piezoelectric crystals oriented to carry loads in three orthogonal directions. A change in the force acting on one of the piezoelectric quartz crystals in a dynamometer causes it to output a charge proportional to the magnitude of the force. If the force acting on the crystal does not change, the crystal will not produce an electrical output.

This dynamometer is connected to a charge amplifier, which converts the charge signal to a useful voltage. The charge amplifier used in this study was a high-gain inverting voltage amplifier that used a MOSFET to achieve high input impedance. The voltage signal output by the charge amplifier is linearly proportional to the force values exerted on the corresponding dynamometer channel (Kistler, 2001).

There are two adverse effects of piezoelectric force dynamometer systems: decay and drift.

Decay occurs when the AC circuit in the charge amplifier discharges over time. If a force is held constant, the dynamometer system output will eventually decay down to zero. Charge amplifiers have a selectable setting to control the time constant of the decay (short, medium, long). For short and medium time constants, the discharge is almost immediate. But the long discharge time constant is provided to allow for quasistatic force measurement. The signal will still discharge, but it will be at a slow rate.

Drift is when the output signal changes value independent of the measured force or signal decay. Many reasons including current leak through the charge amplifier's MOSFET and contamination on the high impedance cable connections exist to cause drift. Drift and decay affect every dynamometer force reading. But for short measurements and measurements where the force changes often, they can often be accounted for.

If a measured force were to change its direction periodically, then the decay effect would have to reset every time the signal changed its algebraic sign. The signal simply would not have enough time to decay noticeably before it changed again. Drift might still occur in the measurement, but a linear approximation can be used to account for this. Drift and decay do become problematic when the signal does not change very much over time. If a force were always acting in the same direction with similar magnitudes, then signal decay would decrease the signal strength to at or near zero. Drift could exist here also. But even if drift were accounted for, the signal would still read at or near zero.

3.4 Signal Noise

Initial measurements showed that all signals being measured contained high levels of noise. Figure 3.9 shows a sample recording of all 5 measured signals.

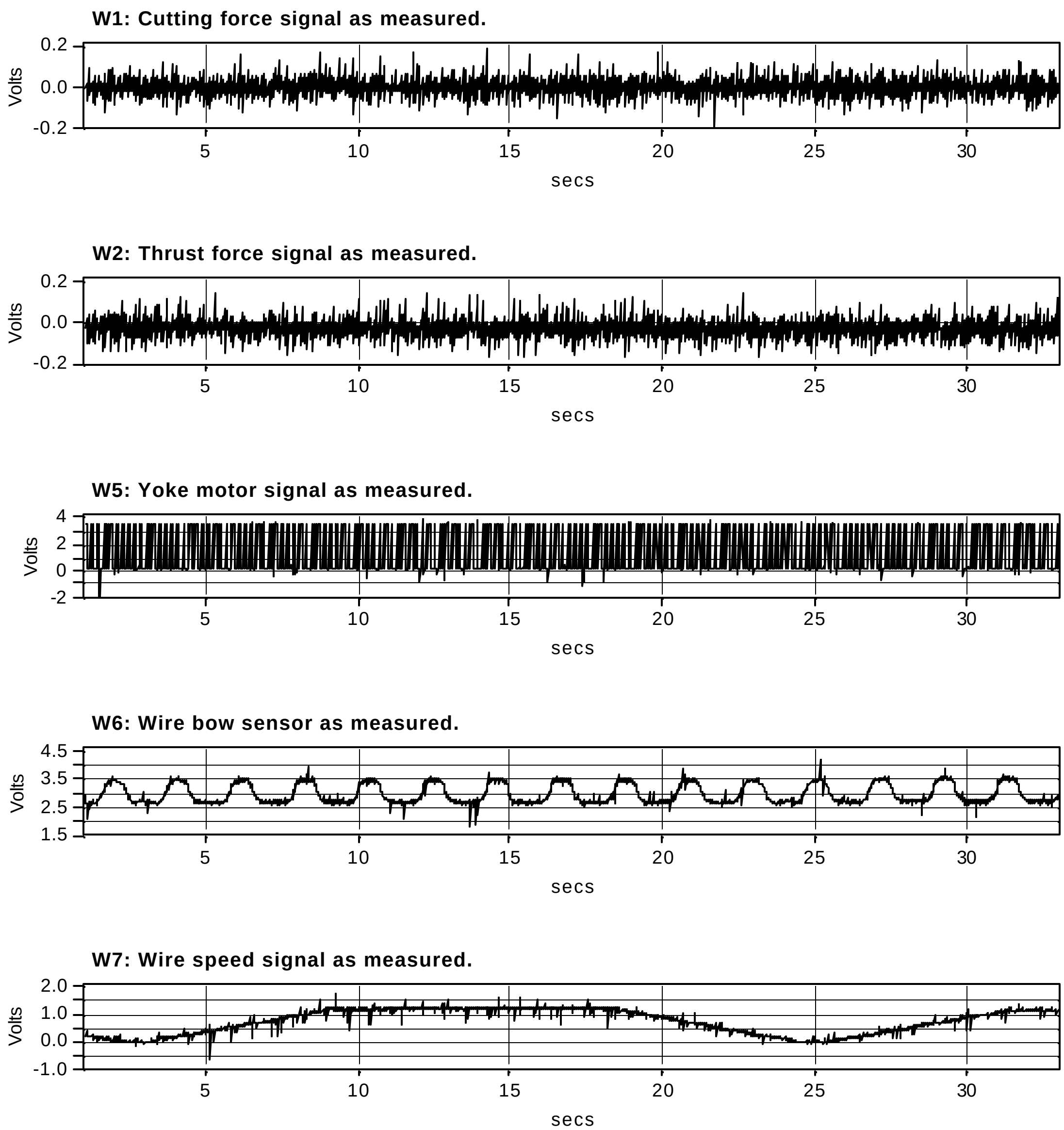

Figure 3.9: Recorded signals with noise.

The level of noise present in each signal is at least 0.1 V. This makes almost no difference to the yoke motor signal since it's amplitude is 3.5 V. This does make a large difference to the force signals, which occur at much smaller voltages than the noise. In fact, the force readings are completely useless as recorded.

Initially, it was theorized that vibration caused by the wire saw during operation was creating inertial forces on the dynamometer's top plate. However, these same levels of noise were found in force recordings taken while the wire saw was at rest.

Electromagnetic interference was not initially considered since every component in the data acquisition system was thoroughly shielded from external interference. Also, spectral analysis of the noisy signals did not contain any dominant frequency peak. An example of the noise spectrum of a zero force recording is shown in Figure 3.10. The common electrical interference frequency of 60 Hz does not even have a noticeable peak. This file was recorded while the dynamometer was not touching any moving objects.

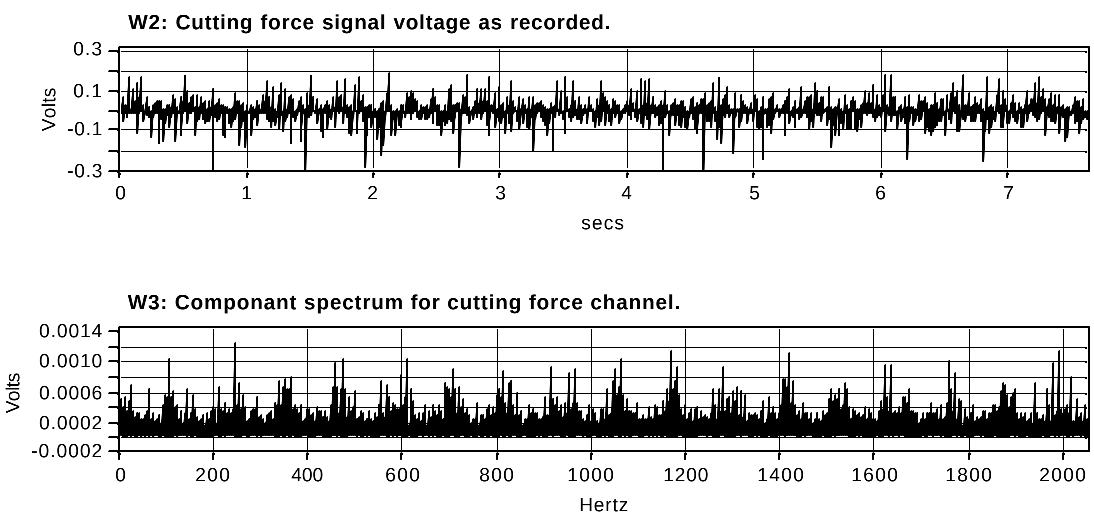

Figure 3.10: Frequency analysis of noise present in a recording of zero force.

Eventually, it was found that the noise in the force channels was caused by the three signals from the wire saw controller. When all five signals were wired into the same NI SCB-69 terminator block, the noise in the force channels appeared as in Figures 3.9 and 3.10. However, when those three wire saw channels were physically disconnected from the terminator block, the noise in the force channels reduced by almost two orders of magnitude. In Figure 3.11, the horizontal cutting force channel is measured while the wire saw is at rest (zero force). Initially, all channels are physically connected to the terminator block. But at a local file time of about 2 seconds, the three signals from the wire saw were disconnected. After this time, the noise in the force channel almost disappears.

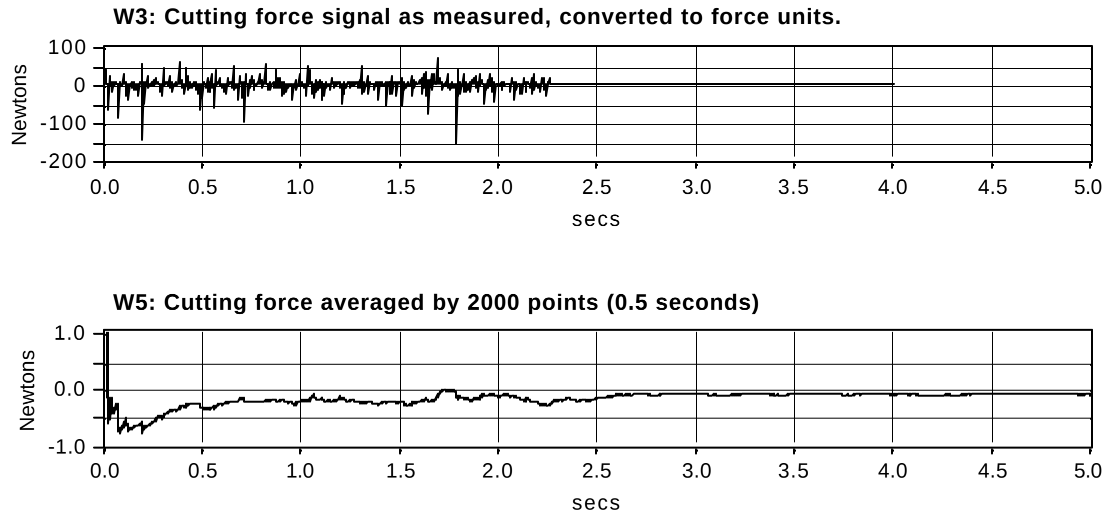

Figure 3.11: Effect on force channel noise of disconnecting signals from wire saw controller.

Several methods were tried to reduce this cross talk noise. Grounding wires were run from both the computer chassis and the wire saw chassis for each signal, but little change was noticed. Readings were taken with only one or two wire saw signals wired in. This had no effect. The use of a second terminator block and data acquisition card to separate force and saw signal measurements was considered, but the difficulty of synchronizing data collection from two different systems prevented that.

Eventually, signal processing consisting of over sampling and localized averaging was selected. This allowed the noise removal to be conducted after the cutting experiments were completed. A description of this process is located in the following section.

3.5 Signal Processing

All of the signals recorded during these experiments required processing before they could be used. First, the noise described in Section 3.4 was accounted for. But even after this was done, each signal required some sort of conversion between the voltages recorded and a useful physical quantity. The following sections describe the work performed on each of the 5 measured signals to obtain the processed data.

3.5.1 Horizontal Cutting Force Signal

As discussed in Section 3.4, the data acquisition channels recording the two force signals were the most affected by the noise. As recorded, the level of noise in the signal was so high that the signal was unreadable. Cutting force data was predicted to exist somewhere on the order of 0-10 N, but the noise in the force signal often exceeded 100 N. For the force readings to be of any use, a method of processing the signal to reduce the effects of the noise to an acceptable level had to be developed.

Several unsuccessful attempts to reduce noise through signal grounding and filtration were attempted as described in Section 3.4.3. Because these methods did not work, the signal was simply sampled at a much faster rate than what was desired. Over-sampling like this allowed the use of localized averaging to remove the noise. Localized averaging is when each recorded data point is averaged with a specified number of data points recorded just before and after it. For example, if a signal was captured at a frequency of 4096 Hz and localized averaging of 2048 points was performed, then each recorded point would be averaged with the 1024 points recorded just before and just after it. In this case, each point would be affected by measurements taken across ½ second (1/4 second before and ¼ second after).

The benefit of localized averaging is that it can remove random noise and expose the centerline signal originally masked by the noise. One drawback to localized averaging is the decreased time resolution of the signal. In the above example, although the signal is originally measured at a frequency of 4096 Hz, the final frequency of completely independent readings is only 2 Hz. Localized averaging can also fall victim to non-random noise. Statistically, if a larger amount of noise exists above the actual signal value than below it, then localized averaging will result in too high a value.

Figure 3.12 shows a force measurement subjected to localized averaging of different rates. Clearly visible at local times of 2.5 and 24.5 seconds are two wire reversals. At these times, the wire slows down, stops, changes direction, and starts back up again. This process causes the wire to undergo a complete sign change, yet these two events are unrecognizable in the data as recorded.

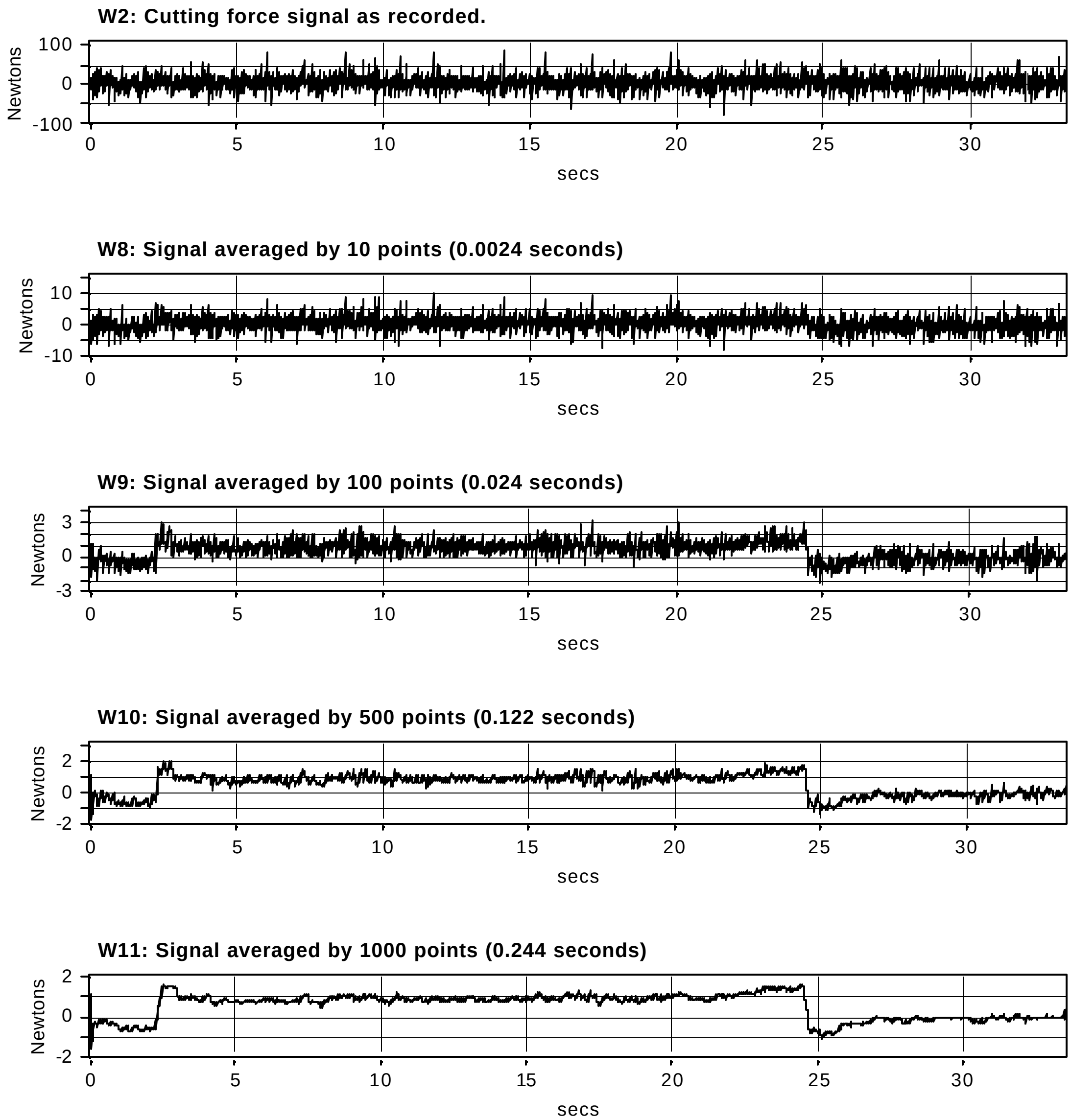

Figure 3.12: Cutting force record before and after different rates of localized averaging.

The four steps used to process this signal are described below.

1. The force signals come out of the charge amplifier as a voltage. The first step is to use a linear calibration factor to convert these signals to units of force. During static calibrations, the calibration factor was found to be 444 N/Volt for both force channels used in this experiment. The signal used in Figure 3.12 was already converted to Newtons to highlight the magnitude of the noise. The first graph in Figure 3.13 shows the signal as the DAQ card measured it. The second graph in Figure 3.13 shows the signal after it was converted from a voltage to a force reading in Newtons.
2. Next, localized averaging was applied to reduce the amplitude of signal noise. An averaging width of 1000 points was selected to ensure the force signal was readable.

This averaging rate allowed for a time resolution of ¼ second in the final signal. The third graph in Figure 3.13 shows the signal after localized averaging was performed.

3. The last force sampling file for a cut was examined, and the point where wire-workpiece contact ends was identified. Force levels are zero when the wire and workpiece do not touch, so any force reading there was due to dynamometer signal drift. The force values at this point and the total time since the cut's beginning were recorded.
4. Linear offsets for signal drift were developed and applied for any force reading of interest. For any force reading, the slope of the line was found from step 3 and the starting offset was found by multiplying the slope with the start time of the recording. For example, if the offset slope from step 3 was found to be 0.005 N/s for a cut, and the force reading of interest began 120 seconds into the cut program, then the offset equation becomes:

$$f(x) = 120s * 0.005N/s + 0.005N/s * t$$
$$f(x) = 0.6 + 0.005t$$

In this equation, t is the time in seconds for this particular recording. These offset equations can then be added to the force dataset to account for the signal drift. An example drift correction line is shown plotted alongside the averaged force reading in the third graph of Figure 3.13. The two curves in that graph were added together to obtain the curve found in the fourth graph.

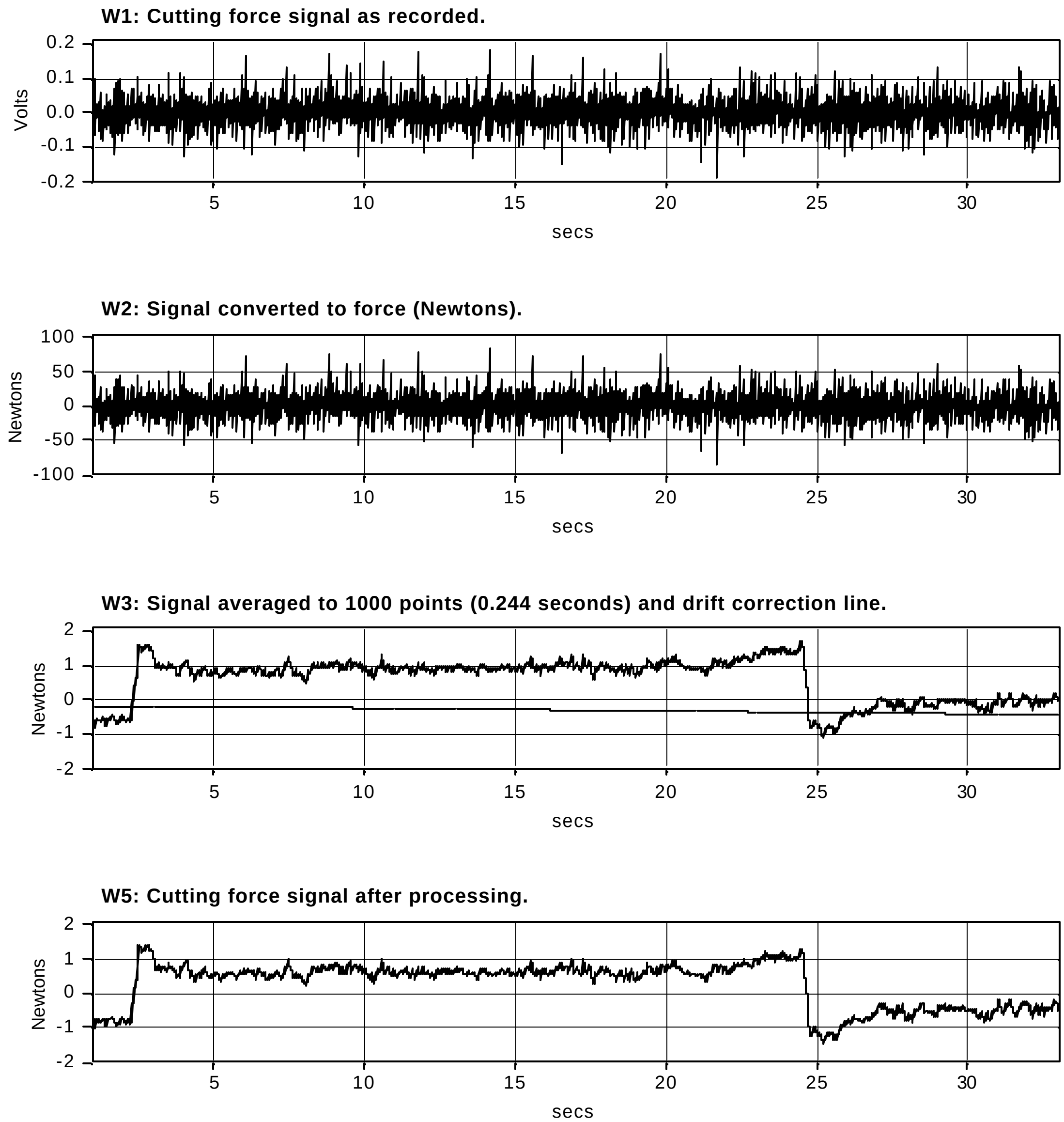

Figure 3.13: Cutting force signal processing.

Also, any redundant data points can be removed by decimating the force dataset. The high frequency rate of the original recordings produce too many data points for the results to be loaded into many popular spreadsheet analysis programs. For example, Excel 2000 allows a maximum of 32,000 data points for each column. The force readings were sampled at a rate of 4096 data points every second, so Excel could only load about 8 seconds of this data. But if the processed signal was decimated by a ratio of 100:1, then any of the force recordings from this study could be loaded into Excel.

3.5.2 Vertical Thrust Force Signal

The steps to process the thrust force signal are essentially the same as those described for the cutting force signal. The signal was recorded as a voltage and then converted to force units. Localized averaging at a rate of 1000 points was performed. Drift correction lines were found and applied.

But after the signals were processed, the data was found to be of no good. The values for the thrust force would remain relatively similar throughout a cut. Since the values were always negative, the signal had plenty of time to decay in the charge amplifier. The charge amplifier's long time constant was used, but that could not keep the force readings from decaying over the length of each cut.

Since dynamometer measured thrust force readings did not achieve usable results, another method for obtaining vertical thrust force values was used. This method is described in the bow sensor processing procedure in Section 3.5.4.

3.5.3 Yoke Motor Signal

As recorded by the software, this signal was a series of square waves with 3.2-volt amplitude. Each square wave represents the yoke positioning motor turning through one step. There are 250 motor steps for each rotation, and each motor rotation moves the saw's yoke 2.54 mm vertically. Therefore, each square wave pulse represents a change in the yoke's vertical position by 0.01016 mm. This signal is identical regardless of whether the motor is indexing the yoke up or down.

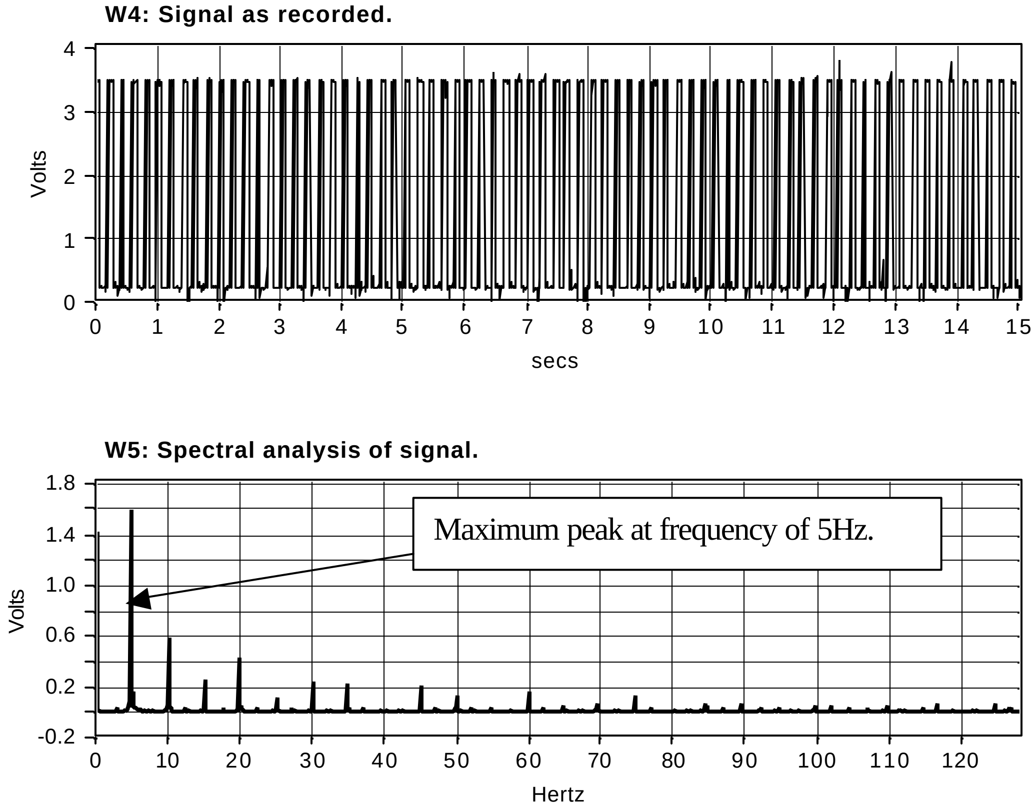

Figure 3.14: Yoke motor signal processing.

The yoke motor output signal can provide two possible outputs. The first output is a yoke position indicator. Counting the number of pulses and multiplying by the vertical displacement per pulse can provide the magnitude of the yoke's vertical displacement over the range examined. This was used in this study to determine the yoke depth at specific times in the fir cutting experiments.

The second output is a yoke velocity indicator. The frequency of the occurrence of the output pulses can be found. This frequency can then be converted to a vertical velocity by multiplying by the conversion factor of 0.01016 mm/pulse. In this study, the frequency of the yoke motor output signal was found by using the spectrum analysis command in the software package DADiSP. This function displays the relative magnitude of each frequency present in the source signal. The maximum non-zero peak represents the frequency of the motor output pulses. Figure 3.14 shows a sample yoke motor output series and the resulting spectrum analysis. The pulse frequency of 5 Hz represents the linear velocity of 0.0508 mm/s used in several of the cuts in this study.

Knowledge of the yoke velocity proved useful in many circumstances, despite the fact that all cutting experiments were conducted with a specified, constant downfeed rate. For example, during the calibration sequence for the saw's capacitance bow sensor, the yoke motor output signal was used to determine exactly when the yoke downfeed paused. Each 0.2-second pause occurred when the wire had bowed to a specified angle. Once the time of each pause was known, corresponding capacitance sensor output voltages and vertical force dynamometer readings could be found and compared.

The yoke motor output signal was also used to locate the times in a data file when a cut program started, when a programmed cut depth was reached, and when the dwell period ended.

3.5.4 Wire Bow Signal

The signal from the capacitance bow sensor is an analog voltage corresponding to the inverse of the capacitance between the sensor and the wire segment in front of it. The baseline signal value occurs when the wire is stretched horizontally with no bow. The signal increases in magnitude when positive wire deflection occurs. This is when the wire is deflected up, causing less wire to be near the sensor face. The signal will also decrease when more wire length passes in front of the sensor face. As described in Section 3.1.2, the initial height of the wire relative to the sensor face can vary, so the baseline voltage corresponding to no wire bow can also change. It is for this reason that the bow sensor was calibrated for every wire segment used. For normal wire bow of less than 6 degrees, the signal magnitude ranged between 2.5 and 5 V. The magnitude of noise in this signal usually stayed within 0.5 V, as described in Section 3.4. An example of a bow sensor signal as it was recorded is shown in the first graph of Figure 3.15.

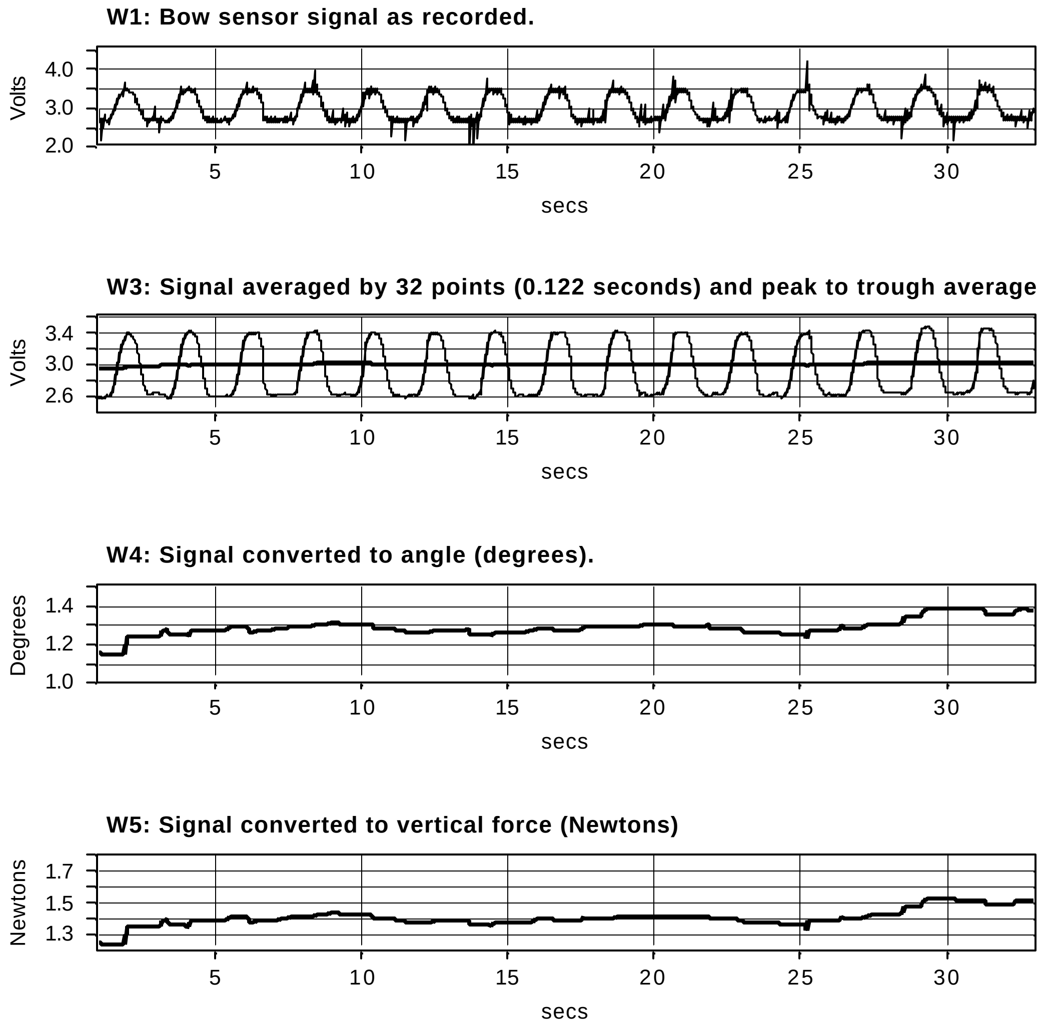

Figure 3.15: Capacitance bow sensor signal through processing.

The general signal steps used to process this signal are described below:

1. Remove the 0.5 V signal noise through localized averaging. The sampling rate used for this signal was 256 Hz, and the time-value response of +-1/16 seconds. The second graph in Figure 3.15 shows the results of localized averaging on the signal.
2. If rocking motion was present, its effects have to be accounted for. The sinusoidal response from the sensor caused by rocking motion does not correspond to actual wire bow. It is instead a result of relative motion between the two wire guide pulleys, which shortens and lengthens the section of wire passing in front of the sensor face. A clockwise rocking motion increases the signal magnitude while a counterclockwise motion lowers the signal magnitude. The average peak to trough signal value represents the sensor output when the two wire guide pulleys are positioned perfectly horizontal to each other. Therefore, to account for rocking motion, a linear curve is fit to the sinusoid's cyclic average. This line tracks the sensor value when the guide pulleys are

aligned horizontally. The second graph in Figure 3.15 also shows the signal's peak to trough average line.

3. The next step in the wire bow signal processing is to use the bow calibration data to convert the sensor voltage into a wire bow angle. As described in section 3.1.2, each bow calibration resulted in a polynomial equation capable of converting between sensor output voltage and wire bow angle θ in degrees. If the cut used rocking motion, the peak to trough line was input into this polynomial equation to obtain the wire bow angle. If rocking motion was not used, then the signal after localized averaging was input into the equation instead. At this point, the value for the wire bow angle can be read from the chart as shown in the third graph in Figure 3.15.
4. An additional step was performed on the capacitance sensor output signal in this study to find the vertical thrust force. During the bow calibration sequence, an additional equation that relates sensor output voltage to the vertical force measured with the dynamometer was found. This equation was also polynomial in nature and could be applied the same way as the angle equation in step 3. The output from this equation is the vertical reaction force in Newtons. The fourth graph in Figure 3.15 shows the results of this step.

3.5.5 Wire Speed Signal

As mentioned earlier in Section 3.1.3, the wire drive motors that spool and unspool the wire output a linear voltage that can be used to approximate the wire's axial velocity. This voltage is linearly related to the wire spool rotational speed. If a constant wire spooling diameter is assumed, then the signal linearly relates to wire axial velocity. The output voltage is zero while the motors are stationary, and it is 3 volts when the motors rotate at their maximum programmable speed. The signal is a scalar quantity indicating speed and is positive regardless of wire direction. An example of the signal is shown in Figure 3.16. Two wire reversals can be identified at times of 3 and 25 seconds into the file. Also, the slope of the wire speed while accelerating and decelerating can be seen as recognized as linear.

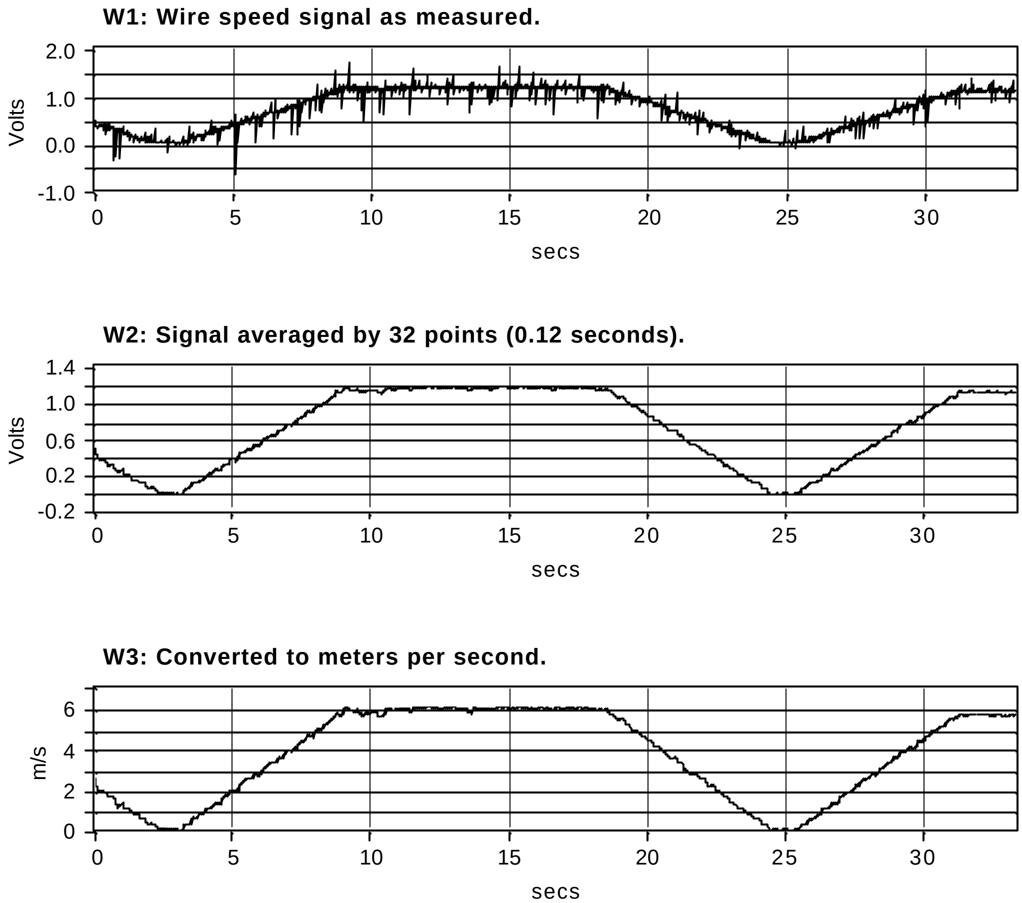

Figure 3.16: Wire speed signal through processing.

The general steps used to process this signal are described below:

1. Just as in the other signals, there is a significant amount of noise present in this signal as recorded. The first step in processing this signal is to perform localized averaging to remove the effects of the noise. As before, use of localized averaging assumes that the noise is random or evenly distributed above and below the level of the signal. This signal was collected at the same 256 Hz collection frequency used for the yoke motor and bow sensor signals. The width of the localized averaging used was the same 1/16-second (+-16 points) as for the bow sensor signal. This averaging rate was selected because it reduced the noise to acceptable levels. The first and second graphs in Figure 3.16 show a wire speed signal as recorded and after localized averaging was performed.
2. The next step in processing this signal is to apply the correct linear calibration factor to relate the measured signal voltage to linear axial wire speed. The use of a linear calibration factor is only an approximation, but is still useful in this case. The factor used to convert voltage to meters per second in this study was 5.08. The selection of this factor was described in section 3.1.3. The third graph in Figure 3.16 shows the wire speed signal after being converted to meters per second.

Once these steps were carried out, the signal could be used to verify that the machine used the specified wire velocity. The signal could also be used to identify the times when the wire was stopped to reverse direction. Also, the wire speed record could be used to determine the acceleration rate of the wire drive motors. With the acceleration values, the relationship between the time between wire reversals and wire speed can be found. For example, if a wire speed of 12 m/s were desired and full wire speed was wanted for at least 80% of the total cut time, then the motor acceleration rate could be used to find the minimum acceptable wire length.

4 FORCES

One of the major goals of this study is to gain knowledge of the forces generated during fixed abrasive diamond wire machining. In the following section, the overall cut program and the force measurement schedule are described. Then in section 4.2, the results of the force measurements are presented for each material type. Finally, section 4.3 describes some of the kinematics involved in wire saw machining.

4.1 Force Measurement

To understand how the forces were measured, it is important to first know the overall structure of a wire saw cut. While many machine parameters can change for each cut, the overall cut process described below remains very similar.

A cut program is first designed and programmed into the machine controller. Factors such as depth of cut, number of cuts, wire speed, rocking motion speed and magnitude, yoke downfeed rate, length of post cut dwell time, and wire tension are input here. The last option from the controller is to begin the program.

The wire spool motors initiate wire velocity as the yoke positioning motor begins moving the yoke down. Also, any programmed rocking motion begins to occur. The wire travels back and forth between the spools, pausing only to change direction. As the wire plunges into the workpiece, there is a transition period where forces and wire bow gradually increase.

Once the initial transition period ends, the cut reaches a steady state cutting period. In this period, wire reversals, rocking motion, and yoke downfeed are essentially constant. This steady state cutting phase continues until the yoke feeds down to the programmed cut depth.

When the yoke reaches the programmed cut depth, the machine enters what the manufacturer calls the dwell stage. At this point, the yoke stops moving and any rocking motion ceases, but the wire continues to run at the same speed. This allows the wire to continue cutting to flatten any left over workpiece surface arc. Also, the wire can cut through any left over bow-induced cut depth discrepancy H, as described in section 3.1.4. The machine continues in the dwell stage until the programmed dwell time is finished and the wire bow drops below 1 degree.

Once the programmed dwell time ends and the measured wire bow angle drops below 1 degree, the yoke positioning motor begins to rise, reversing the wire back out of the cut. The wire is still run at its programmed cutting speed here allowing it to cut through any debris or binder present in the cut. This continues until the yoke is returned to its starting height.

If multiple cuts are included in the program, the machine table indexes to the next position to begin the next cut. If there is only one cut in the program, the wire is wound onto one spool and then stopped. At this point, the program is finished, and the machine is at rest.

Due to the noise present in the signals, which was described in section 3.4, data signals were sampled at rates much higher than would normally be desired. For example, the desired sampling frequency for the cutting force is only a few points per second. However, the noise present in the signal resulted in the signal processing procedure described in section 3.5. This processing required a sampling rate of over 4 kHz. For some of the ceramic cutting experiments, where the entire cut lasted less than a minute, the force readings could be collected continuously for the entire program. But each one-inch deep wood cutting program lasted over 500 seconds. If force readings were collected continuously throughout an entire cut program, there would be more than 2 million data points for each force channel.

To simplify data storage, signals were recorded in shorter 20-30 second intervals at various times throughout the cut program. These short recordings, or snapshots, can be started at set times to record specific events, such as the start of the cut or the end of the cut. If the recording of specific events is performed consistently across different cuts, then they can be used to compare the results of different cutting parameters.

The measurement schedule for each cut was very similar. There were usually four types of measurements made.

1. The first snapshot recorded the cut program start. The charge amplifier was reset to zero at the beginning of this recording so that force levels start at zero. This recording shows the start of the cut program as wire speed, yoke velocity, and rocking motion begin.
2. Each cut program has a recording that shows the end of wire downfeed and the beginning of the dwell period. At this end point, any rocking motion stops, but the wire continues to move as it does during cutting.
3. The programmed amount of dwell time is known, but as stated above, there may be additional dwell time added to reduce wire bow. For this reason, a reading was started at a known time a few seconds before the programmed dwell period ended. This recording was continued until the yoke raised enough that there was no contact between the wire and workpiece. Since there is no wire-workpiece contact at the recording's end, the forces would be zero by definition. Knowledge of this force reading's magnitude and the time relative to the cut's beginning is used as in section 3.5.1 to calculate the dynamometer drift rate.
4. Additional snapshots were captured at various times throughout the steady state cutting period. These recordings show the consistency of the rocking motion, yoke downfeed motor output, and wire velocity during the bulk of the cutting program.

4.2 Force Results

There were essentially four experiment designs used in this study, as described in Section 2.3. The first was a wire endurance test where pine was cut repeatedly to determine the feasibility of using fixed abrasive diamond wire to machine wood. The second was the main cutting experiments for the pine and oak material that tested variations in wire speed and rocking motion. Douglas fir was another wood material sliced in the third experiment to determine the effect of wood grain type. The last experiment dealt with the slicing of ceramic foam materials. The following Sections contain the force results from these experiments and an introduction to wire saw cutting mechanics.

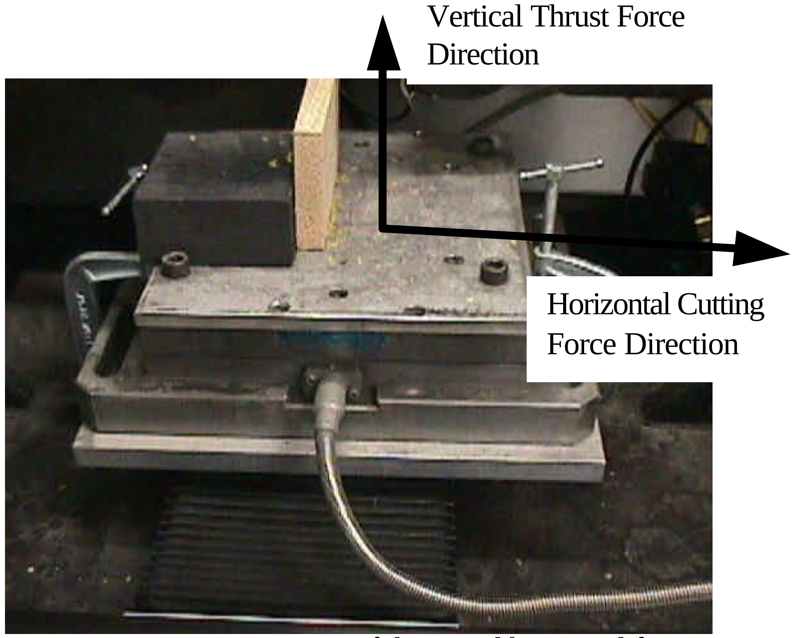

Figure 4.1: Directions of thrust and horizontal forces.

Force results are presented for both the horizontal cutting direction and the vertical thrust direction. Ratios of these two forces are also presented. The directions of the vertical thrust force F_T and the horizontal cutting force F_C are along the directions of wire downfeed DF and wire velocity V as shown in Figure 4.1.

4.2.1 Endurance Test Force Results

The initial wire endurance test was conducted to determine whether the fixed abrasive diamond wire could last long enough to complete the later slicing experiments. A series of 16 identical slices were made through a wood material, and the results from each successive slice were compared. Pine was used as the workpiece, and the parameters used in each slice are listed in Table 2.1.

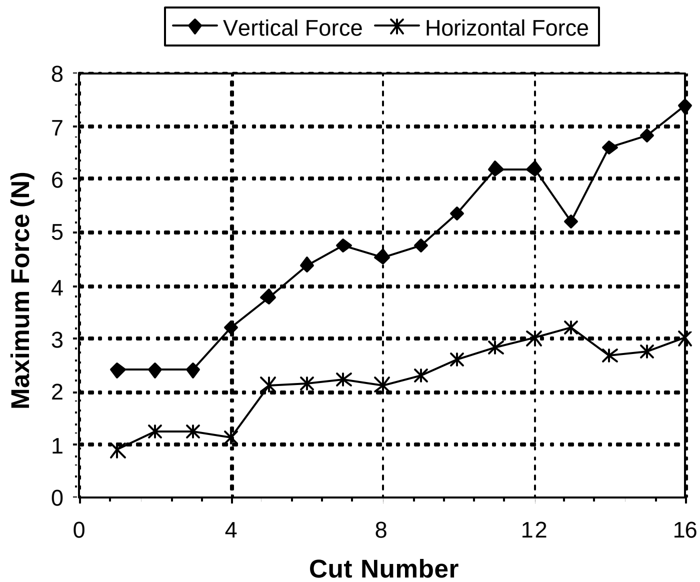

Figure 4.2: Wire endurance test force results.

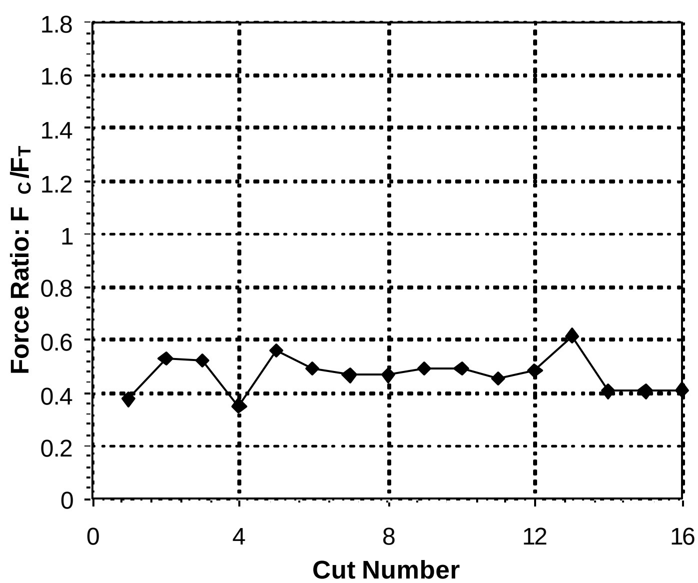

Figure 4.3: Wire endurance test force ratios.

The results for the maximum vertical and horizontal forces, F_T and F_C are shown in Figure 4.2. The first few cuts had very similar force results, but overall, the force values increased with successive cuts. The values for the vertical thrust force F_T were always higher than the horizontal F_C values. Also of interest is the ratio of the horizontal to vertical forces, F_C / F_T as shown in Figure 4.3. This shows that even as the force levels increased, the ratio of the forces remained between 0.4 and 0.6 for the cuts.

4.2.2 Pine and Oak Force Results

The primary wood cutting experiments used oak and pine as the workpiece as wire speed and rocking motion conditions were used as variables. In all, 12 slicing tests were performed for each of the two materials. The process parameters used for these tests are listed in Tables 2.2 and 2.3. The maximum horizontal cutting force F_C values were recorded with the dynamometer system and processed with the methods described in Section 3.5.1. The vertical thrust force F_T signal was obtained from the amount of wire bow. Relations between the amount of wire bow and the magnitude of vertical forces measured during wire bow calibrations were obtained and used as described in Section 3.1.2.

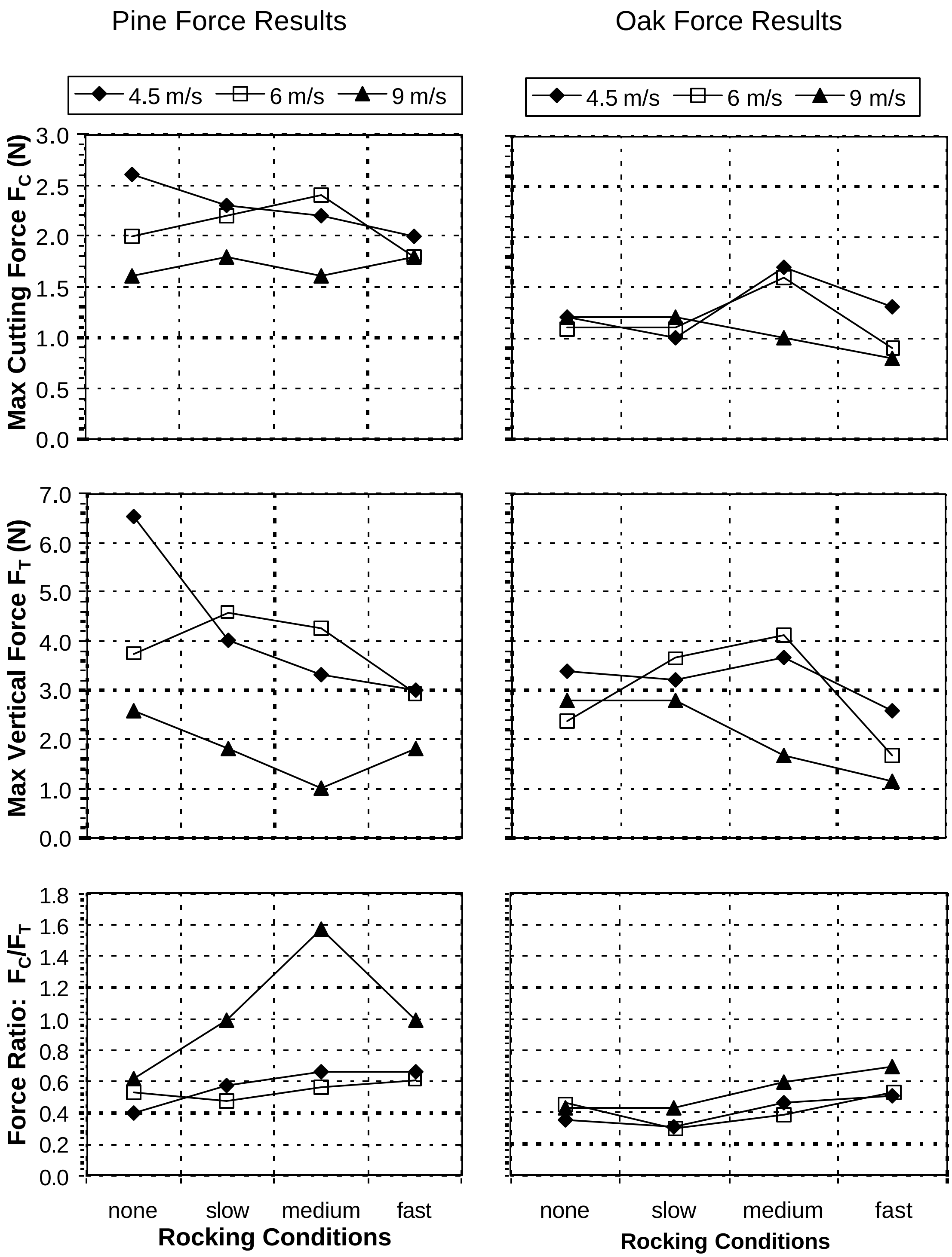

Figure 4.4: Force results from pine and oak cutting experiments.

Figure 4.4 shows the force results from the pine and oak cutting experiments. The maximum cutting force F_C values for pine showed that the highest wire speed resulted in the lowest forces. This also held true for the maximum thrust force F_T values for pine. The difference between the two slower wire speeds is not immediately recognizable. Rocking motion did not produce any discernable trends in the values of F_C for pine. But there is a noticeable drop in the F_T values for pine between the extreme cases of no rocking motion and fast rocking motion.

In the oak cutting experiments, the fastest wire speed usually resulted in the lowest force readings. However, there was one cut where the 6 m/s wire speed case resulted in lower values for F_C and F_T, and there was one cut where the 4.5 m/s wire speed case resulted in a lower F_C value. The effects of rocking motion on the maximum cutting force F_C is not clear from the graph. There was a drop in the maximum thrust force F_T between the two extreme rocking motion conditions.

For the two slower wire speeds in the pine cutting experiments, the force ratio shown in Figure 4.4 remains between 0.4 and 0.6. The force ratios for all the oak cutting experiments are also within a similar 0.4 to 0.7 range. The force ratios obtained from the 9 m/s wire speed cuts of pine ended up significantly higher. The reasons for this are not clear.

4.2.3 Fir Force Results

Douglas Fir was used due to its relatively straight grain structure. This allows the wire to pass cut only earlywood or only latewood at a given time. A cut program was used without rocking motion to ensure that the wire remained parallel with grain boundaries. Force recordings were taken at times when the wire cut from one grain type to the other. Figure 4.5 shows an example of the earlywood and latewood grain types.

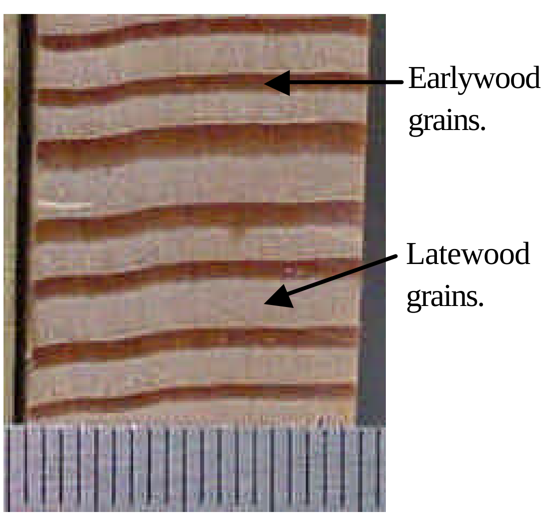

Figure 4.5: Douglas Fir grain examples.

There was no noticeable change in the horizontal cutting force F_C due to grain type. There was a small noticeable change in wire bow and the vertical thrust force F_T when the cut moved from one grain to another. The wire bow angle was consistently measured at values between 1.2 and 1.3 degrees when the wire was cutting earlywood. The wire bow angle rapidly dropped down to 0.75 degrees, however, when the cut moved into latewood. When the cut passed back into earlywood, the wire bow gradually increased back to 1.2 or 1.3 degrees.

4.2.4 Ceramic Force Results

Initially, the ceramic foam materials were machined at the same downfeed fate DF of 0.0508 mm/s that was used for the wood materials. Cutting at this downfeed rate did not result in any noticeable amounts of force data or wire bow. Since the ceramic materials are open celled foams, the material removal rate for a given downfeed rate will be much lower than for a continuous workpiece material like wood.

To examine the forces generated in cutting the foam ceramic materials, the downfeed rate was increased to the machine's maximum downfeed rate of 0.635 mm/s. Two wire speeds and the two extreme rocking motion conditions were compared at this downfeed rate. The complete list of process parameters is contained in Table 2.4. Table 4.1 lists the maximum values for the cutting force F_C and the thrust force F_T for the different ceramic foam cutting experiments.

Table 4.1: Force values for foam ceramic cutting experiments.

		SiC		TTZ		ZTA	
Wire Speed	Parameter	No Rock	Fast, 5^o Rock	No Rock	Fast, 5^o Rock	No Rock	Fast, 5^o Rock
4.5 m/s	F_C (N)	*	0.1	1.50	1.50	2.50	3.00
	F_T (N)	2.23	2.23	4.26	4.29	5.86	6.06
	Ratio (F_C / F_T)	0	0.04	0.35	0.33	0.43	0.50
6 m/s	F_C (N)	0.1	0.1	1.30	1.10	2.50	2.75
	F_T (N)	2.23	2.23	3.96	4.11	5.19	5.86
	Ratio (F_C / F_T)	0.04	0.04	0.33	0.27	0.48	0.47

*: Force level was too small to measure.

The SiC material produced very small horizontal cutting force values. For the 4.5 m/s wire speed test with no rocking, this value was too small to show up in the force recordings. For the other three cutting tests on SiC, the maximum horizontal cutting force values were only 0.1 N. The maximum F_T value obtained for each of the SiC cutting tests was the same at 2.2 N. The force ratios were all very small due to the values obtained for the cutting force F_C.

The TTZ foam ceramic material produced higher values for both F_C and F_T than those produced by the SiC. At the 4.5 m/s wire speed tests, the use of rocking motion did not have any affect on the maximum F_C value. At 6 m/s wire speed, however, the use of rocking motion reduced the maximum F_C value from 1.3 to 1.1 N. The use of rocking motion did not affect the maximum F_T values much. For both wire speeds, the maximum F_T value did increase some with rocking motion use, but this increase was small. The force ratio remained between 0.27 and 0.35 for each of these four of the TTZ cutting experiments listed above.

The ZTA foam material produced maximum force readings higher than either of the other two ceramic materials. The maximum F_C values increased for both wire speeds when rocking motion was added, the increase was 50% less with the faster wire speed. The maximum F_T values also increased when rocking motion was used. The force ratios stayed within the range of 0.43 to 0.5 for all four ZTA cutting tests listed above.

4.3 Kinematics

The fixed abrasive wire saw machining process is complex due to its use of easily deformable wire. In order to explain the development of equations to describe the relationship between process parameters, the system can be built up with increasing levels of complexity. This is attempted the following paragraphs.

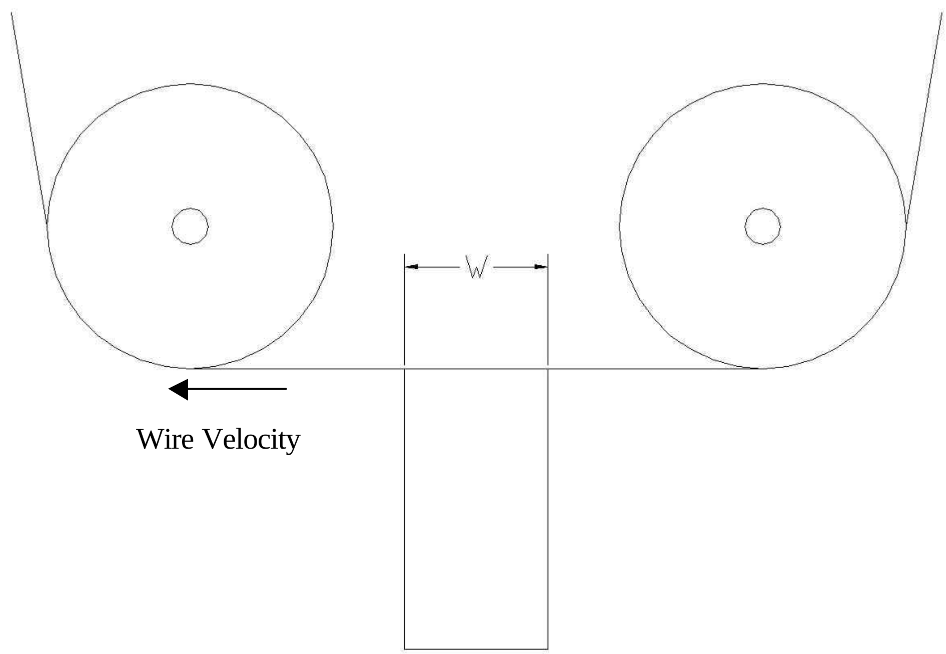

Figure 4.6: Rigid wire ideal wire cutting with no rocking motion.

First, examine the ideal cutting scenario in Figure 4.6 where the wire is rigid and there is no rocking motion. Since the wire is rigid, and therefore unable to deflect, the tangent of the wire defines the cutting surface on the workpiece. For these conditions, the cut profile on the workpiece is simply a horizontal straight line at nominal wire depth. This depth is at the level of the base of the wire guide pulleys. The length of wire-workpiece contact is simply the width of the workpiece at that depth. If the workpiece width changes, so will the contact length.

If the wire is considered a rigid body, then the distributed vertical force (thrust force) from the workpiece is countered by opposing forces from the guide pulleys. This is shown in the free body diagram of a section of wire in figure 4.7. The horizontal force (cutting force) F_C acting on the wire by the workpiece is countered by the difference between wire tensions on either side of the workpiece. In this configuration, the cutting and thrust forces align with the X and Z horizontal and vertical axes. Note that in this case, there is no direct relationship between the thrust forces and the wire tension.

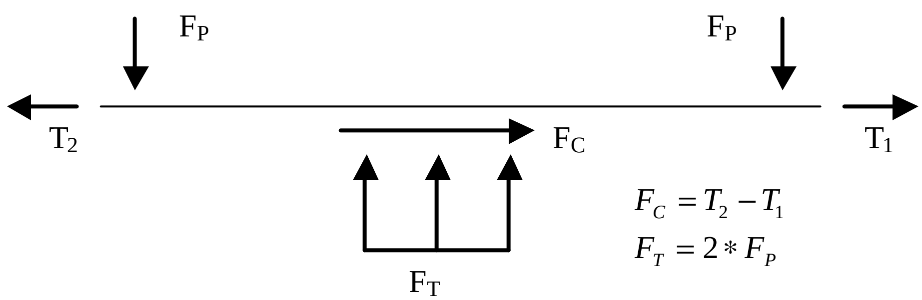

$$F_C = T_2 - T_1$$
$$F_T = 2 * F_P$$

Figure 4.7: Free body diagram of wire section shown in Figure 4.6.

The free body diagram in Figure 4.7 demonstrates that the horizontal cutting force generated by wire saw cutting is related to the change in tension of the wire as it contacts the workpiece. The leading wire will always have a higher tension than the trailing wire.

The direction of the cutting force F_C changes when the wire reverses and changes the direction of its movement. Since the leading side of the wire has a higher tension, the side with the leading edge will also change. Figure 4.6 shows the wire moving to the left, and the free body diagram force equations are based on this. If the wire were instead moving to the right, the only difference would be sign change.

If you add rocking motion to the above case, but keep the wire rigid, the cut wire path and cut profile both change. Again, since there is no wire deflection, the wire tangent will again define the shape of the cut profile. Since the rocking motion rotates the wire between positive and negative angles θ, as shown in Figure 4.8, the workpiece cut profile will be bounded by tangents of θ on either side. The entire profile would be a circular arc of angle 2θ and radius $W/(2\sin\theta)$.

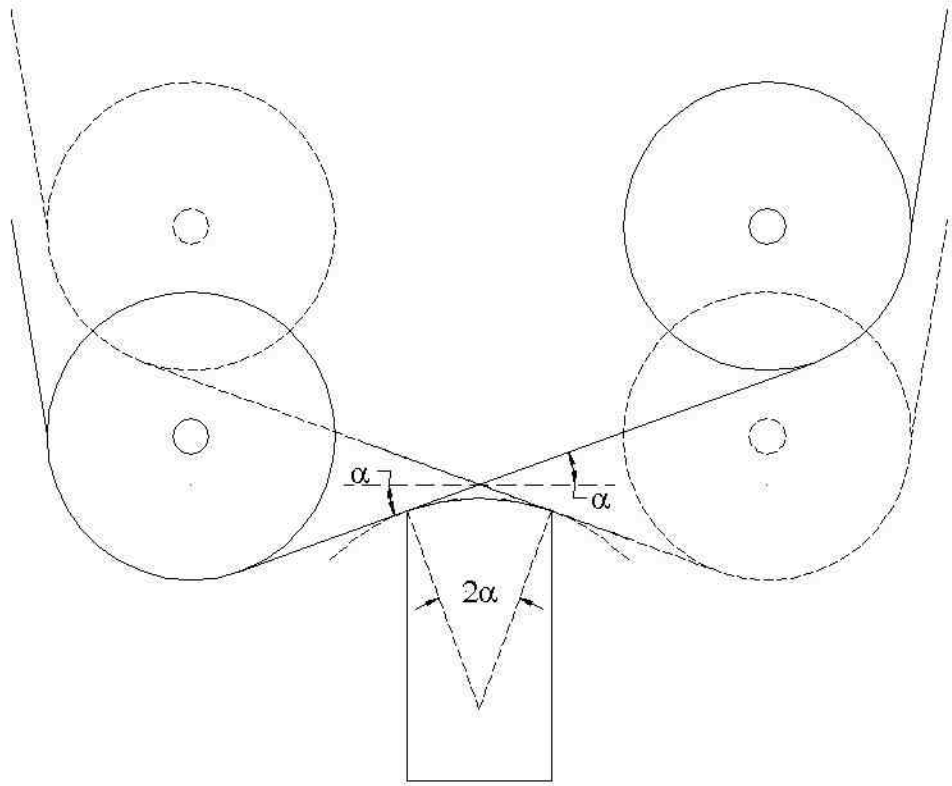

Figure 4.8: Rigid wire cutting with rocking motion of amplitude α.

Consider the free body diagram in Figure 4.9. If the same workpiece-orientated coordinate system is used, then the vertical and horizontal forces F_X and F_Z show their dependence on the inclination angle of the wire as shown in the above equations. If a wire-orientated coordinate system is used, then the force equations for the cutting and thrust forces F_C and F_T remain the same as in the first case. Since the wire is rigid, the angle of inclination α will be the same on both sides of the workpiece.

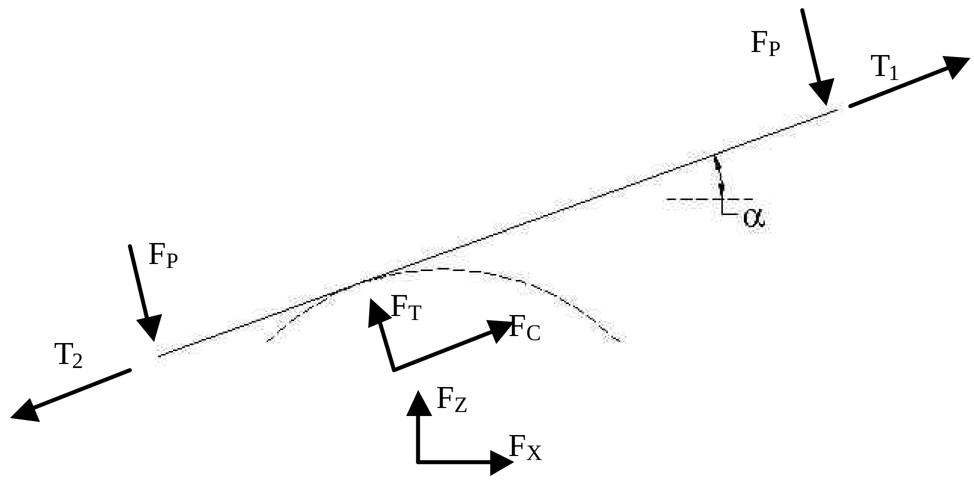

$$F_X = (T_2 - T_1)Cos\,a - 2F_P Sin\,a$$
$$F_Z = 2F_P Cos\,a + (T_2 - T_1)Sin\,a$$
$$F_C = T_2 - T_1 = F_X\,Cos\,a + F_Z\,Sin\,a$$
$$F_T = 2 * F_P = F_Z Cos\,a - F_X\,Sin\,a$$

Figure 4.9: Free body diagram of wire section shown in Figure 4.19.

In this case, measurements of F_X and F_Z would not always equal the cutting and thrust forces F_C and F_T. However, during each cycle of rocking motion, the wire guide pulleys would become horizontal to each other twice. At these two times, the system would resemble the diagram in Figure 4.6. Also, the amplitude of rocking motion is limited to 5 degrees. At angles this small, the error induced by neglecting these trigonometric terms is small.

Next, consider the real world case from Figure 4.10 of wire cutting where the wire is allowed to bend without the use of rocking motion. Any vertical thrust force will deflect the wire. If you assume the symmetry caused by a centered workpiece, then there will be an identical wire deflection of θ on both sides of the workpiece. Even if there is a asymmetric aspect to cutting such as improved cutting on the trailing edge of the wire, this symmetry assumption is still valid. This is because any nonsymmetrical effects would be removed as the wire reverses its direction. Any directional dependant effects should therefore be small enough to neglect.

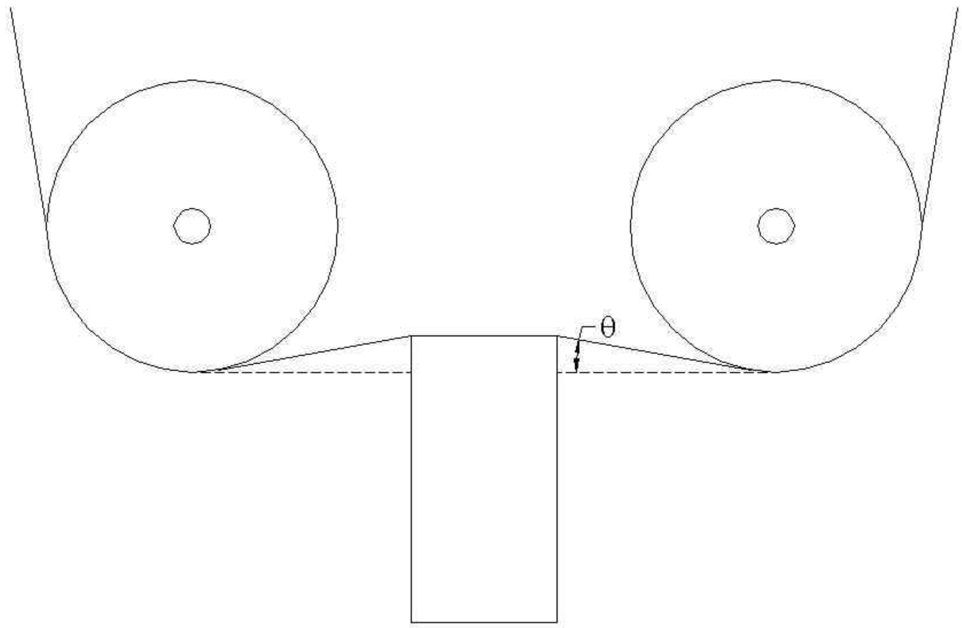

Figure 4.10: Real world wire cutting with no rocking motion.

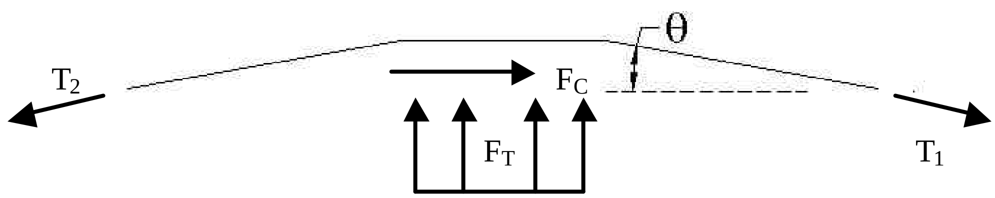

$$F_C = (T_2 - T_1)Cos\theta$$
$$F_Z = (T_2 - T_1)Sin\theta$$

Figure 4.11: Free body diagram of wire section shown in from 4.10.

The profile of the cutting surface of the workpiece is not inherently predictable. It could be straight or curved to some unknown radius. The overall force equations from the free body diagram of the system shown in Figure 4.11 would be the same regardless of if the actual profile were curved or flat. The force equations show that both the horizontal and vertical forces generated through cutting would be dependant on the wire bow angle θ. As the bow angle θ approaches zero, the Sin(θ) term causes the vertical force to do the same. This demonstrates how any thrust force will deflect the wire. Note that symmetry of the system results in the same wire bow angle θ on both sides of the workpiece.

Finally, add rocking motion to the real world case just described. As before, there will be a wire rotation of magnitude α. However, instead of point contact between the wire and workpiece, wire bow will cause a contact length of finite length. This amount of contact length will depend on the amount of wire bow, which depends on many different factors as mentioned in section 3.1.4. Also introduced in section 3.1.4 is the ideas that wire bow during rocking motion will cause the angle of wire inclination to be different on either side of the workpiece and that the wire bow sensor used in this study was not calibrated to measure either of those angles. This system is shown in Figure 4.12 below.

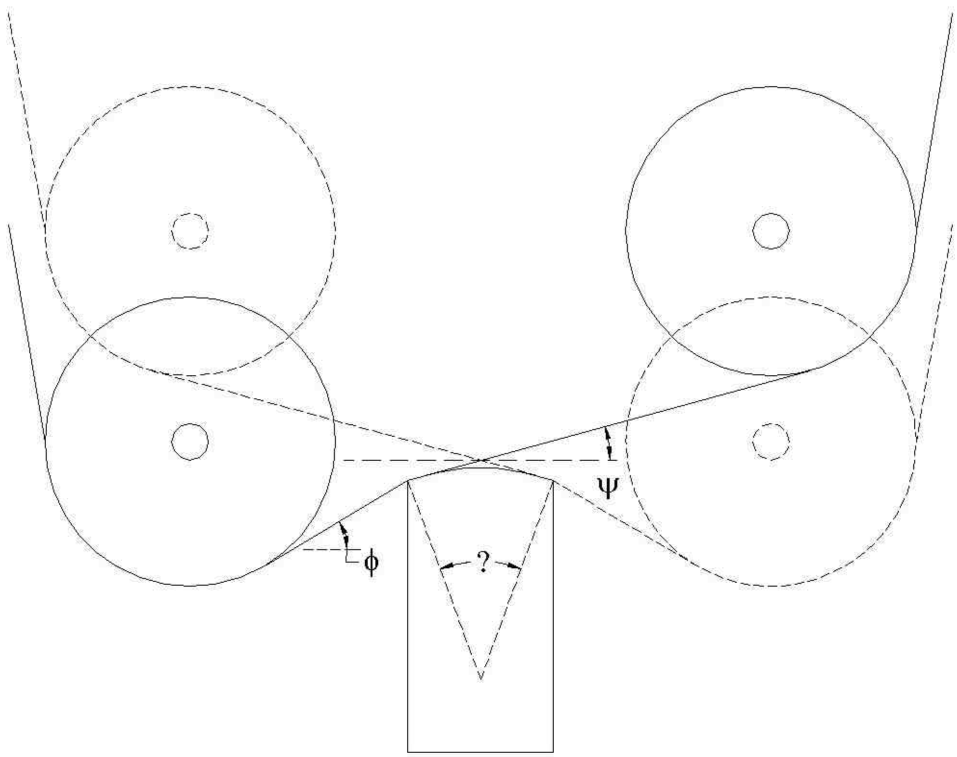

Figure 4.12: Real world wire cutting with rocking motion.

Due to the rocking motion of the wire assembly, the overall cut profile should remain a circular curve. The radius of the circular profile and the length of wire-workpiece contact cannot be easily predicted.

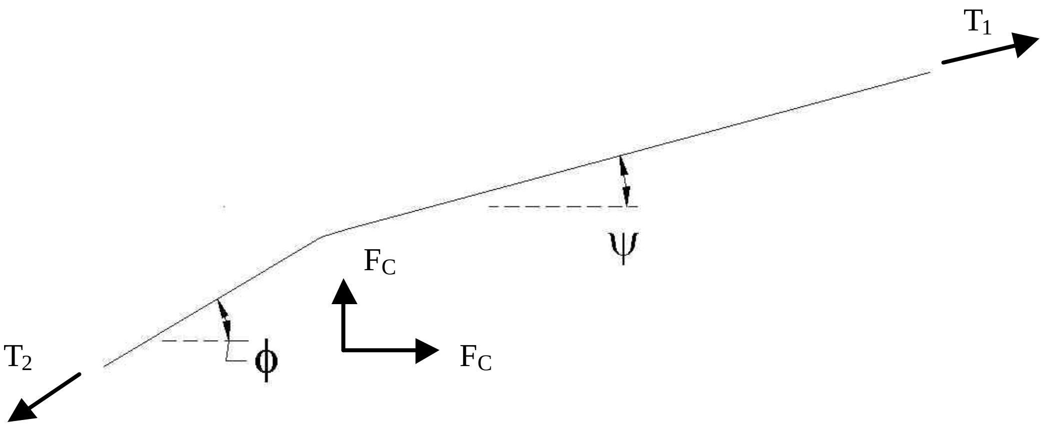

$$F_C = T_2 Cos\ f - T_1 Cos\ y$$
$$F_T = T_2 Sin\ f - T_1 Sin\ y$$

Figure 4.13: Free body diagram of wire section shown in Figure 4.12.

The equations for the forces exerted on the wire as shown in the FBD in Figure 4.13 are also more complex. Due to the finite wire contact length and the wire rocking motion, the wire inclination angles ψ and ϕ may be different. Because of this, the equations cannot be simplified any further.

Since the wire inclination angle will not be the same on both sides, a single wire bow sensor will not provide enough detail to find the cutting and thrust forces at a given time. However, when rocking motion rotates completely clockwise, the system will be a mirror image of the above diagrams. At that time, the wire to the right of the workpiece will be inclined to the angle ϕ. A single bow sensor would measure both angles during a given rocking motion cycle, so a record of the wire inclination angle would allow for calculation of the force values.

5 SURFACE ROUGHNESS

Surface roughness measurements were not obtained for the ceramic foam materials due to the small cross sectional area of their ligaments. However, surface roughness measurements were taken for the cut wood surfaces. These measurements were primarily conducted with a Talysurf 120 contact stylus machine. This machine drags a stylus across the workpiece surface for a specified length, recording the surface profile as it goes.

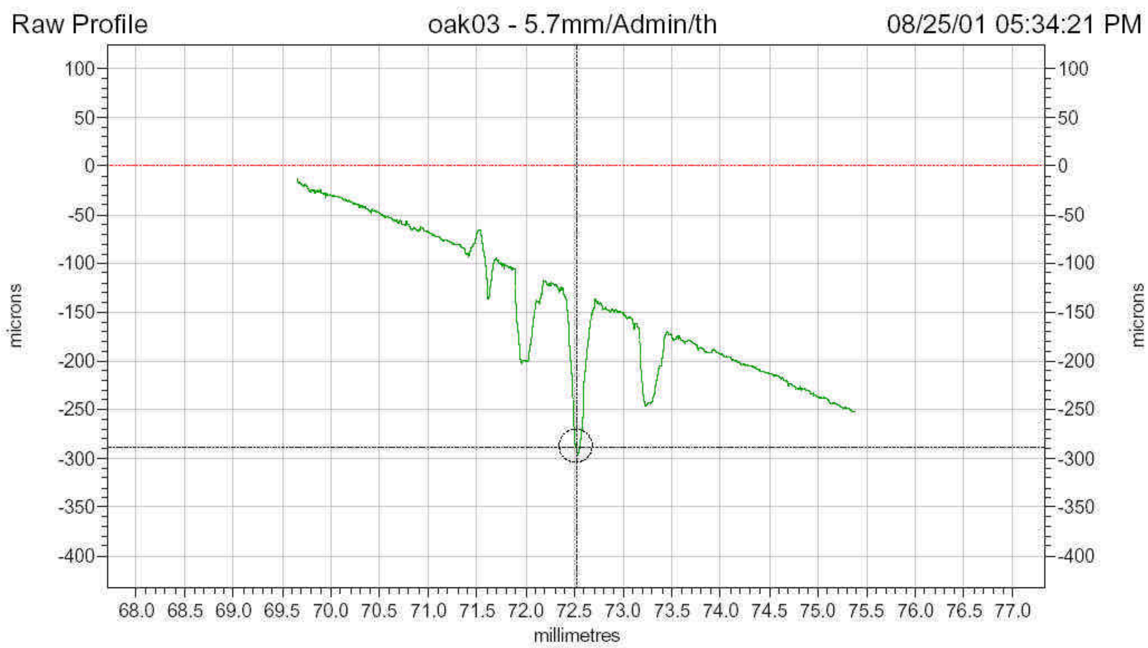

Figure 5.1: Sample measured Talysurf profile.

To account for any overall workpiece surface tilt, the Taylor Hobson software used a least squares method to produce the mean line. The least squares line was fitted so that the areas above and below the resulting mean line were the same. Figure 5.1 shows a sample profile trace as measured, and Figure 5.2 shows the resulting mean line after the least squares tilt correction. The mean line profile data in shown n Figure 5.2 could then be used to calculate surface roughness parameters over the profile measured.

The average surface finish, R_a, is defined as the arithmetic mean of the absolute departures of the roughness profile from the mean line (Dagnall, 1997). This is the most widely used surface roughness parameter.

Figure 5.2: Sample modified Talysurf profile.

The root mean square surface finish, R_q, is simply the root mean square parameter corresponding to Ra. This parameter is often regarded as more significant when conducting statistical measurements (Dagnall, 1997).

The peak value R_p represents the maximum peak value above the mean line over a trace. This is useful to distinguish between roughness caused by a few discrete points (holes) and roughness caused by more numerous small peaks.

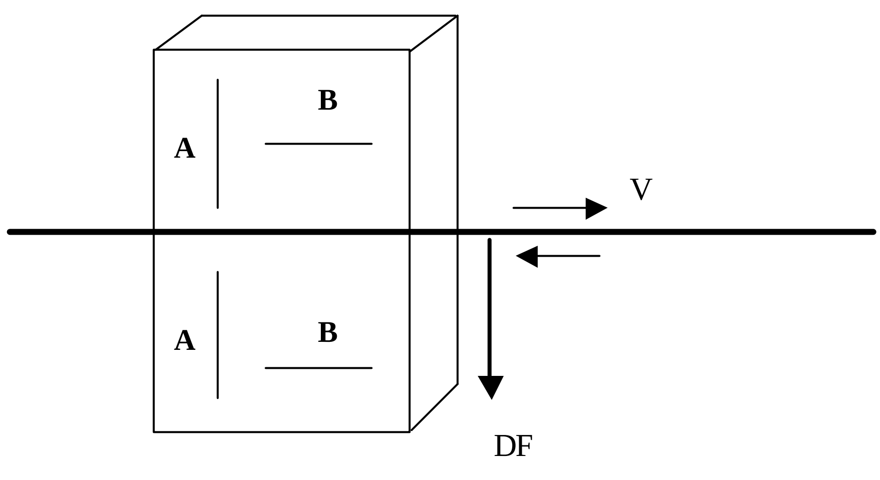

Figure 5.3: Location of surface roughness measurements on wood cut surface.

In fixed abrasive wire saw machining, surface roughness profiles can be taken in different directions and locations. These are shown in figure 5.3 below. In the figure, a machined surface exists for which the wire downfeed DF progressed down and the wire axial velocity V alternated between left to right. The profile can be measured along the direction the DF, indicated by A in Figure 5.3. Alternately, the profile can be measured along the direction of V, indicated by B in Figure 5.3. Also, numerous profiles can be taken across the workpiece and the results averaged to gain

5.1 Wire Endurance Test Surface Roughness

The original cutting test was a series of slices of pine material carried out with the same process parameters. Medium speed rocking motion was used on pine in these cuts along with 4.5 m/s wire speed and 0.0508 mm/s downfeed rate. The complete listing of parameters is contained in Table 2.1.

The results of the surface finish parameter R_a from the first 10 cut surfaces in this experiment are shown in Figure 5.4. With the exception of one cut surface, the values for the surface roughness parameter are all very similar. The average surface finish Ra value for the slices was always less than 3 μm.

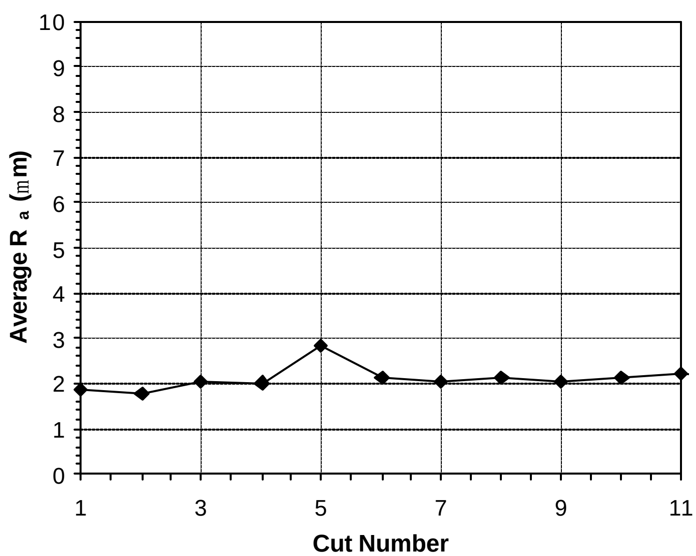

Figure 5.4: Surface roughness values for wire endurance test surfaces.

5.2 Pine And Oak Surface Roughness

The main wood cutting experiments for pine and oak materials contained six machining tests where the wire speed and rocking motion conditions were used as process variables. The surfaces machined during these tests were collected and the Talysurf contact stylus machine measured their surfaces to obtain roughness values. Different measurements for each surface were averaged to provide a more representative value for the roughness. The results from these measurements of pine and oak surfaces are shown below in Figure 5.5.

For the average Ra surface finish values for pine, the values exist between 2 to 3 μm. There is no noticeable effect of either rocking motion or wire speed on this parameter. The average R_p and R_q values for pine surfaces follow similar trends. The RMS R_q values fall between 2 and 4 μm, and show no great variation due to wire speed or rocking motion. The surface peak R_p values again stay within the small range of 6 to 8 μm and are again not noticeably affected by wire speed or rocking motion.

The average R_a values for the oak surfaces exist over the much wider range of 1 to10 μm. For wire speeds of 6 and 9 m/s, increasing rocking conditions result in larger roughness values. The results from the 4.5 m/s wire speed tests are not as clear. The average R_p and R_q values for oak surfaces follow the same trends. Their values exist over much larger ranges than do the similar values for pine surfaces. Also, for wire speeds of 6 and 9 m/s, the R_p and R_q values increase with increasing rocking motion frequency.

The average results listed in Figure 5.5 are averages of several different measurements across each surface. The measurements on each surface often varied depending on where the measurement took place. As shown in Figure 5.3, measurement profiles were taken in directions parallel to the wire downfeed direction and parallel to the wire axial velocity. Measurements in these different directions resulted in different values of surface roughness parameters. Figure 5.6 shows examples of corresponding Ra values taken in directions parallel to the wire downfeed DF and parallel to the wire velocity V. The roughness values were almost always higher when measured in the direction of wire downfeed. For all three surface roughness parameters, the oak surface machined with 4.5 m/s DF without rocking motion produced the lowest values.

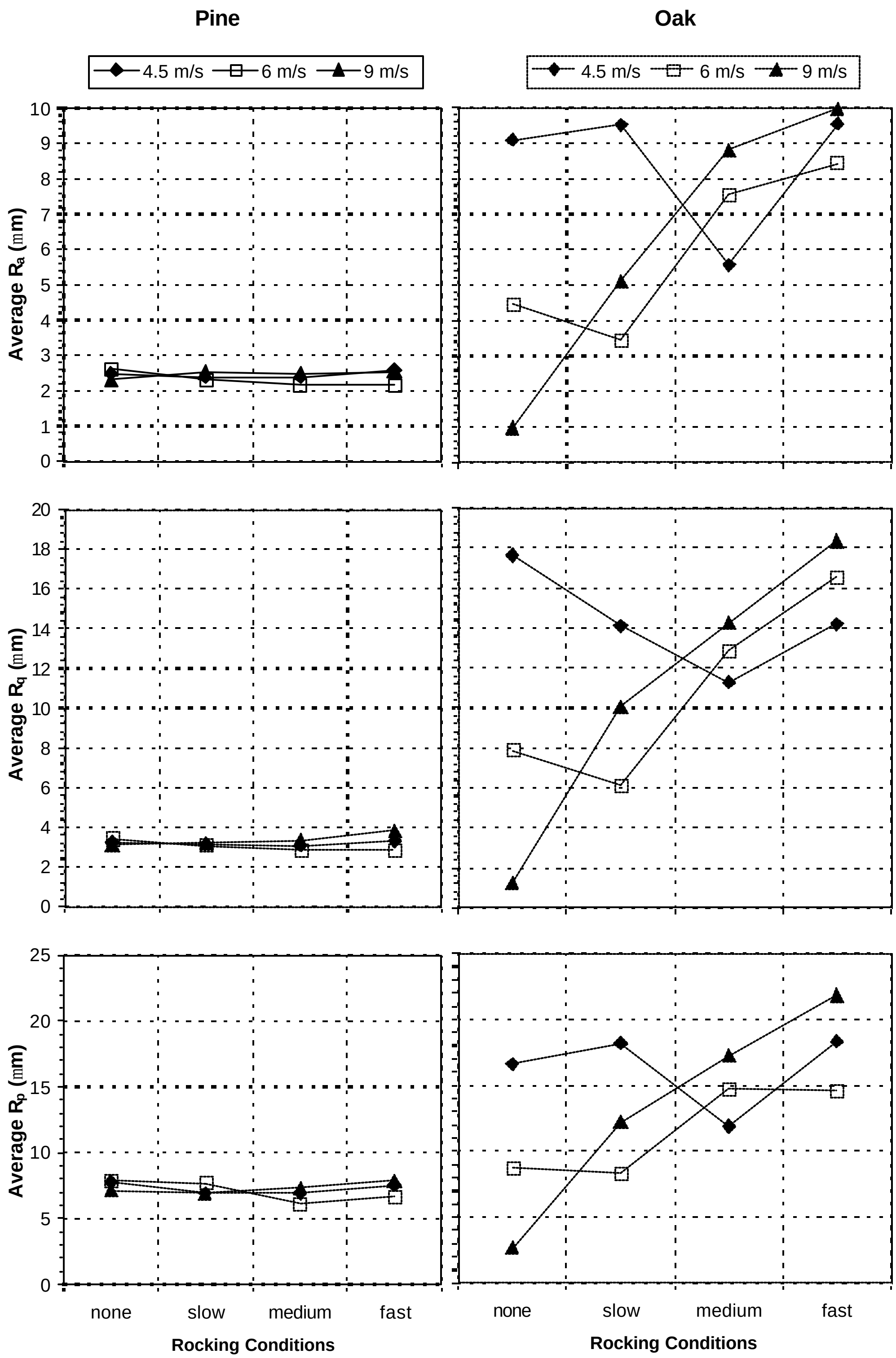

Figure 5.5: Surface roughness results from oak and pine cutting experiments.

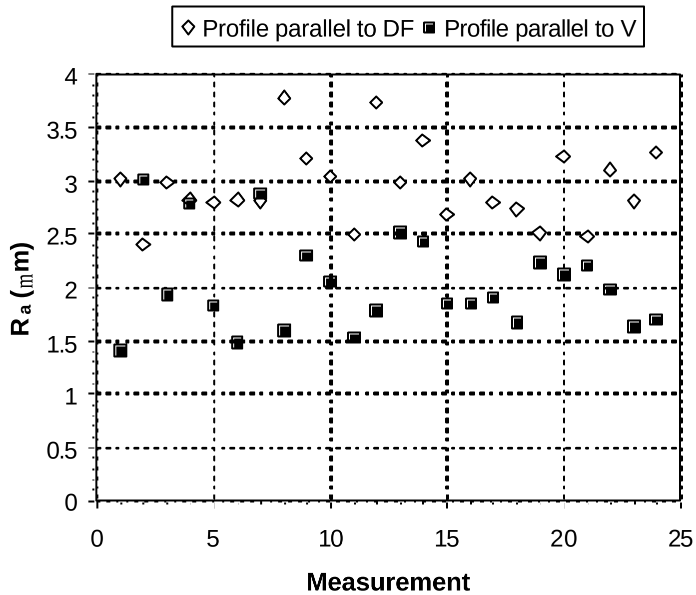

Figure 5.6: Measurement path effects on roughness for pine surfaces.

The roughness values measured on oak surfaces varied greatly. This was due largely to the presence of porous holes through the workpiece, which were unrelated to the wire machining. The porous holes can be seen in Figure 5.7 existing in the earlywood grains. In certain other species of oak, these pores are filled with tyloses (Forest Products Laboratory, 1987). The grains containing these holes are oriented so that they cam intersect profile measurements in both directions. The sample surface profile trace shown in Figure 5.1 and Figure 5.2 were taken on an oak surface, and the presence of the holes can be easily seen.

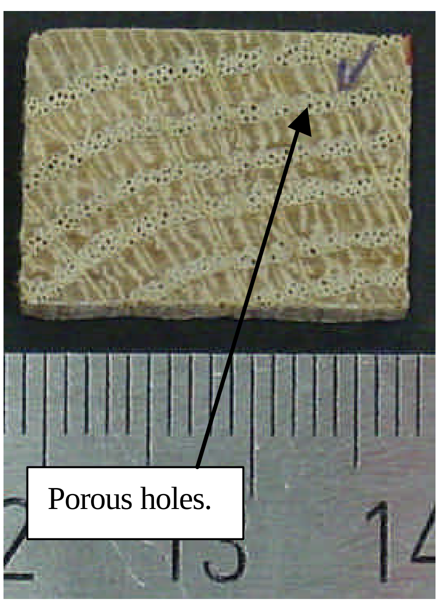

Figure 5.7: Machined oak surface.

For measurements of oak surfaces, the resulting surface roughness values are determined largely on whether or not the profile intersected any holes. Figure 5.8 shows the Ra values from different measurements. There are many measurements with roughness values smaller than 2 μm, but there are even more measurements that encountered holes, resulting in Ra values above 5 µm. The effects of the porous holes, not by the effects of wire machining, therefore dominate the surface roughness values for the oak surfaces. The oak cutting experiment conducted with a wire speed of 4.5 m/s with no rocking motion resulted in the lowest average surface roughness values of any surface. This does not mean that its surface is any less rough than any other oak surface. The measurement traces on this surface just did not intersect any holes.

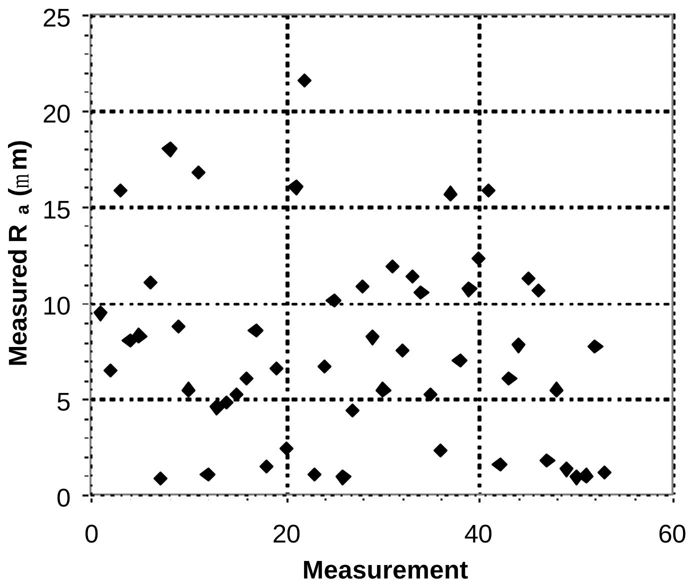

Figure 5.8: Variability of R_a roughness values for oak surfaces.

5.3 Contact vs. Optical Measurement

The Talysurf machine drags a diamond stylus across the workpiece surface. Because of the nature of the workpiece materials, there was a concern that the hard stylus might plow into the softer wood. This plowing effect, if it exists, would result in unrealistically low surface roughness values. To check for evidence of this plowing effect, an optical Rodenstock surface roughness measurement machine was used to measure selected samples. Surfaces from one cut of each wood type were measured at various points with the Rodenstock machine, and the results were averaged for each surface. The resulting average R_a and R_p values are compared to corresponding measurements made with the Talysurf stylus machine in Table 5.1.

The results in the table show that the Rodenstock and Talysurf machines obtain similar values for the average surface roughness parameter R_a. For the pine surfaces from the wire endurance test and the pine experiments, the Talysurf machine found slightly lower R_a values. For the oak surfaces, the Rodenstock machine found a lower average value. The differences in average R_a values from the two machines were between 0.35 and 2.36 μm.

Table 5.1: Effects of measurement method on surface roughness values.

	Average R_a (mm)		**Average R_p (mm)**	
Material Source	Rodenstock	Talysurf	Rodenstock	Talysurf
Wire endurance test cut #9	2.47	2.12	10.27	5.86
Pine experiments cut #6	3.25	2.40	19.06	6.93
Oak experiments cut #2	6.43	8.79	28.33	17.24

For the average peak parameter R_p, the Rodenstock machine found much larger values for all three cases. The differences in average R_p values from the two machines were between 4.2 and 12.1 μm. The Rodenstock measurements consistently record higher peak values, but this does not necessarily result in higher roughness values.

The roughness values for the oak material are again higher than what was caused by the wire machining due to the presence of porous holes through the workpiece. The roughness values for both materials, however, are similar enough between the two methods to indicate that both methods are equally valid.

5.4 Fir Surface Roughness

Douglas Fir wood was machined to determine the effect of different grain types on machining results. Surface roughness measurements were performed several times in both directions on the machined surface with the Talysurf machine, and the results were averaged to obtain overall values for the surface. The resulting average surface finish parameters for the Douglas Fir material are listed in Table 5.2 below.

Table 5.2: Surface roughness values for Douglas Fir machined surface.

Average R_a (μm)	Average R_p (μm)	Average R_q (μm)
2.38	4.81	2.52

The resulting average values for the R_a, R_p, and R_q surface roughness values are similar to those obtained during the pine cutting experiments.

6 SEM

The first research model SEM was built in the RCA Laboratory in 1942 (Zworkykin, 1942). Advances in signal processing and amplification led to the first commercial model SEM to be produced in 1964 (Watt, 1985). Since then, SEM has become a standard tool in examining the exterior features of objects in fine detail.

In SEM, an aligned wide beam of electrons is scanned across an object under observation. As the electrons in the beam strike the object, some are reflected and some are absorbed by the material, causing it to emit other electrons. Detectors use the direction and energy of the emitted and reflected electrons to produce a picture of the geometric features of the material. The picture is formed over time as the electron beam scans across the material surface (Watt, 40).

The surface absorbing and reflecting the electrons from the beam needs to be electrically conductive or else it can build up a net charge. This charging of the surface can result in spots in the image too bright to record properly. To prevent this, nonconductive materials are sputter coated with a layer of conductive material.

The main goal of using the SEM in this study was to investigate the wear of fixed abrasive diamond wire. First, it was necessary to examine new unused wire. Then, wire samples used to machine different materials were examined and compared to the unused wire. Debris collected during machining tests was also examined.

A Hitachi S-800 field emission-gun scanning electron microscope was used for the majority of pictures presented in this study. The SEM was operated at 5 kV with a working distance of 15 mm.

The following sections describe the results of the SEM investigation of new, unused fixed abrasive diamond wire, used wire, and machining debris.

6.1 New Diamond Wire

The wire used in this study was 0.3 mm diameter Laser Technology West brand wire with 80 μm size diamonds. The diamonds are electroplated onto the wire before it is all coated in a metal binding material. Some diamonds were left exposed, but most are buried beneath the binding material. Because most diamonds are buried beneath the binding material, the exact number of diamonds present in the wire cannot be easily determined.

As this wire is first used, the binding material covering the diamond particles will erode, causing the diamonds to become exposed beyond the surface. As a diamond is used to plow through workpiece material, it can undergo wear in several ways:

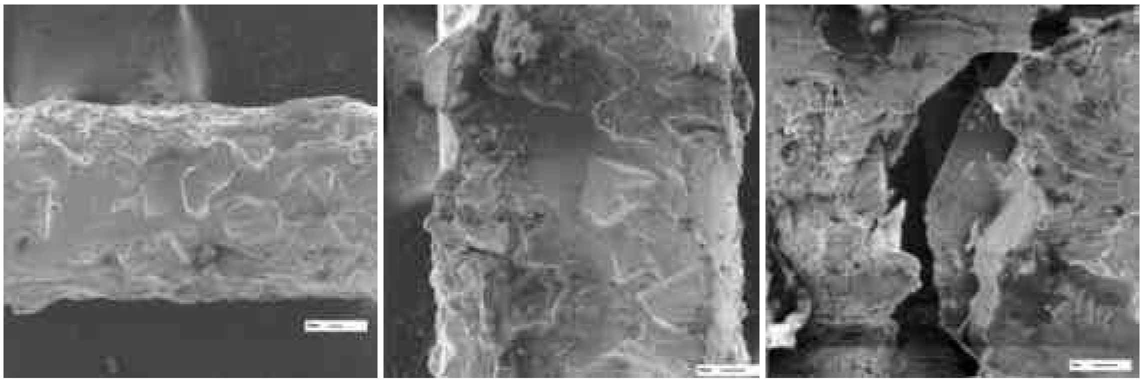

(a) (b) (c)

Figure 6.1: Unused LTW wire at (a) 1x magnification, (b) 1x mag., and (c) 3kx mag.

Unused wire from two other manufacturers was also examined with the SEM. The fist wire from Well Diamond Wire Saws is shown in Figure 6.2 under three different levels of magnification. The diameter of this wire is larger than for the LTW wire. The process to affix the diamond particles to the wire must be different, since the diamonds are not covered in any binding material. The diamond in Figure 6.2(c) appears to have been mechanically forced into the wire binding material. There is only one layer of diamonds present on this wire, and they all are exposed to allow cutting initially. Due to the exposed nature of the diamonds, it is easy to see each diamond on a new wire.

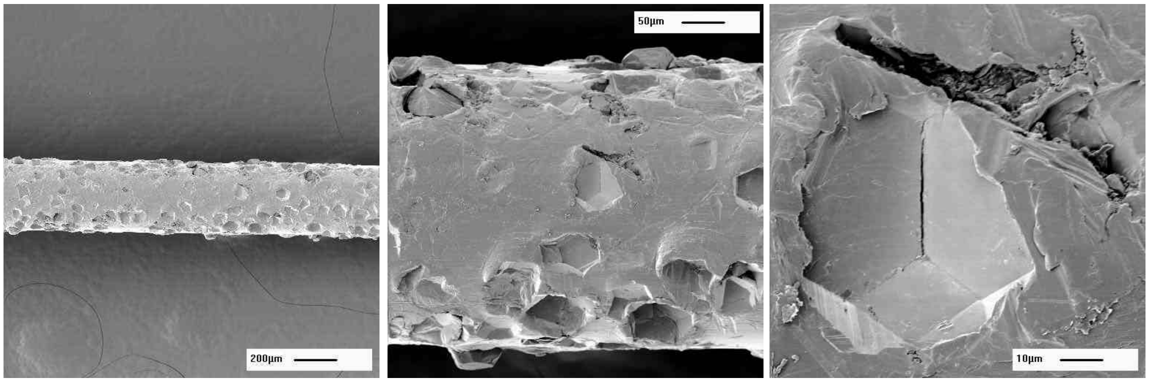

(a) (b) (c)

Figure 6.2: Unused Well wire at (a) 1x magnification, (b) 1x mag., and (c) 3000x mag.

The third type of new wire is Winter wire from Saint-Gobain Winter Diamantwerkzeuge GmbH & Co. This wire is approximately the same diameter as the LTW wire used in this study, but the diamond particles are much smaller at sizes of 20 to 40 μm. The diamond particles can be seen exposed on the surface of the wire, but Figure 6.3(c) shows one diamond particle that is mostly buried beneath the wire material.

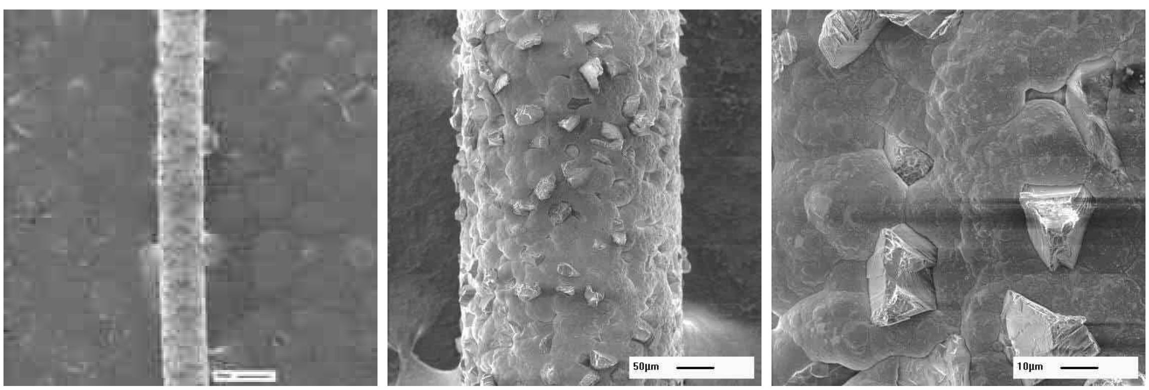

(a) (b) (c)

Figure 6.3: Unused Winter wire at (a) 1x magnification, (b) 1x mag., and (c) 3kx mag.

6.2 Used Diamond Wire

After the completion of a material's set of cutting experiments, the wire used to machine it was cut to obtain a sample. For example, after the completion of the initial wire endurance test, the wire used in the test to cut pine was cut near the wire mid point to obtain a sample of wire. The wire sample was obtained from the center of the length to ensure it was used to cut the workpiece material.

In total, five wire lengths were used in this study. One wire was used in the original wire endurance cutting test, one was used in the pine cutting experiments, one was used in the oak cutting experiments, one was used in the Douglas Fir experiment, and one wire was used to cut the ceramic foam materials. The wire from the Douglas Fir cutting experiment was the only wire not examined with the SEM.

Although the diamond particles are not electrically conductive, the wire samples were not coated to prevent charging. The only sample preparation technique conducted on the wires was to clean them in an ultrasonic bath to remove any debris from their surface.

The wire from the endurance test is shown in Figure 6.4 under three magnification levels. In the low magnification picture in Figure 6.4(a), it can be seen that the wire does not change much along the section examined. The higher magnification pictures in Figure 6.4(b) and Figure 6.4(c) demonstrate that the wire still has exposed and buried diamonds in its surface.

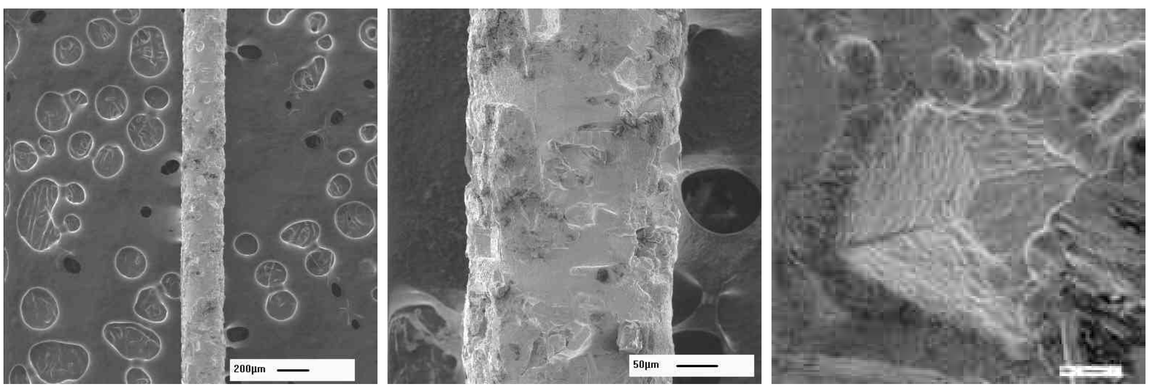

(a) (b) (c)

Figure 6.4: Used wire from original endurance test at (a) 40x magnification, (b) 200x mag., and (c) 1000x mag

The wire from the pine cutting experiments is shown with three different magnifications in Figure 6.5. In the low magnification picture in Figure 6.5(a), several dark regions consisting of non-conductive debris can be seen. The binding material appears to be much more uniform circularly, suggesting it may have been worn during cutting. Also, there do not seem to be as many diamonds present on the wire surface as there were in the previous example. Holes left by pulled out diamonds can be seen in both Figure 6.5(b) and 6.5(c). Additional examples of this wire can be seen in the appendix.

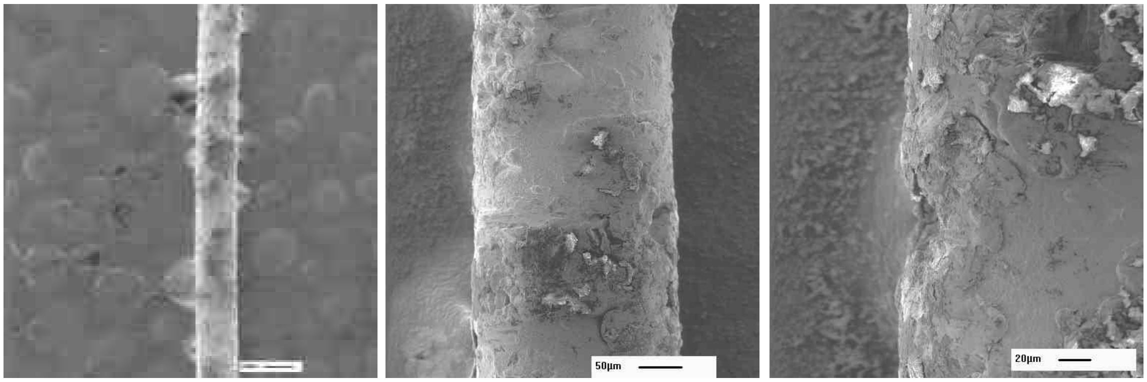

(a) (b) (c)

Figure 6.5: Used wire from pine cutting experiments at (a) 40x magnification, (b) 200x mag., and (c) 400x mag.

The wire used in the oak cutting experiments is shown under three levels of magnification in Figure 6.6 below. This wire appears very similar to the wire used in the wire endurance test. There are still many diamonds left exposed in the surface and buried beneath the binding material. There are also holes left by pulled diamonds, as seen in Figure 6.6(c). Additional examples of the oak experiment wire can be seen in the appendix.

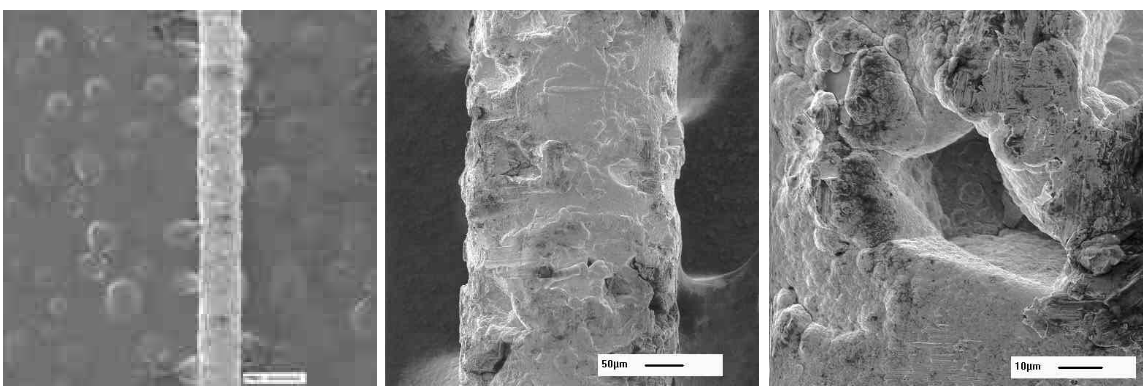

(a) (b) (c)

Figure 6.6: Used wire from oak cutting experiments at (a) 40x magnification, (b) 200x mag., and (c) 1000x mag.

The wire used to cut the ceramic foam materials is shown in Figure 6.7. Of the used wires, this one appears to have the least amount of wear. There are more diamonds exposed on the surface than there were on the other wires. The shapes of diamonds buried under the binding material can still be seen on the surface of Figure 6.7(b). Sheared diamond particles still attached to the wire can be seen in both Figure 6.7(b) and Figure 6.7(c). The appendix contains additional pictures of this wire sample.

Although this wire was used to cut three different materials, the total amount of workpiece material removed by this wire is actually small compared to the wires used to cut wood. This is because of the open cell nature of the ceramic workpieces, where large amounts of the workpiece volume is actually taken up by air. This could explain why the diamond does not appear to have worn much.

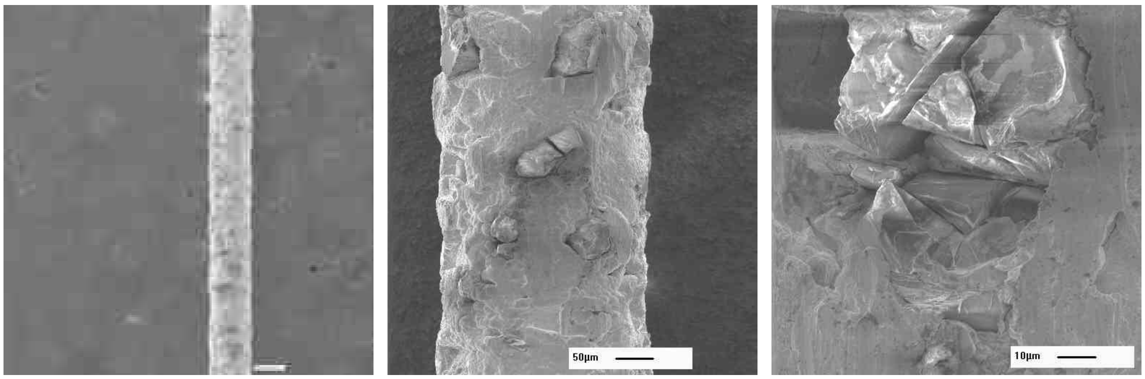

(a) (b) (c)

Figure 6.7: Used wire from ceramic cutting experiments at (a) 40x magnification, (b) 200x mag., and (c) 1000x mag.

The samples of used LTW wire show that the quantification of its wire wear is a difficult task. Diamond particles are not inherently visible beneath the binding material, and the wire does not have an easily determined effective diameter. The effective diameter should be caused by heights of protruding diamond particles. The relatively large spacing between exposed diamond tips makes measuring this distance by observation subjective. Because of this, quantification of wire wear amounts could be pursued in other areas such as in-process laser-based diameter measurement.

A sample picture of a worn piece of Well brand diamond wire is shown in Figure 6.8. This sample was not from this study, but it does demonstrate how different types of fixed abrasive diamond wire wear. In this wire sample, the holes left by pulled diamonds can clearly be seen and counted. The metal wire remaining appears worn, possibly from wire-workpiece rubbing. For this wire type, when the diamond particles are pulled out, there are no replacements to appear to replace

Figure 6.8: Well wire after wear.

them. Wire wear for this type of wire could be defined based on the number or percentage of diamonds pulled out.

6.3 Cutting Debris

During cutting tests, a paper trap was placed beneath where the wire exited the workpiece. Debris pulled from the cut by the wire fell into the trap, and was stored for later examination with the SEM. Many cut programs did not produce enough debris in the trap for analysis. Therefore, the trap would be used for consecutive cuts of the same material until there was a noticeable amount of debris. For this reason, debris cannot be compared across wire speeds and rocking motion conditions as was done for forces and surface finish. This examination attempts to determine what the debris consists of and what types of workpiece chips are generated during wire saw machining.

After cutting wood, the inside of the saw enclosure was coated in a layer of fine dust.

The collected debris was deposited onto double-sided carbon tape on an SEM mounting slide. Because the debris consisted of small discrete particles, some of which being non-conductive workpiece material, the slides with the debris samples were coated in a layer of gold-platinum. Even after coating, many large debris segments would charge too much for the SEM to be able to focus on it.

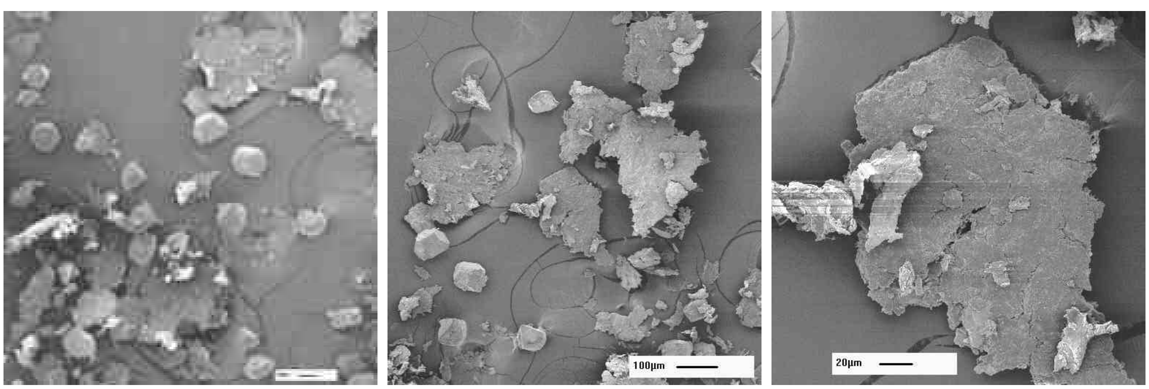

(a) (b) (c)

Fig 6.9: Debris collected from wire endurance test at (a) 100x magnification, (b) 100x mag, and (c) 400x mag.

Figure 6.9 shows debris collected during the wire endurance test under three levels of magnification. Figures 6.9(a) and 6.9(b) both show the presence of diamond particles and workpiece chips among the debris. The chips in Figure 6.9(b) are wider than the diamonds and almost as wide as the diameter of the cutting wire. The diamond particles appear to have been pulled from the wire before any noticeable amount of wear occurred.

Figure 6.10 shows micrographs at three magnification levels of debris collected during the pine cutting experiments. As in the previous example, there are many pulled diamonds among the debris. Also, the workpiece chips are often significantly larger than the diamonds, as seen in Figure 6.10(a). Additional photos of this debris collection are provided in the Appendix.

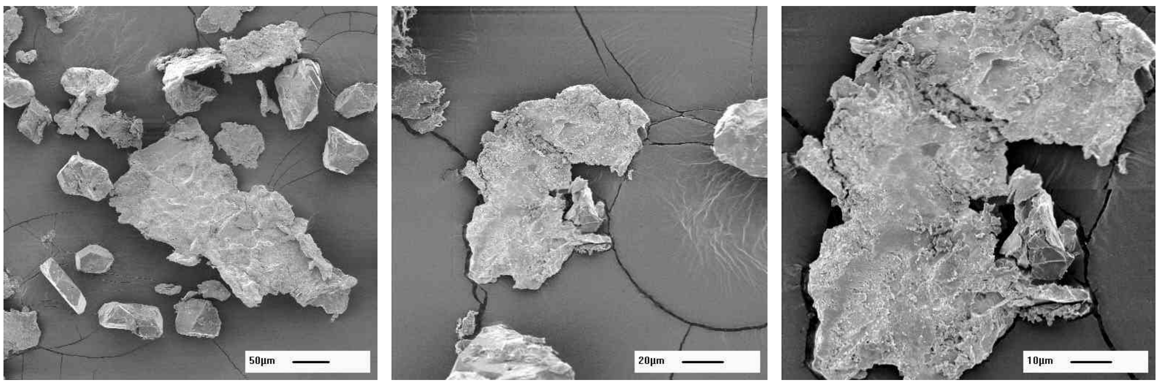

(a) (b) (c)

Figure 6.10: Debris collected from pine cutting experiment at (a) 200x magnification, (b) 500x mag, and (c) 1000x mag.

The debris collected from the oak cutting experiments is shown under three magnification levels in Figure 6.11. As with the previous two examples, there were many diamonds present in the debris. There were some workpiece chips as large as those found in the pine debris, but as seen in Figures 6.11(a) and 6.11(c), many of the workpiece chips were smaller than the diamonds. Figure 6.11(b) shows a diamond that appears to have fractured.

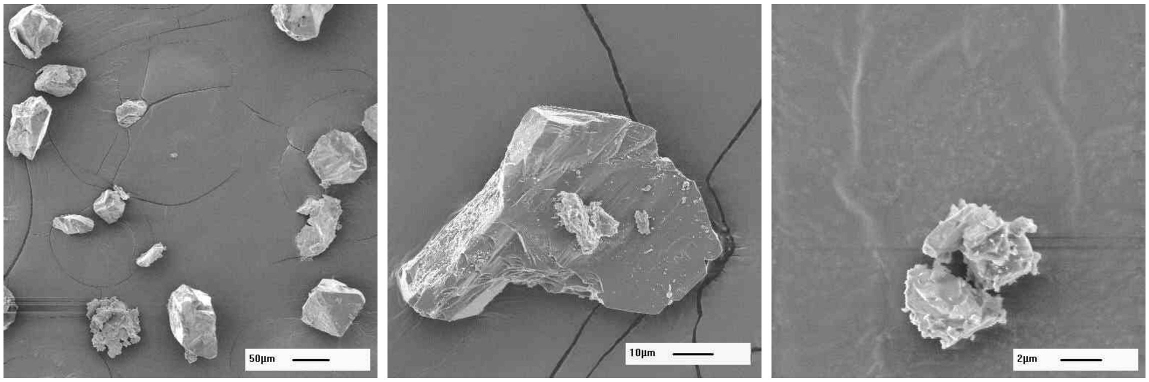

(a) (b) (c)

Figure 6.11: Debris collected from oak cutting experiment at (a) 200x magnification, (b) 1000x mag, and (c) 5000x mag.

Figure 6.12 provides views of debris collected from SiC cutting at three magnification levels. The most noticeable feature is the presence of mm-scale debris as seen in Figure 6.12(a). Several pieces of debris appeared to be SiC foam ligaments that broke off from the workpiece away from where the wire was cutting. The debris contains diamonds as in the other collections. Figures 6.12(b) and 6.12(c) show examples of small 10 µm size diamond particles. Additional pictures of SiC debris are provided in the Appendix.

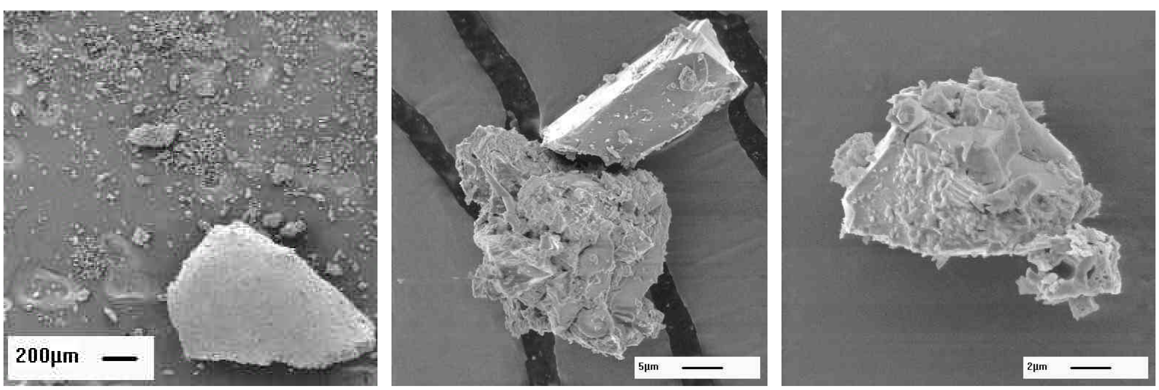

(a) (b) (c)

Figure 6.12: Debris collected from SiC cutting experiment at (a) 40x magnification, (b) 2000x mag, and (c) 5000x mag.

Debris from TTZ cutting experiments is shown in Figure 6.13 at three magnification levels. This debris consisted of diamonds and workpiece chips just as before. The workpiece chips were mostly in the 20 to 100 mm size range. The large chips appear to be pieces of foam that broke away from the workpiece. The smaller chips show evidence of having being machined, as shown by the chip in Figure 6.13(b). Figure 6.13(c) shows a diamond particle, which appears to be still partially coated by wire binding material.

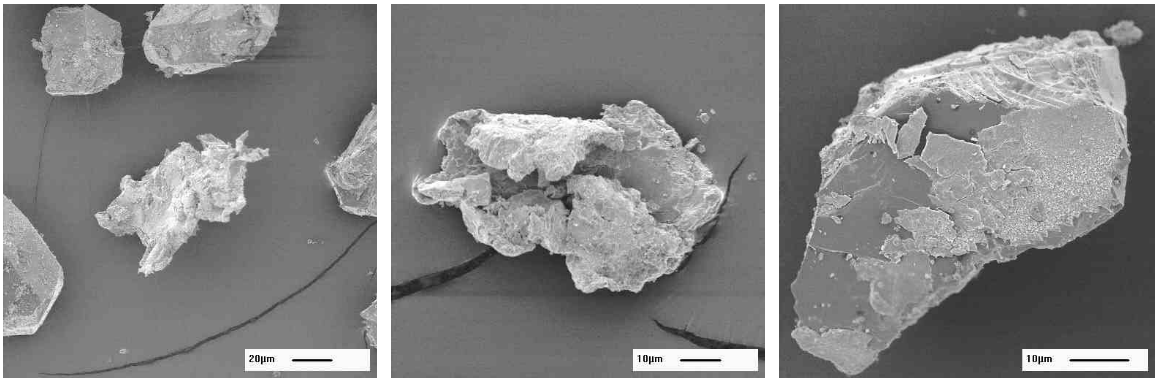

(a) (b) (c)

Figure 6.13: Debris collected from TTZ cutting experiment at (a) 500x magnification, (b) 1000x mag, and (c) 1500x mag.

Figure 6.14 contains images of debris collected during ZTA cutting at three levels of magnification. This debris collection contained numerous examples of large ZTA pieces as seen in Figures 6.14(a) and 6.14(b). These pieces were machined by the wire on one edge, but were simply broken on other edges. The piece shown in Figure 6.14(a) demonstrates how the ligaments of ZTA contain hollow cores left over from when it was created. Figure 6.14(c) shows a diamond particle, which shows no sign of wear.

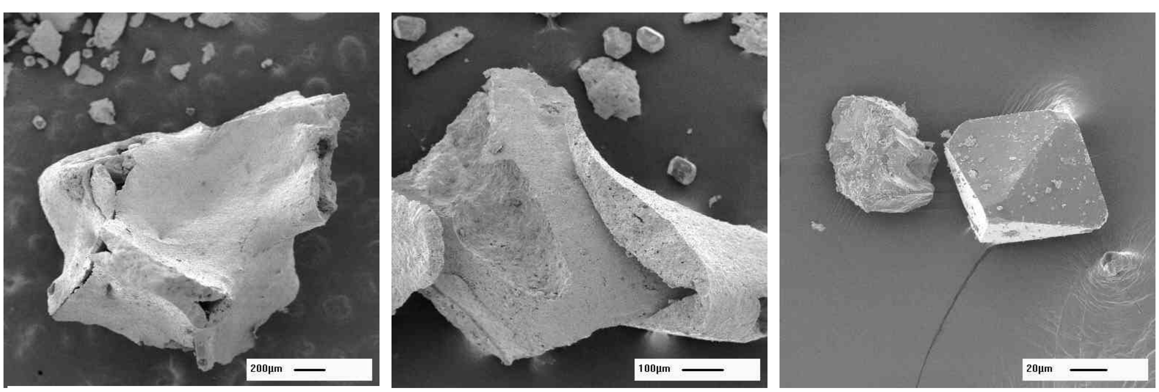

(a) (b) (c)

Figure 6.14: Debris collected from ZTA cutting experiment at (a) 40x magnification, (b) 100x mag, and (c) 500x mag.

6.4 Machined Surfaces

A sample of machined oak and TTZ surfaces were examined with the SEM. The surfaces required extensive coating to reduce the amount of surface charging. Example pictures of the surfaces are provided here, and additional images are located in the Appendix.

The machined oak surface is shown in Figure 6.15. Figures 6.15(a) and 6.15(b) show the porous holes that exist on the workpiece surface. These holes were responsible for the large surface roughness values measured and presented in Chapter 5. However, as seen in Figure 6.15(c), the features on the workpiece surface are rather small, indicating a locally low roughness value. The orientation of the oak surface pictures is such that wire velocity V was horizontal on the page and wire downfeed DF progressed down on the page.

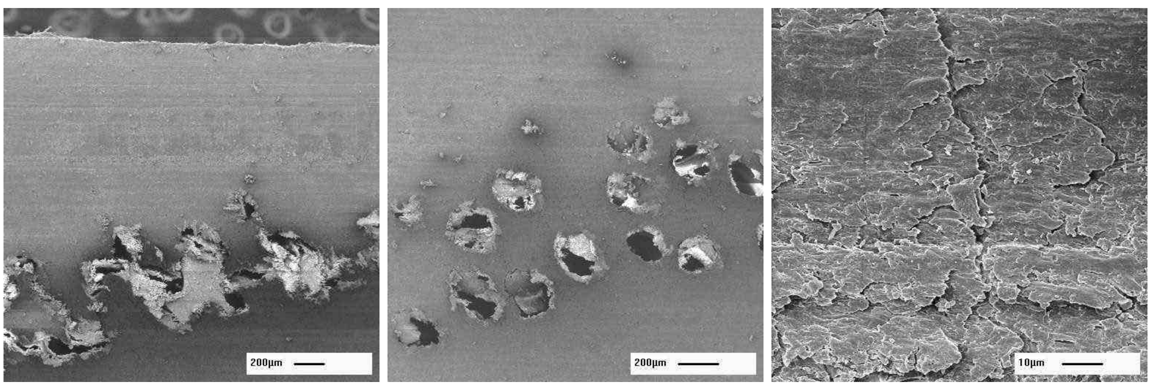

(a) (b) (c)

Figure 6.15: Machined oak surface at (a) 40x magnification, (b) 50x mag, and (c) 1000x mag.

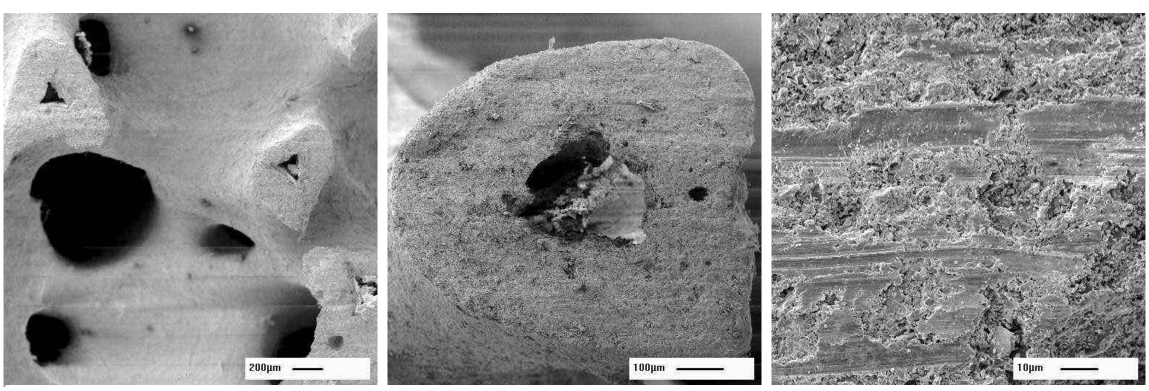

(a) (b) (c)

Figure 6.16: Machined TTZ surface at (a) 40x magnification, (b) 120x mag, and (c) 1000x mag.

Figure 6.16 shows example pictures of a machined TTZ surface at three levels of magnification. Figures 6.16(a) and 6.16(b) show the presence of hollow cores in the TTZ ligaments. Figure 6.16(c) shows the surface under 1000x magnification. The smoothened surface tracks show where the diamonds passed horizontally across the surface.

7 CONCLUSION

With increasing material costs for wood materials, there exists a need for a method of machining with lower kerf loss. Fixed abrasive diamond wire saw machining was investigated for use in cutting wood. Wood machining is traditionally dominated by the use of steel saw blades. The fixed abrasive diamond wire developed for use by the semiconductor industry to slice crystal ingots is significantly thinner than even the most advanced thin kerf saw blades. This can lead to significant material cost savings in a production environment.

Two common wood materials, pine and oak, were selected as the main workpiece materials. First, an experiment was conducted to gage the wire's ability to machine wood for extended amounts of time. The effect of wood grain type in wire machining was then examined. Next, experiments were carried out to determine the effects of wire speed and wire rocking motion in wire machining. Experiments were also conducted to determine the effectiveness of machining foam ceramic materials with fixed abrasive diamond wire.

Horizontal cutting forces were measured with a piezoelectric dynamometer, and vertical thrust forces were approximated through measurements of wire bow during cutting. Forces were shown to gradually increase through subsequent cuts with the same parameters. The ratio between horizontal and vertical forces, however, stayed near 0.5. Results showed that machining latewood grains resulted in lower wire bow and vertical thrust forces than machining of earlywood grains.

The horizontal forces ranged between 1.5 and 2.7 N for cutting pine and between 0.8 and 1.3 N for cutting oak. There was no clear indication of the effect of rocking motion on horizontal forces. Higher wire speeds could be shown to result in lower horizontal forces. Vertical forces ranged between 1 and 6.8 N for pine and between 0.6 and 4.2 N for oak. Higher wire speeds usually resulted in lower vertical forces, and maximum rocking motion resulted in lower vertical forces when compared to no-rock conditions. The force ratios for oak and pine remained between 0.3 and 0.65 except when pine was machined at the highest wire speed. The increased force ratio for that specific wire speed is unexplained, but may indicate a set of efficient cutting conditions.
Wire saw cutting of ceramic foams did not result in noticeable force levels unless machining downfeed rates were greatly increased. The wire saw used in this study was able to slice each ceramic at its maximum programmable downfeed rate. Even at this rate, forces remained within the ranges experienced during wood machining.

Surface roughness remained consistent for all machined pine surfaces, with R_a remaining near 2.5 μm. Surface roughness of machined oak surfaces resulted in high values due to preexisting porous holes on the workpiece surface. Due to the presence preexisting holes, the effects of wire saw machining on oak surface roughness is not clear.

SEM analysis demonstrated evidence of wire wear from machining, including the presence of holes left by removed diamonds. However, the use of a binder material to coat the diamond wire has the effect of hiding many diamonds from view. Because of this, SEM analysis was unable to quantitatively determine the amount of wire wear caused by machining the various workpiece materials.

SEM analysis of the debris generated during machining revealed the presence of intact diamond particles and workpiece chips much larger than the individual diamonds. The presence of intact diamonds indicates they are being pulled out of the wire before significant wear can occur.

This fundamental study provides a base for future work in fixed abrasive diamond wire saw machining of wood and wood product materials. There are two obvious areas that deserve additional examination in future studies. The first is a reduction of noise in the collected signals. Noise reduction would allow for increased time response, accuracy, and length of the force recordings. The second is the surface roughness measurements of machined oak surfaces. Measurements could be taken to avoid the grains containing holes. While excluding a large percentage of the workpiece surface, this should provide a better understanding of the effects of wire machining.

Additionally, experiments should be conducted over a much wider range of wire speeds, downfeed rates, rocking angles and speeds, and workpiece materials. This study provides an indication of what fixed abrasive diamond wire can do with wood, but additional data points should be collected.

In this study, fixed abrasive diamond wire has been shown to successfully machine wood products. The small size of the wire results in a lower kerf loss when compared to even the most advanced saw blades. The use of this technology could prove valuable to the wood machining industry as material costs and economic competitiveness continue to increase.

REFERENCES

Asakawa, K., and Oishi, H., 2000, *Ingot Slicing Method and Apparatus Therefore*, US Patent Number 6,065,461.

Bekaert, 1999, *Sawing Wire*, Bekaert Steel Cord Product Group, Zwevege, Belgium.

Bonzo, R., Shafer, H. G., and Trentelman, J. P., 1996, *Apparatus and method for wire cutting glass-ceramic wafers*, US Patent Number 5,564,409.

Buljan, S. T., and Andrews, R. M., 2000, *Brazed superabrasive wire saw and method therefore*, US Patent Number 6,102,024.

Dagnall, H., 1997, *Exploring Surface Texture*, Taylor Hobson Limited, Leicester, England.

Egglhuber, K., 2000, *Wire saw and method of using it*, US Patent Number 6,098,610.

Egglhuber, K., 2001, *Wire saw and process for cutting off shaped articles*, US Patent Number 6,234,159.

Forest Products Laboratory, 1987, *Wood Handbook: Wood as an Engineering Material*, prepared for U.S. Department of Agriculture, pp. 1-26.

Hauser, C., 1998a, *Wire Sawing Device*, US Patent Number 5,758,633.

Hauser, C., 1998b, *Wire Sawing Device*, US Patent Number 5,787,872.

Hauser, C., 1998c, *Device for wire sawing provided with a system for directing wire permitting use of spools of wire of very great length*, US Patent Number 5,829,424.

Hauser, C., 1999, *Wire Saw Device*, US Patent Number 5,910,203.

Hodsden, J. B., 1998, *Apparatus and method for slicing a workpiece utilizing a diamond impregnated wire*, US Patent Number 5,878,737.

Hodsden, J. B., 1999, *Apparatus and method for slicing a workpiece utilizing a diamond impregnated wire*, US Patent Number 5,964,210.

Hodsden, J. B., 2001, *Rocking apparatus and method for slicing a workpiece utilizing a diamond impregnated wire*, US Patent Number 6,279,564.

Hodsden, John B., and Hodsden, Jeffrey B., 2000, *Continuous wire saw loop and method of manufacture thereof*, US Patent Number 6,065,462.

Hodsden, John B., and Hodsden, Jeffrey B., 2001, *Continuous wire saw loop and method of manufacture thereof*, US Patent Number 6,311,684.

Hodsden, J. B., and Luedders, S. M., 2001, *Rocking apparatus and method for slicing a workpiece utilizing a diamond impregnated wire*, US Patent Number 6,279,564.

Ikehara, M., 2000, *Method using a wire feeding device for a multi-wire saw*, US Patent Number 6,109,253.

Ishikawa, K., Suwabe, H., Kanayama, K., Makino, M., and Yoshida, H., 1994, "Study on machining characteristics of wire tool with electrodeposited diamond grains," *Transactions of Japan Society of Mechanical Engineers*, Vol. 60, No. 573, pp. 1815-1820.

Ito, S., and Murata, R., 1987, "Study on machining characteristics of diamond abrasive wire," *Journal of Mechanical Engineering Lab*, Tokyo, Japan, Vol. 41, No. 5, pp. 236-244.

Katamachi, S., 2000, *Wire saw for slicing brittle materials with an ingot loading and unloading mechanism*, US Patent Number 6,135,103.

Kistler, 2001, *The Piezoelectric Effect, Theory, Design, and Usage*, Kistler Instrument Corporation.

Kirbach, E., 1989, "State-of-the-art thin kerf sawing in North American mills," *Timber Processing*, Vol. 14, No. 10, pp. 34-35.

Kurokawa, T, 1990, *Wire saw*, US Patent Number 4,903,682.

Li, J., Kao, I. and Prasad, V., 1998, "Modeling stresses of contacts in wire saw slicing of polycrystalline and crystalline ingots: Application to silicon wafer production," *ASME Transcations, Journal of Electronic Packaging*, Vol. 120, pp. 123-128.

McLaughlin, H. B., 1977, *Use X and Y table to contour cut the workpiece*, US Patent Number 4,016,856.

Mech, H., 1974a, *Machine and method for cutting brittle materials using a reciprocating cutting wire*, US Patent Number 3,831,576.

Mech, H., 1974b, *Machine for cutting brittle materials*, US Patent Number 3,841,297.

Merritt, D., 1999, Private communication at Merritt Precision Technology.

Mitsubushi, 1998, *Pathway to the Production of High Purity Silicon*, Mitsubushi Advanced Materials.

Miyoshi, K., Suzuki, T., Takahashi, K., Goto, Y., Chiba, A., and Wada, S., 1999, *Wire type slicing machine and method*, US Patent Number 5,944,007.

Mote, C. D., 1964, "Circular saw stability: a theoretical approach," *Forest Products Journal*, Vol. 14, No. 6, pp. 244-250.

Mote, C. D., and Nieh, L. T., 1973, “On the foundation of circular-saw stability theory,” *Wood and Fiber*, Vol. 5, No. 2, pp. 160-169.

Mote, C. D., and Szymani, R., 1977, “A review report on principal developments in thin circular saw vibration and control research part 1: vibration of circular saws,” *Holz als Roh- Und Werkstoff*, Vol. 35, pp. 189-161.

Nagatsuka, S., Okubo, S., Kawarai, H., Oishi, H., Asakawa, K., and Matsuzaki, J., 2001, *Wire saw control method and wire saw*, US Patent Number 6,178,961.

Ohashi, S., and Matsuzawa, M., 2001, *Saw wire assembly, cutting method utilizing the same, and system therefore*, US Patent Number 6,178,962.

Oishi, H., Asakawa, K., and Matsuzaki, J., 2001, *Wire Sawing Machine*, US Patent Number 6,237,585.

Onizaki, K., Keiichiro, and Ogawa, K., 2001, *Wire saw cutting method and apparatus therefore*, US Patent Number 6,283,111.

Parker, R. G., and Mote, C. D., 1989, “Asymmetric tensioning of circular saws,” *Holz als Roh- und Werkstoff*, Vol. 47, pp. 143-151.

Sahoo, R.K., Prasad, V., Kao, I., Talbott, J., and Gupta, K. P., 1998, “Towards an integrated approach for analysis and design of wafer slicing by a wire saw,” *ASME Transactions Journal of Electronic Packaging*, Vol. 120, pp. 35-40.

Schajer, G. S., and Mote, C. D., 1983, “Analysis of roll tensioning and its influence on circular saw stability,” *Wood Science and Technology*, Vol. 17, pp. 287-302.

Super Thin Saws, Saw blade picture. www.superthinsaws.com, 2001.

Szymani, R., and Mote, C. D., 1977, “Principal developments in thin circular saw vibration and control research: Part 2: reduction and control of saw vibration,” *Holz als Roh- und Werkstoff*, Vol. 35, pp. 219-225.

Takeuchi, N., 1991, *Brittle material cutting method*, US Patent Number 5,201,305.

Tokura, H. Nakayama, S., and Yoshikawa, M., 1992, “Cutting performance of diamond plated wire tools,” *Journal of Japan Society of Precision Engineering*, Vol. 58, No. 12, pp. 2013-2018.

Toyama, K., 1998, *Wire saw cutting method synchronizing workpiece feed speed with wire speed*, US Patent Number 5,810,643.

Toyama, K., 1999, *Wire saw cutting apparatus synchronizing workpiece feed speed with wire speed*, US Patent Number 5,947,789.

Toyama, K., Kiuchi, E., Hayakawa, K., 1993, *Wire saw and slicing method using the same*, US Patent Number 5,269,285.

Ueoka, I., Sugawara, J., Mizogouchi, A., Oshita, H., Yamanaka, M., Ogawa, H., Urakawa, N., and Yoshinaga, H., 2000, *Wire-saw and its manufacturing method*, US Parent Number 6,070,570.

Watt, I., 1985, *The Principles and Practice of Electron Microscopy*, Cambridge University Press, Cambridge.

Wells, R. C. and Hatfield, T. J., 1987, *Wire Saw Machine*, US Patent Number 4,655,191.

Wells, R. C., 1985, *Wire Saw*, US Patent Number 4,494,523.

Witte, D. A., and Ragan, T., 2000, *Method of slicing silicon wafers for laser marking*, US Patent Number 6,112,738.

Yu, F. C., 2000, *Diamond wire saw*, US Patent Number 6,105,568.

Zworkykin, V.R., Hillier, J., and Snyder, R.L., 1942, "A Scanning Electron Microscope," *ASTM Bulletin*, No. 117.

APPENDIX A

SEM Catalog

New Wire	40x	200x	300x	1000x
New Supplier 1 (LTW) wire	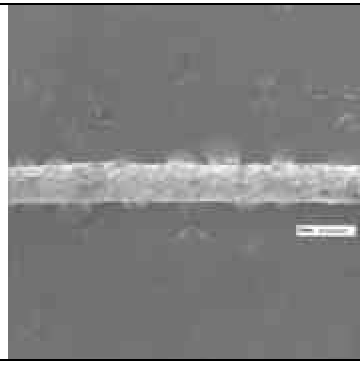	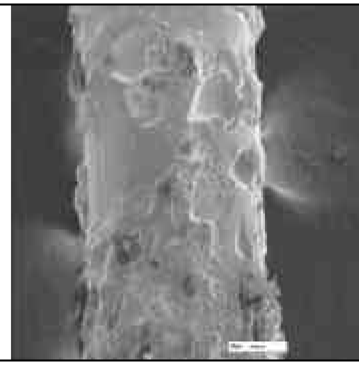	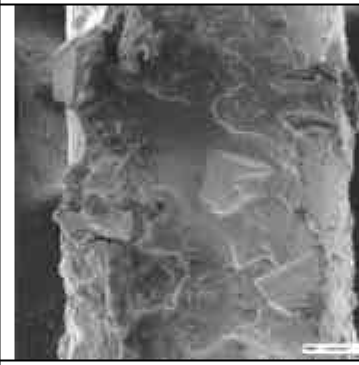	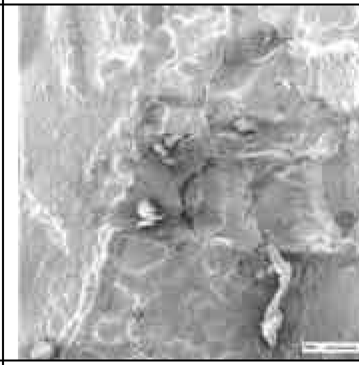
	40x	200x	200x	1000x
New Supplier 3 (Winter) Wire	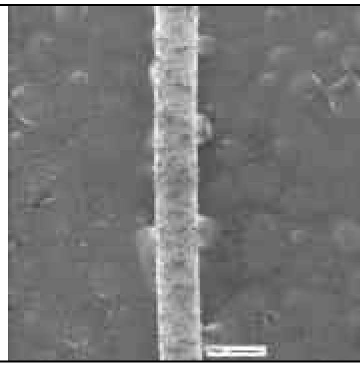	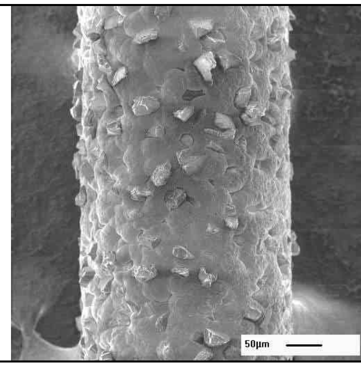	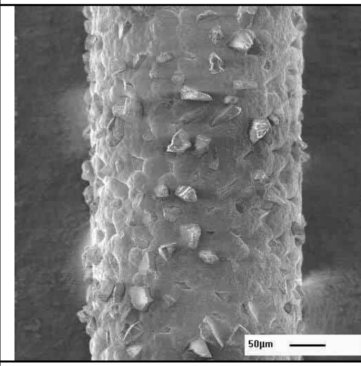	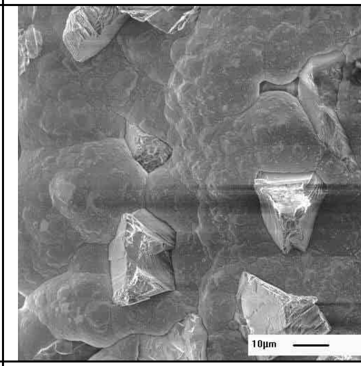
	100x	150x	250x	1000x

New Wire	40x	200x	300x	1000x
New Supplier 2 (Well) Wire	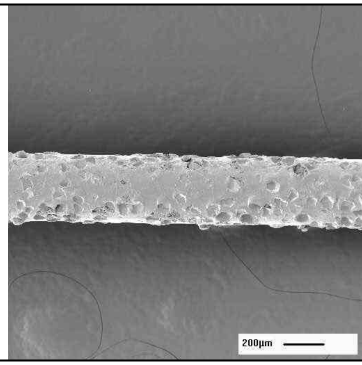	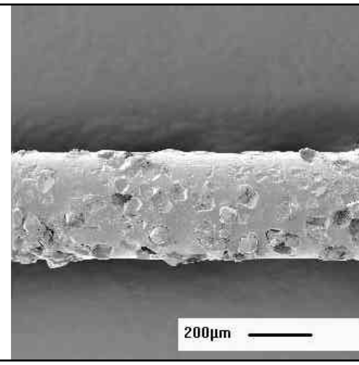	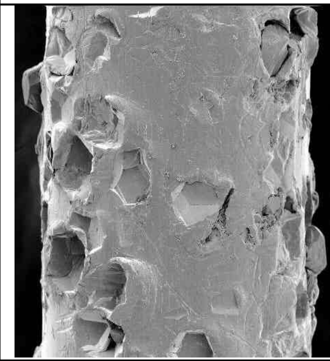	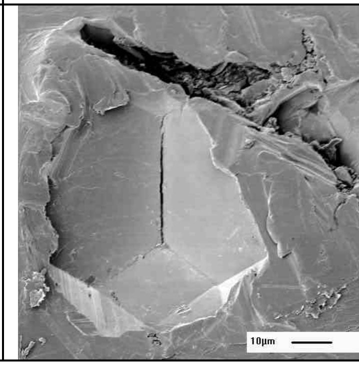

Used wire 1	40x	200x	400x	1000x
Wire used in original wire endurance test.	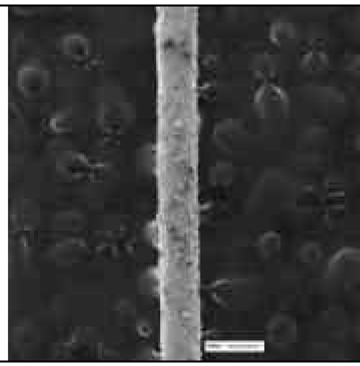	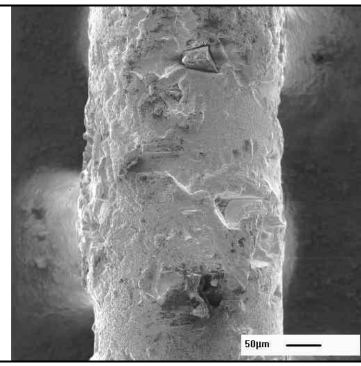	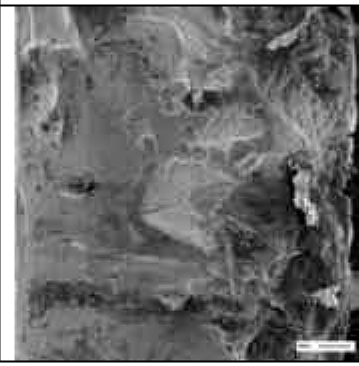	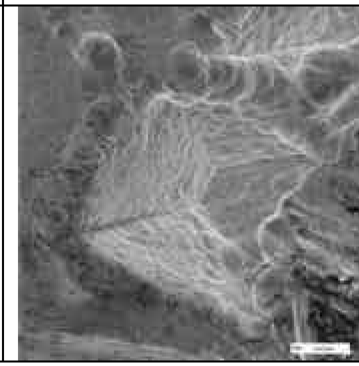

Used wire 1	40x	200x	400x	1000x
Wire used in pine cutting experiments.	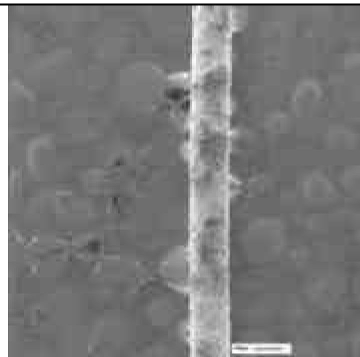	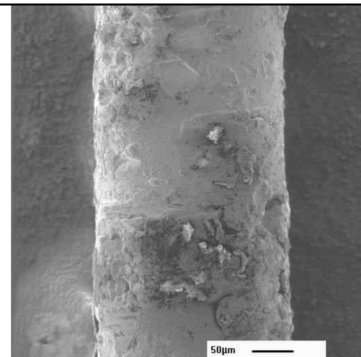	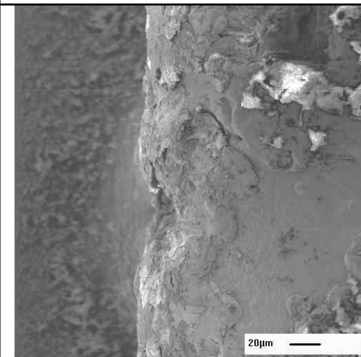	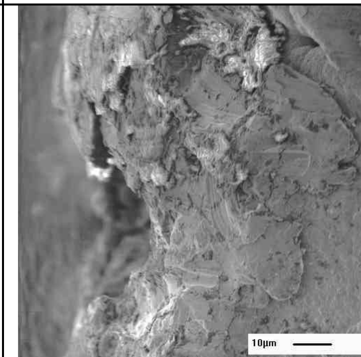
Wire used in oak cutting experiments.	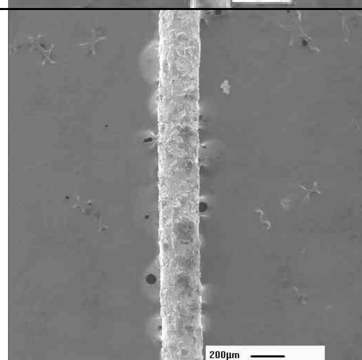	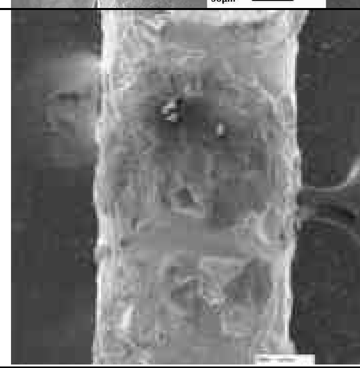	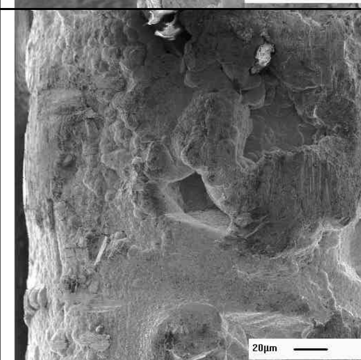	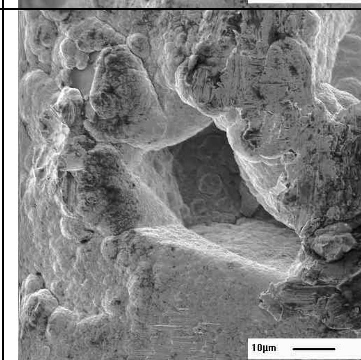
Wire used in ceramic cutting experiments.	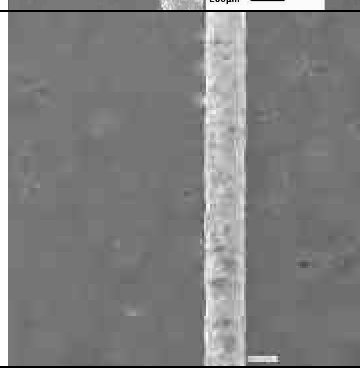	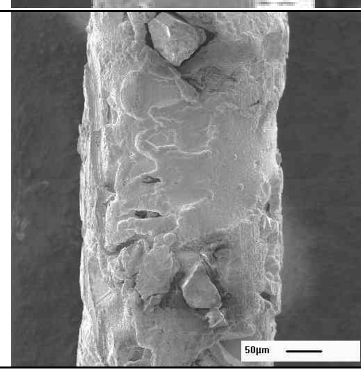	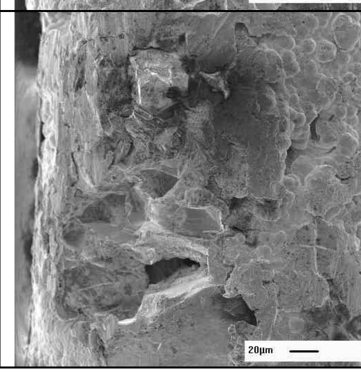	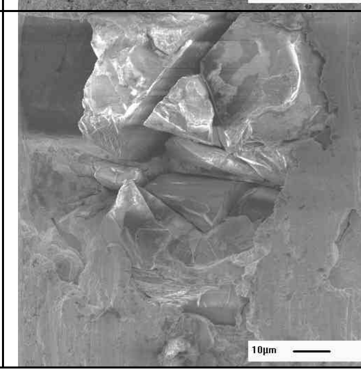

	40x	200x	200x	200x
Wire from pine endurance test	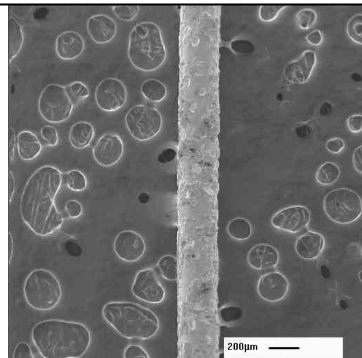	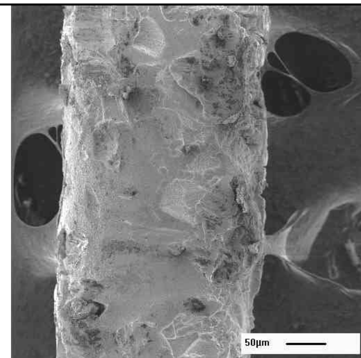	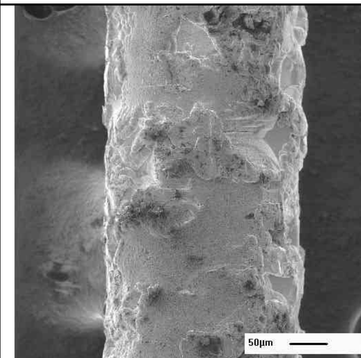	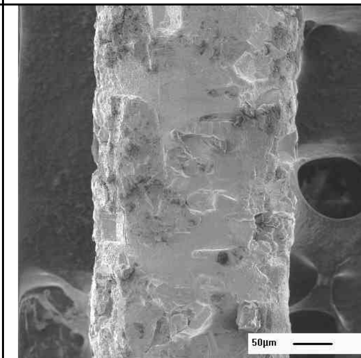
Wire from pine cutting experiment	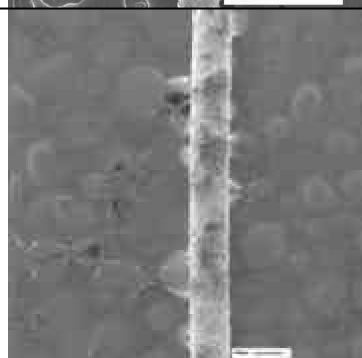	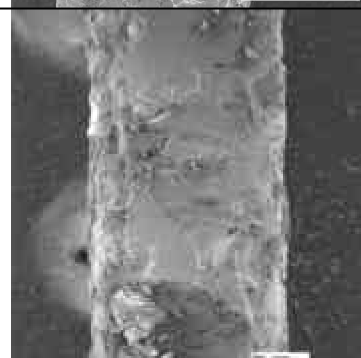	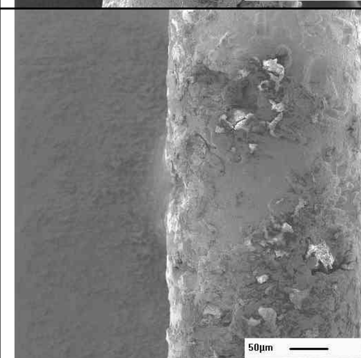	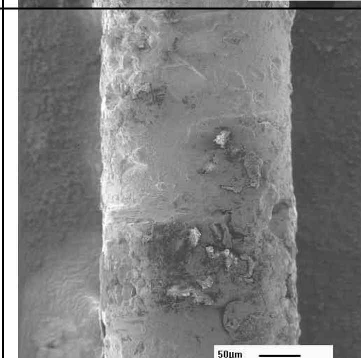
Wire from oak cutting experiment	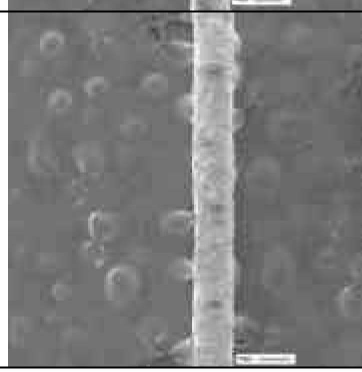	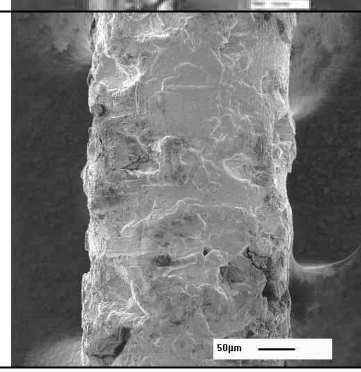	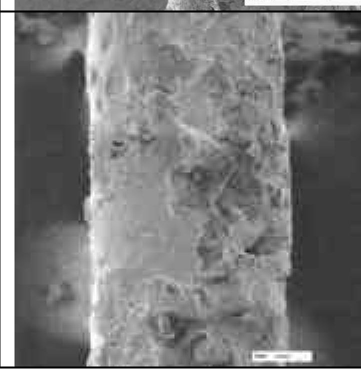	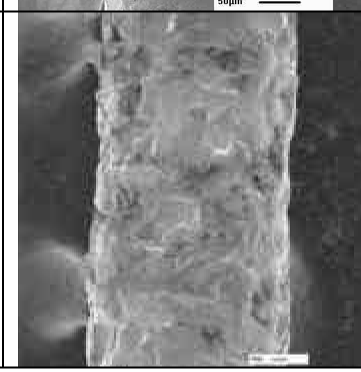

	40x	200x	200x	200x
Wire from ceramic cutting experiments	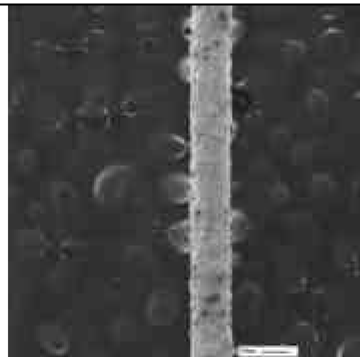	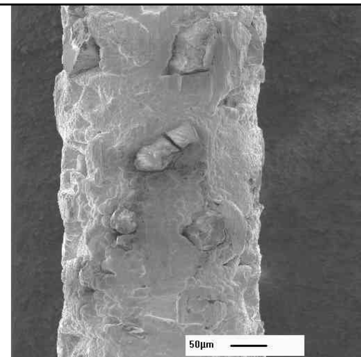	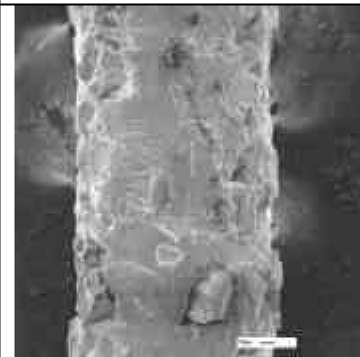	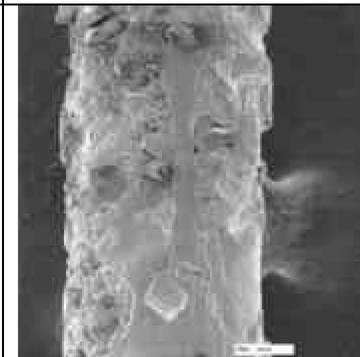
Wire used in other cutting	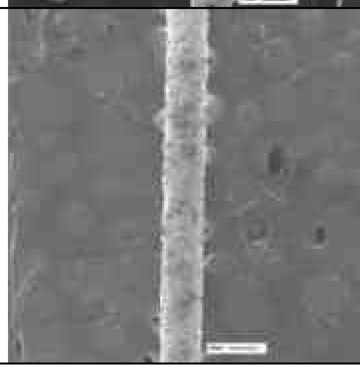	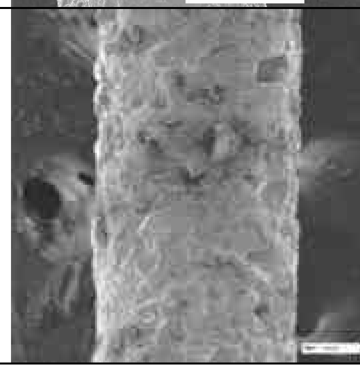	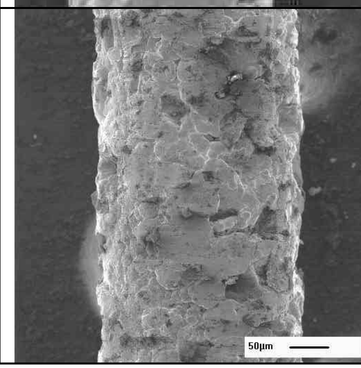	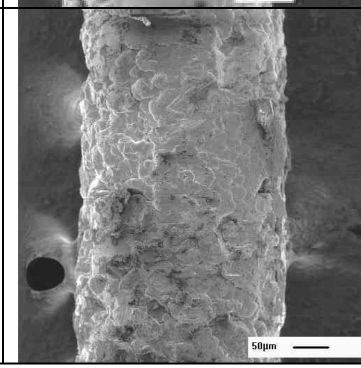

	40x	100x	500x	1000x
Debris from original wire endurance test.	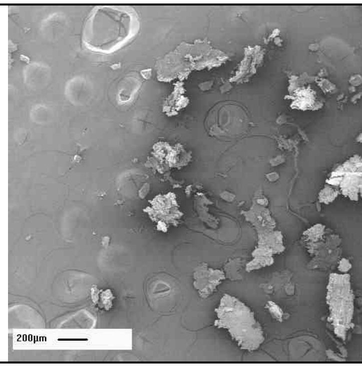	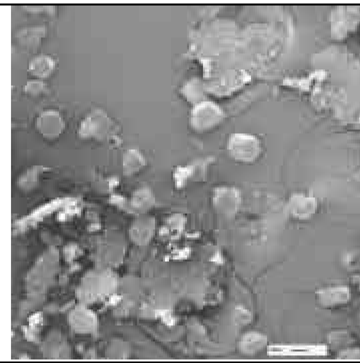	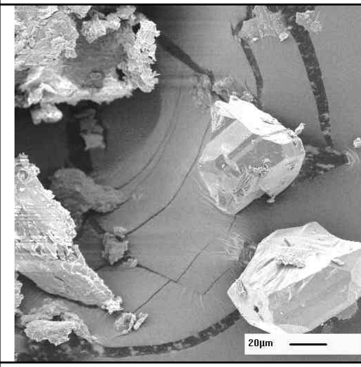	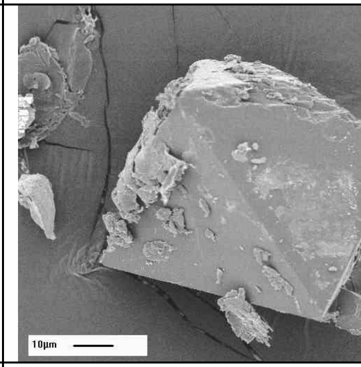
	40x	100x	500x	1000x
Debris from pine experiments.	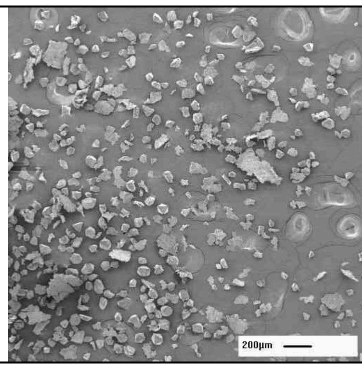	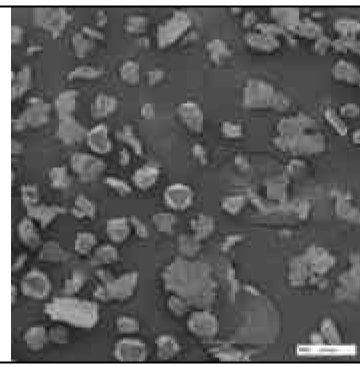	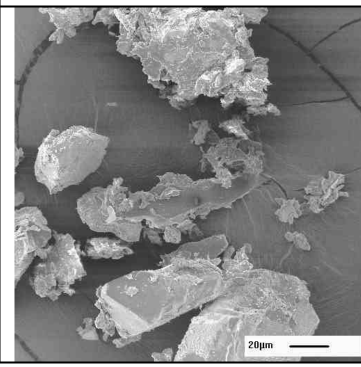	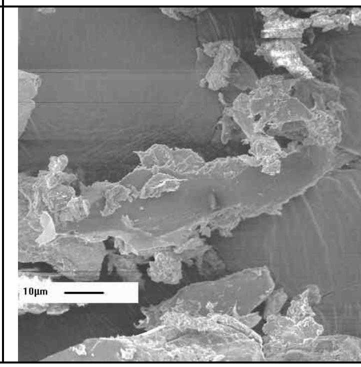

	40x	100x	500x	1000x
Debris from oak experiments.	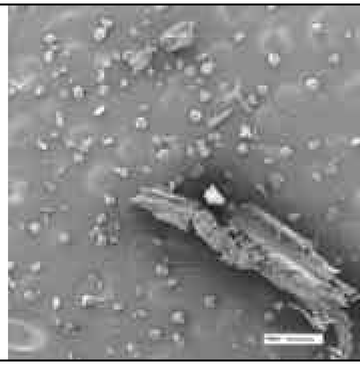	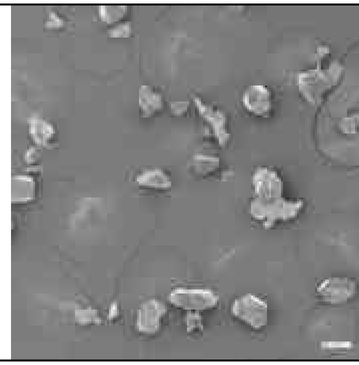	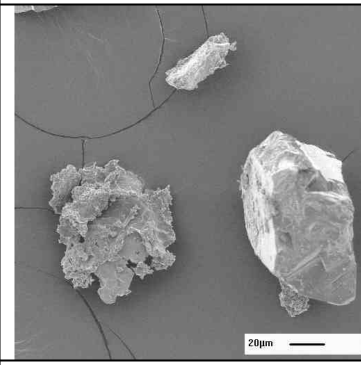	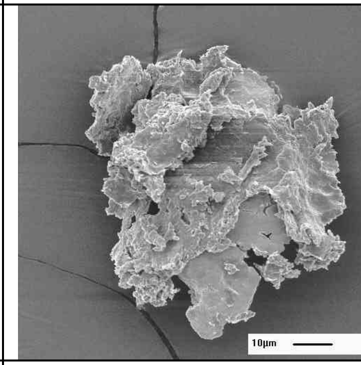
	40x	100x	500x	1000x
Debris from SiC experiments	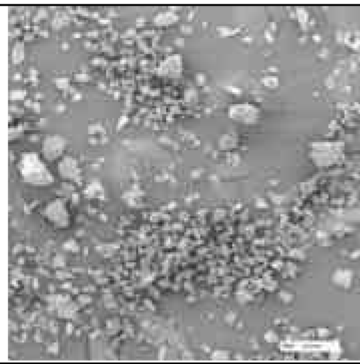	NA	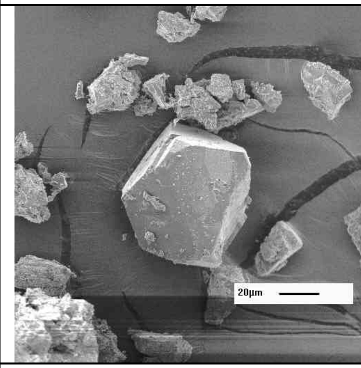	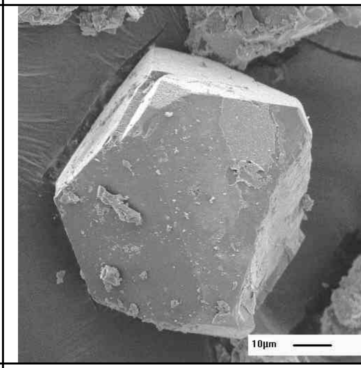

	40x	100x	500x	1000x
Debris from TTZ experiments	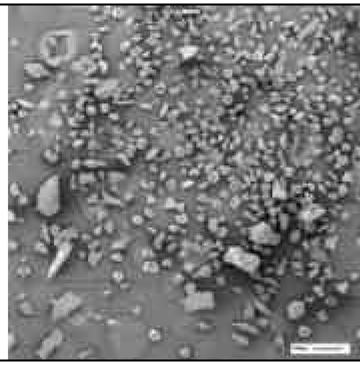	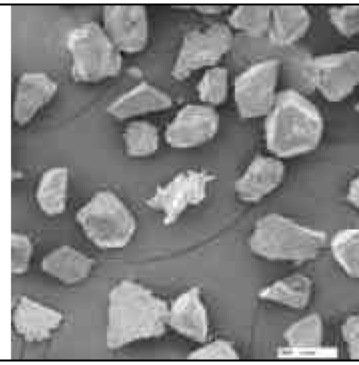	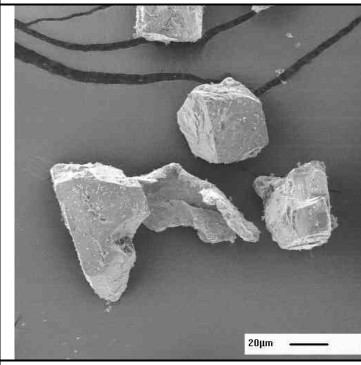	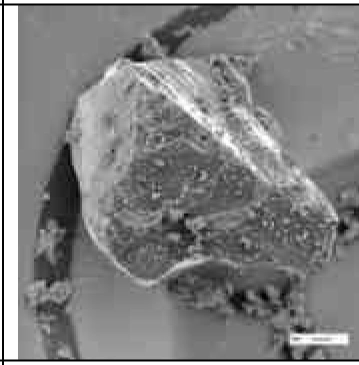
	40x	100x	500x	1000x
Debris from ZTA experiments	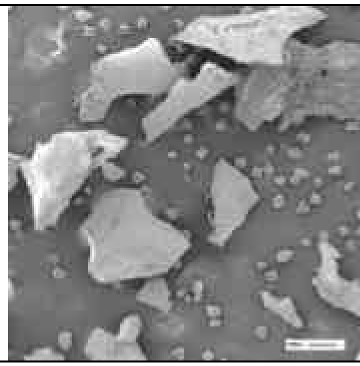	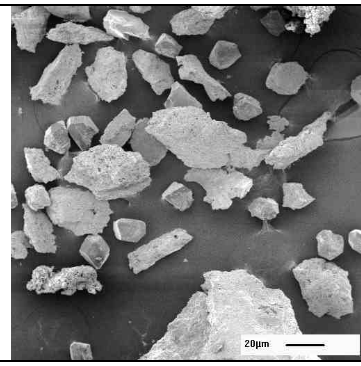	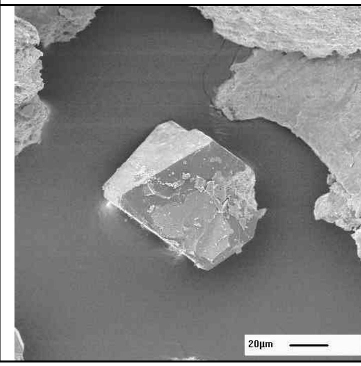	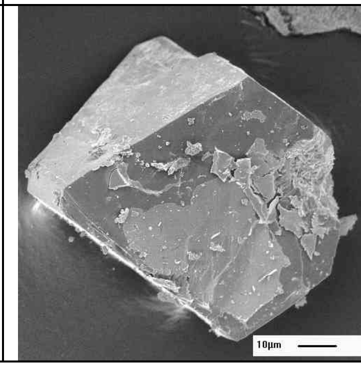

	40x	40x	100x	100x
Cutting debris from endurance test	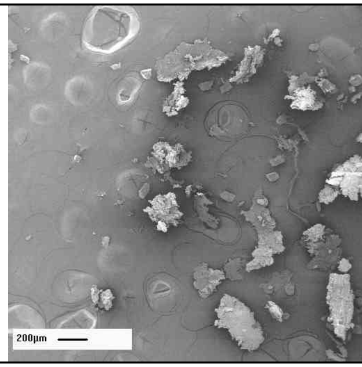	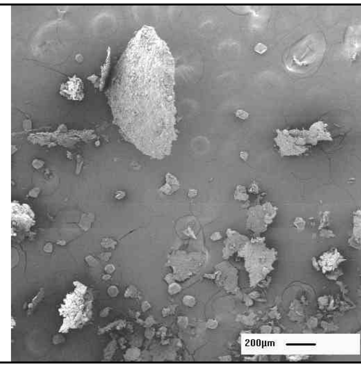	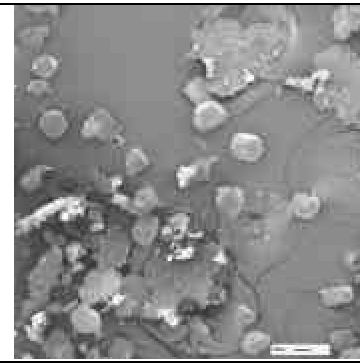	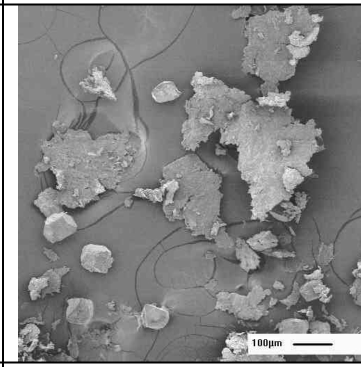
	400x	400x	500x	1000x
	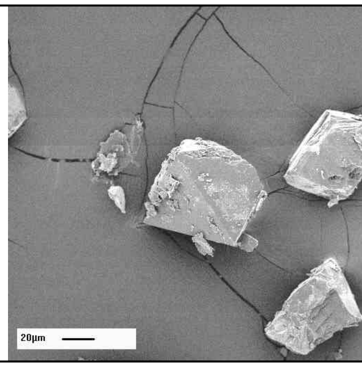	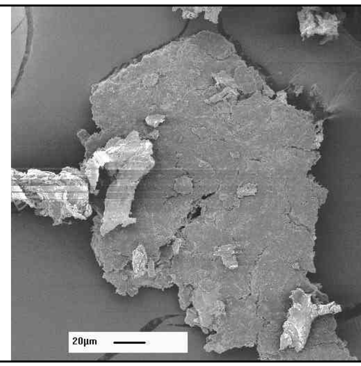	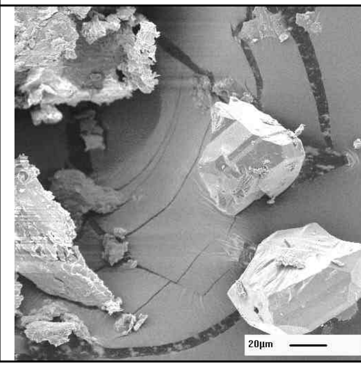	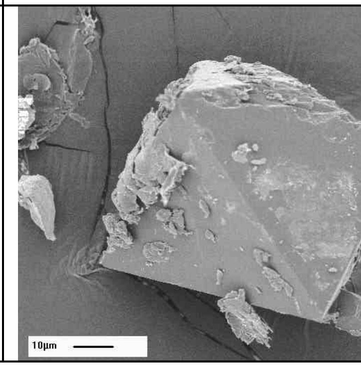

	40x	40x	100x	100x
Cutting debris from pine cutting experiments.	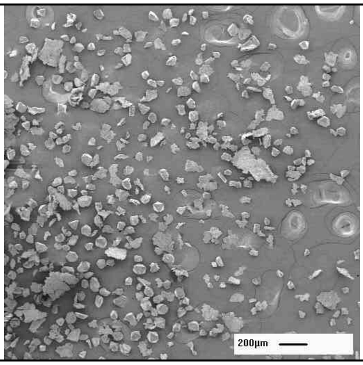	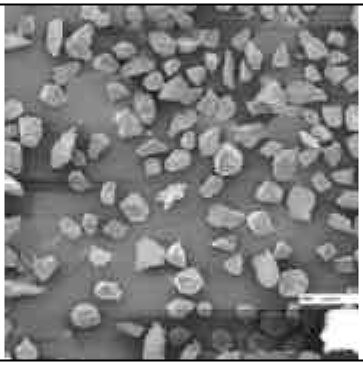	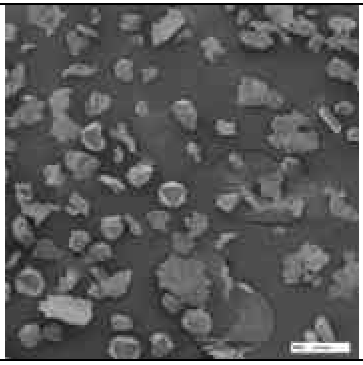	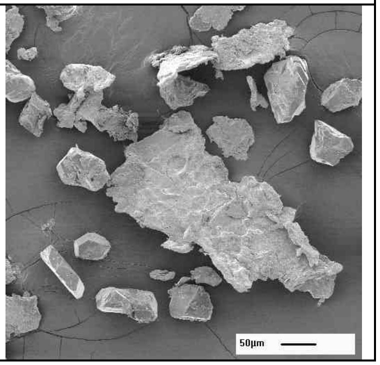

Cutting debris from pine cutting experiments, continued.	500x	500x	1000x	1000x
	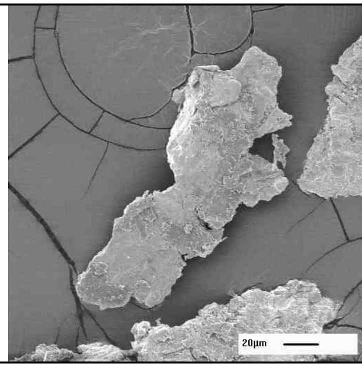	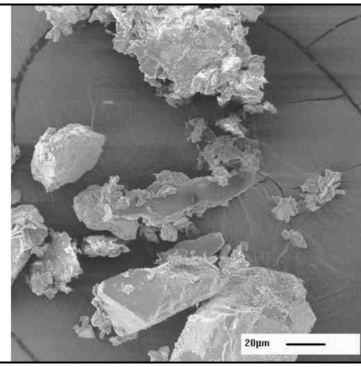	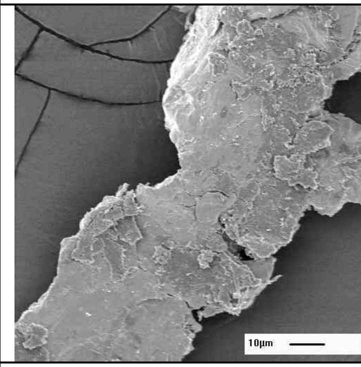	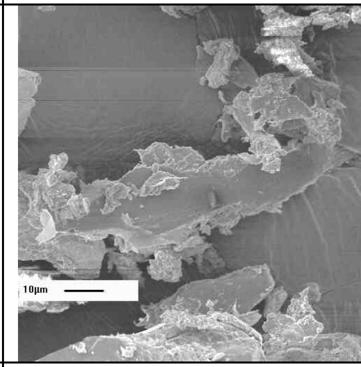
	40x	100x	200x	500x
Cutting debris from oak cutting experiments.	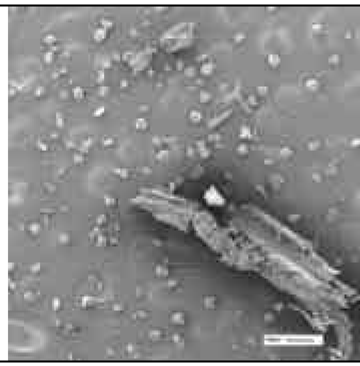	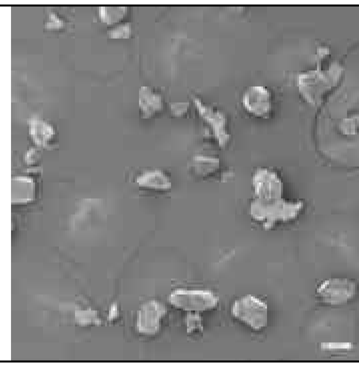	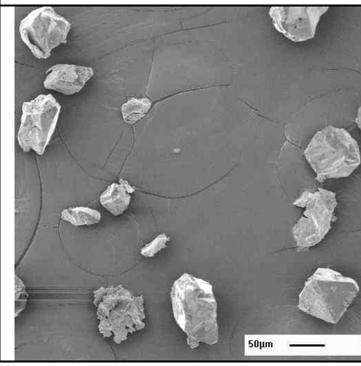	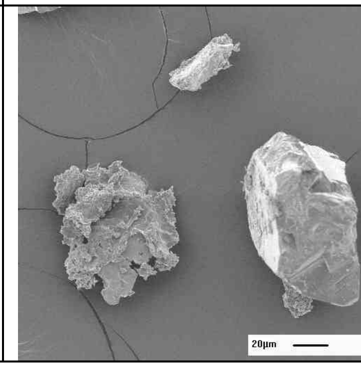

	1000x	1000x	5000x	
Debris from oak experiments, continued.	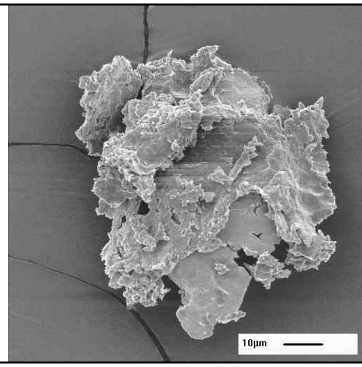	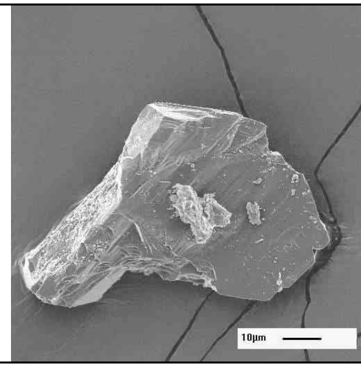	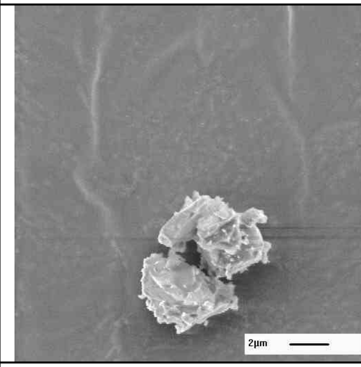	
Cutting debris from SiC experiments.	40x	40x	500x	1000x
	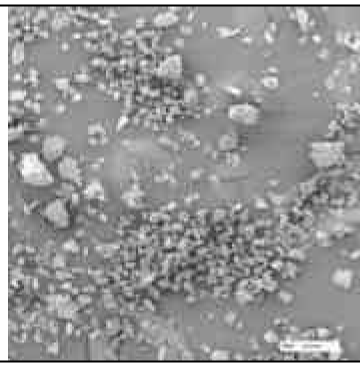	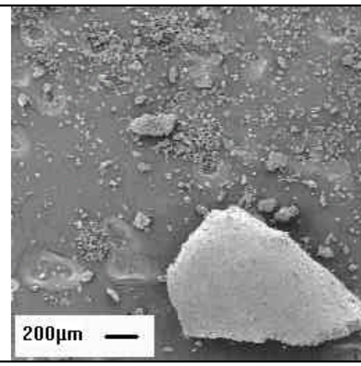	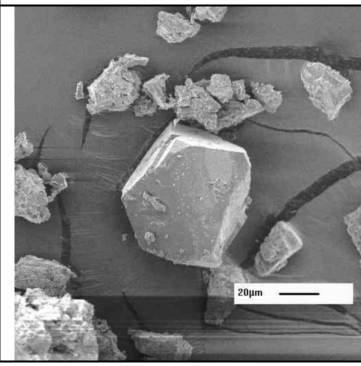	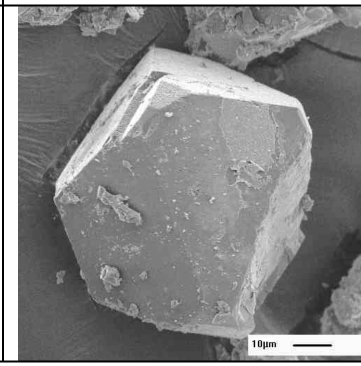

	1000x	2000x	5000x	
	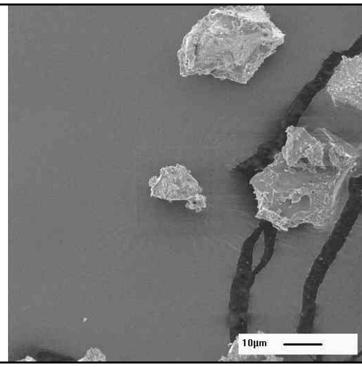	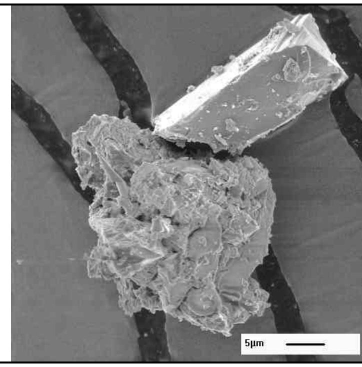	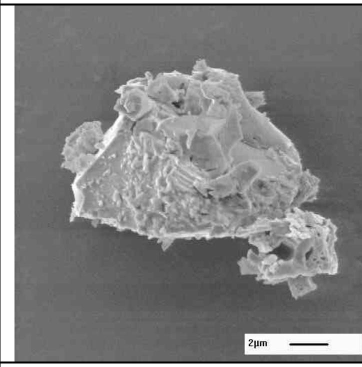	
	40x	50x	200x	500x
Cutting debris from TTZ experiments.	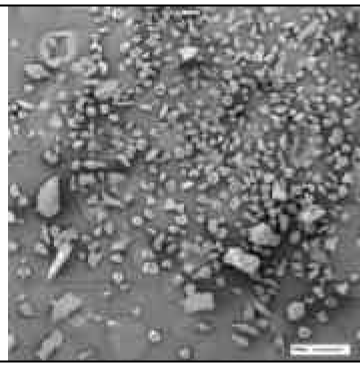	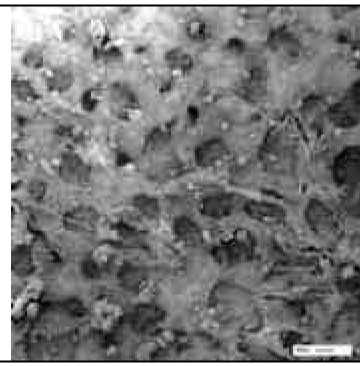	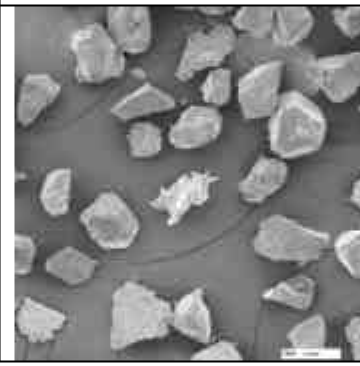	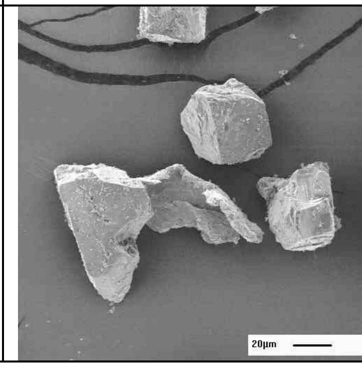

Cutting debris from TTZ experiments, continued.	500x	1000x	1000x	1500x
	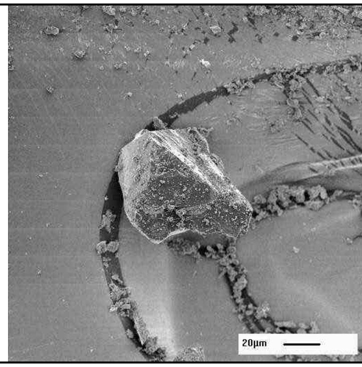	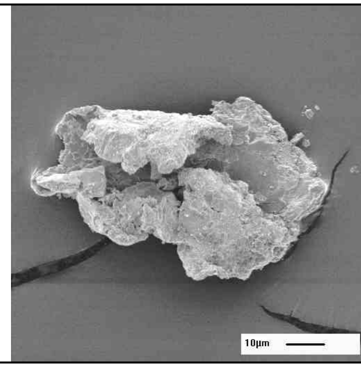	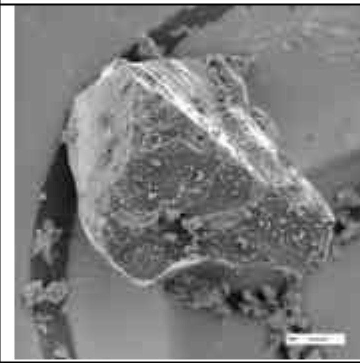	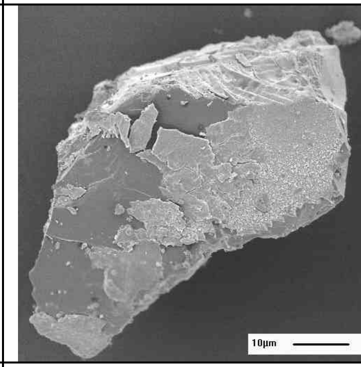
	40x	40x	100x	100x
Cutting debris from ZTA experiments.	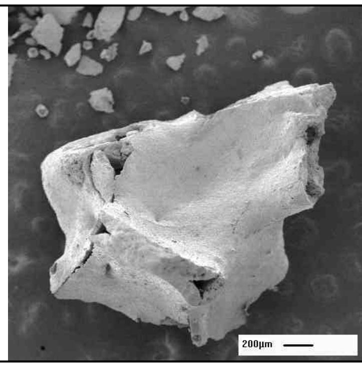	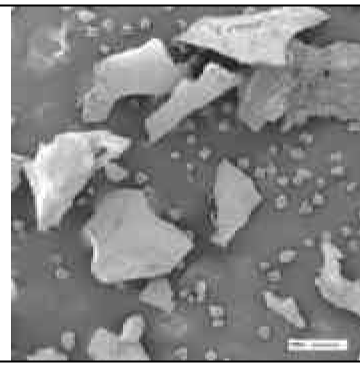	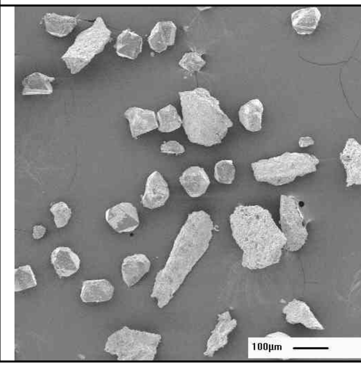	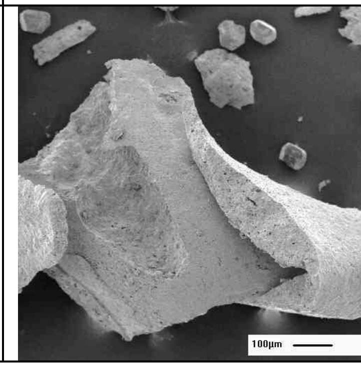

	200x	500x	500x	1000x
	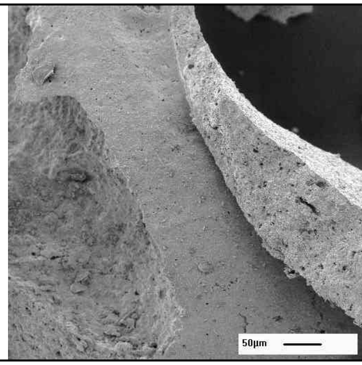	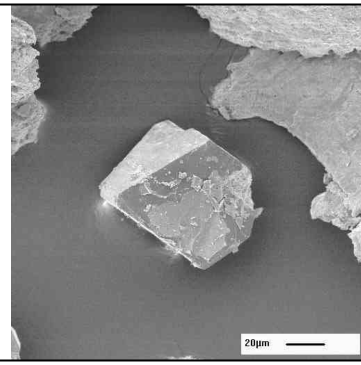	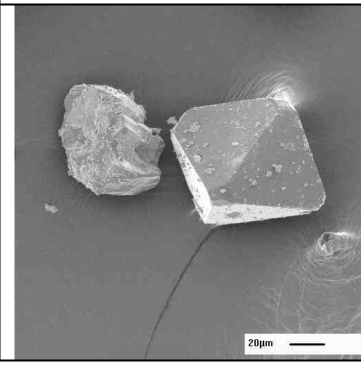	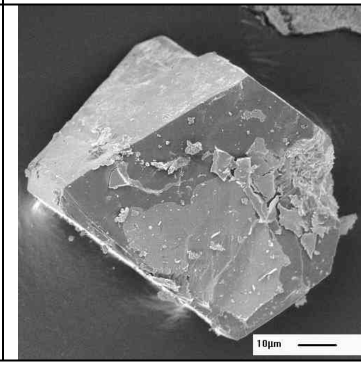

	100x	500x	1000x	2000x
Machined Oak Workpiece	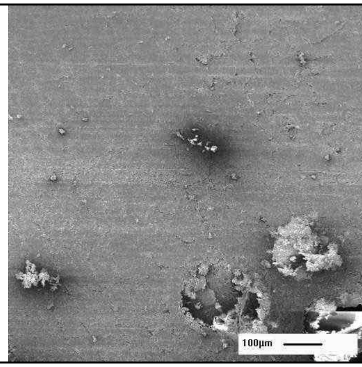	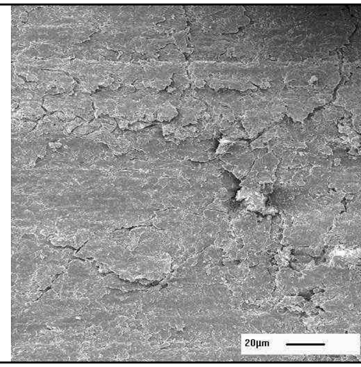	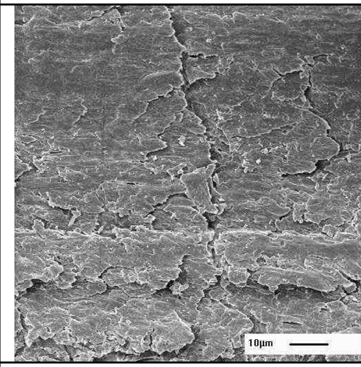	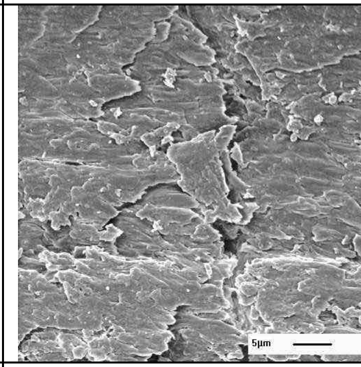
	40x	50x	500x	1000x
Machined TTZ Workpiece